

การเตรียมคอมพอสิตไทเทเนียมไดออกไซด์/คาร์บอนจากไม้ไผ่เป็นขั้วไฟฟ้า

นางสาวชไมพร มุ่งทางธรรม

วิทยานิพนธ์นี้เป็นส่วนหนึ่งของการศึกษาตามหลักสูตรปริญญาวิทยาศาสตรมหาบัณฑิต

สาขาวิชาปิโตรเคมีและวิทยาศาสตร์พอลิเมอร์

คณะวิทยาศาสตร์ จุฬาลงกรณ์มหาวิทยาลัย

ปีการศึกษา 2551

ลิขสิทธิ์ของจุฬาลงกรณ์มหาวิทยาลัย

PREPARATION OF TITANIUM DIOXIDE/BAMBOO BASED CARBON
COMPOSITE AS ELECTRODE

Miss Chamaiporn Mungthangtham

A Thesis Submitted in Partial Fulfillment of the Requirements
for the Degree of Master of Science Program in Petrochemistry and Polymer Science
Faculty of Science
Chulalongkorn University
Academic Year 2008
Copyright of Chulalongkorn University

Thesis Title **PREPARATION OF TITANIUM DIOXIDE/BAMBOO
BASED CARBON COMPOSITE AS ELECTRODE**

By **Miss Chamaiporn Mungthangtham**

Field of Study **Petrochemistry and Polymer Science**

Advisor **Aticha Chaisuwan, Ph.D.**

Co-Advisor **Associate Professor Orawon Chailapakul, Ph.D.**

Accepted by the Faculty of Science, Chulalongkorn University in Partial
Fulfillment of the Requirements for the Master's Degree

.....Dean of the Faculty of Science
(Professor Supot Hannongbua, Dr.rer.nat.)

THESIS COMMITTEE

.....Chairman
(Professor Pattarapan Prasassarakich, Ph.D.)

.....Advisor
(Aticha Chaisuwan, Ph.D.)

..... Co-Advisor
(Associate Professor Orawon Chailapakul, Ph.D.)

.....Examiner
(Associate Professor Wimonrat Trakarnpruk, Ph.D.)

.....Examiner
(Assistant Professor Kulaya Otaka, Ph.D.)

ชไมพร มุ่งทางธรรม: การเตรียมคอมพอสิตไทเทเนียมไดออกไซด์/คาร์บอนจากไม้ไผ่เป็นขั้วไฟฟ้า. (PREPARATION OF TITANIUM DIOXIDE/BAMBOO BASED CARBON COMPOSITE AS ELECTRODE) อ.ที่ปรึกษาวิทยานิพนธ์หลัก:
อ.ดร. อธิชา ฉายสุวรรณ, อ.ที่ปรึกษาวิทยานิพนธ์ร่วม: รศ.ดร. อรวรรณ ชัยลภากุล,
107 หน้า

งานวิจัยนี้ได้นำเสนอวิธีใหม่ในการเตรียมนาโนคอมพอสิตไทเทเนียมไดออกไซด์/คาร์บอน ที่มีความเสถียรต่ออุณหภูมิสูงสำหรับนำไปประยุกต์ใช้ในงานตัวเก็บประจุ โดยตะกียบไม้ไผ่ที่ใช้แล้วถูกนำมาเป็นแหล่งของคาร์บอน วิธีใหม่ที่นำเสนอต้องผ่านกระบวนการ 2 ขั้นตอนคือ การอิมเพกนชันผงตะกียบไม้ไผ่ด้วยไทเทเนียมเพอร์ออกไซด์โพรพอกไซด์ซึ่งละลายอยู่ใน 2-โพรพานอล ตามด้วยคาร์บอนในเซชันที่อุณหภูมิที่ต้องการศึกษาคือ 500, 600, และ 700 องศาเซลเซียส ข้อมูลจากเทคนิคการเลี้ยวเบนรังสีเอ็กซ์แสดงให้เห็นว่าทั้งสามอุณหภูมิเกิดโครงสร้างไทเทเนียมไดออกไซด์แบบแอนาเทสและเป็นที่น่าสนใจว่าไม่พบโครงสร้างแบบรูทิลเลย การเตรียมไทเทเนียมไดออกไซด์ด้วยวิธีอื่นเป็นที่รู้จักกันโดยทั่วไปว่าจะเกิดการเปลี่ยนแปลงโครงสร้างจากแอนาเทสเป็นรูทิลได้เมื่ออุณหภูมิสูงขึ้นในช่วง 600-700 องศาเซลเซียส และกลายเป็นรูทิลอย่างสมบูรณ์ที่อุณหภูมิสูงกว่า 700 องศาเซลเซียส ขึ้นไป นั่นแสดงให้เห็นว่าคาร์บอนจากไม้ไผ่ในคอมพอสิตช่วยเพิ่มความเสถียรต่ออุณหภูมิสูงถึง 700 องศาเซลเซียส อุณหภูมิคาร์บอนในเซชันและวิธีในการเตรียมคอมพอสิตมีผลต่อขนาดผลึกของแอนาเทส โดยวิธีใหม่นี้ได้ผลึกนาโนแอนาเทสที่มีขนาดเล็กเป็นครึ่งหนึ่งของวิธีดั้งเดิมและใช้เทคนิคการถ่ายภาพด้วยกล้องจุลทรรศน์อิเล็กตรอนแบบส่งกราดในการตรวจสอบลักษณะพื้นผิวและขนาดผลึกของไทเทเนียมไดออกไซด์ ไอโซเทิร์มการดูดซับไนโตรเจนของคอมพอสิตแสดงลักษณะของสารที่มีรูพรุนขนาดเล็กและคอมพอสิตที่เตรียมโดยวิธีใหม่มีค่าพื้นที่ผิวจำเพาะน้อยกว่าวิธีแบบดั้งเดิม เหตุผลเพราะไทเทเนียมเพอร์ออกไซด์ที่ใช้เป็นแหล่งของไทเทเนียมสามารถแทรกซึมเข้าไปในรูพรุนของผงไม้ไผ่และเกิดเป็นผลึกของนาโนแอนาเทสในรูพรุนของคาร์บอนที่ได้จากไม้ไผ่เมื่อผ่านกระบวนการคาร์บอนในเซชัน โดยสิ่งที่เกิดขึ้นพร้อมๆกันคือเกิดการพัฒนาของโครงสร้างรูพรุนของคาร์บอนไปห่อหุ้มผลึกแอนาเทสที่เกิดขึ้นให้อยู่ในรูพรุนของคาร์บอนขณะที่ได้รับความร้อนนั่นเอง ซึ่งต่างจากไทเทเนียมไดออกไซด์ที่เตรียมจากวิธีดั้งเดิมจะปรากฏอยู่ข้างนอกรูพรุนของคาร์บอน ดังนั้นจึงเกิดผลึกขนาดใหญ่บนรูพรุนของคาร์บอนทำให้เหลือพื้นที่ผิวในรูพรุนมากค่าพื้นที่ผิวจำเพาะของวิธีดั้งเดิมจึงมีค่ามากกว่า เทคนิคไซคลิกโวลแทมเมทรีและอิมพีแดนซ์สเปกโทรสโกปีใช้สำหรับตรวจสอบลักษณะจำเพาะทางเคมีไฟฟ้าของขั้วไฟฟ้าตัวเก็บประจุคอมพอสิต โดยอุณหภูมิในการคาร์บอนในเซชันและปริมาณไทเทเนียมไดออกไซด์ในคอมพอสิตล้วนมีผลต่อค่าการเก็บประจุจำเพาะของขั้วไฟฟ้าคอมพอสิตทั้งสิ้น อย่างไรก็ตามคอมพอสิตที่เตรียมโดยผ่านกระบวนการใช้กรดฟอสฟอริกมีแนวโน้มให้ค่าการเก็บประจุจำเพาะสูงขึ้น ดังนั้นคอมพอสิตที่เตรียมได้ในงานวิจัยนี้จึงมีประโยชน์สามารถนำไปประยุกต์ใช้กับงานทางด้านตัวเก็บประจุได้

สาขาวิชา ปิโตรเคมีและวิทยาศาสตร์พอลิเมอร์ ปลายมือชื่อนิติศ.....

ปีการศึกษา..... 2551..... ปลายมือชื่อ อ.ที่ปรึกษาวิทยานิพนธ์หลัก.....

4872262823: MAJOR PETROCHEMISTRY AND POLYMER SCIENCE

KEYWORDS: BAMBOO/CARBON/TITANIUMDIOXIDE/CAPACITOR/ELECTRODE

CHAMAIPORN MUNGTHANGTHAM: PREPARATION OF TITANIUM
DIOXIDE/BAMBOO BASED CARBON COMPOSITE AS ELECTRODE.

ADVISOR: ATICHA CHAISUWAN, Ph.D., CO-ADVISOR: ASSOC. PROF.

ORAWON CHAILAPAKUL, Ph.D., 107 pp.

In this research, we report a novel method for preparation of the titanium dioxide/carbon nanocomposite with high thermal stability for application in a capacitor using the disposed bamboo chopsticks as carbon source. The proposed preparation method contains 2 steps which are impregnation of the bamboo powder with a solution of titanium tetraisopropoxide in 2-propanol and subsequently carbonization at a required temperature. The effect of carbonization temperatures was studied at 500, 600 and 700°C. The XRD data showed that crystalline TiO₂ was readily formed as anatase structure at all of the three temperatures. It is very interesting that rutile phase was not observed at all. It is well known that titanium dioxide prepared by other methods normally undergoes anatase-to-rutile phase transformation in the temperature range from 600 to 700°C and anatase is completely converted to rutile above 700°C. It indicates that carbon from bamboo can obviously stabilize the nano-anatase phase up to 700°C. The crystal size of anatase is affected by the carbonization temperature and method of preparation. This method provided nanocrystals of anatase with about one half smaller crystal sizes than that prepared by the conventional method which was performed in the alternative sequence of preparation steps. SEM was used for the identification of the surface morphology and particle size. The adsorption isotherms of the composites show the characteristic of micropores. The composite prepared by this novel method has lower BET specific surface area than that prepared by the conventional method. It can be explained that TTIP can penetrate into wide pores of the bamboo texture and convert to nanocrystals of anatase inside the pores of resulted porous carbon. Simultaneously, carbonization results in encapsulation of the anatase particle within the pores of carbon. The composites from the conventional method contain TiO₂ outside the pores of carbon. The latter causes relatively larger crystals on the outer surface of carbon and leaves more space inside the carbon pores. Cyclic voltammetry and electrochemical impedance spectroscopy were employed to characterize the electrochemical performances of the composite electrode. The specific capacitance of the composite electrode is affected by the carbonization temperature and TiO₂ content in the composite. However, the composite treated by phosphoric acid shows an enhanced specific capacitance. The composite is potential to be applied further as electrode materials for electric double layer capacitors.

Field of Study: Petrochemistry and Polymer Science Student's Signature:.....

Academic Year:.....2008..... Advisor's Signature:.....

ACKNOWLEDGEMENTS

The success of this thesis can be attributed to the extensive support and assistance from Dr. Aticha Chaisuwan and Associate Professor Dr. Orawon Chailapakul, the author's advisor and co-advisor, respectively. She deeply thanks them for their valuable advice and guidance in this research and their kindness throughout this study.

She would like to gratitude to Professor Dr. Pattarapan Prasassarakich, Associate Professor Dr. Wimonrat Trakarnpruk and Assistant Professor Dr. Kulaya Otake as the chairman and members of this thesis committee, respectively, for all of their kindness and useful advice in the research.

She would like to thank Department of Chemistry and Program of Petrochemistry and Polymer Science, Faculty of Science, Chulalongkorn University for the valuable knowledge and experience. This thesis is financially supported by the government budget of the year 2008 through the National Research Council of Thailand. Furthermore, she would like to thank the members of Materials Chemistry and Catalysis Research Unit for generosity, especially their very good corporation in work, sharing of colorful emotion and friendly working atmosphere. She truly realizes their support and standing by her throughout her work.

For all of her friends, she greatly appreciates their help and encouragement throughout the course of her research and study.

Finally, she would like to express her deepest gratitude to her beloved family for their entirely care and support, endless love and eternal understanding throughout her life. The usefulness of this thesis, she dedicates to her family, all teachers who have taught her since her childhood and you who are always stand by her.

CONTENTS

	Page
ABSTRACT (THAI)	iv
ABSTRACT (ENGLISH)	v
ACKNOWLEDGEMENTS	vi
CONTENTS	vii
LIST OF TABLES	x
LIST OF FIGURES	xii
LIST OF SCHEMES	xviii
LIST OF ABBREVIATIONS	xix
CHAPTER I INTRODUCTION	1
1.1 Background.....	1
1.2 Objective.....	8
1.3 Scopes of This Work.....	8
CHAPTER II THEORY	9
2.1 Carbon.....	9
2.2 Titanium Dioxide.....	10
2.3 Structure of Titanium Dioxide.....	11
2.4 Synthesis Methods for Titanium Dioxide Nanostructures.....	13
2.4.1 Sol-Gel Method.....	13
2.4.2 Hydrothermal Method.....	13
2.4.3 Solvothermal Method.....	14
2.4.4 Chemical Vapor Deposition.....	14
2.4.5 Sonochemical Method.....	14
2.4.6 Microwave Method.....	15
2.4.7 TiO ₂ Aerogels.....	15
2.5 Modifications of Titanium Dioxide Nanomaterials.....	15
2.5.1 Metal-Doped TiO ₂ Nanomaterials.....	16
2.5.2 Nonmetal-Doped TiO ₂ Nanomaterials.....	16

2.6	Applications of TiO ₂ Nanomaterials.....	17
2.6.1	Photocatalytic Applications.....	17
2.6.2	Photovoltaic Applications.....	18
2.7	Faradaic and Nonfaradaic Processes.....	18
2.8	Nonfaradaic Processes and the Nature of the Electrode-Solution Interface.....	18
2.8.1	The Ideal Polarized Electrode.....	18
2.8.2	Capacitance and Charge of an Electrode.....	19
2.9	Electric Double Layer Capacitors (EDCLs).....	19
2.10	Electrochemical Impedance Spectroscopy (EIS).....	21
2.10.1	Definition of Impedance.....	21
2.10.2	Electrical Circuit Elements.....	22
2.10.3	Charge Transfer Resistance, R_{ct} (or Polarization Resistance, R_p).....	22
2.10.4	Double Layer Capacitance, C_{dl}	23
2.10.5	Constant Phase Element (CPE).....	24
2.10.6	Warburg Impedance (Z_w).....	24
2.11	Characterization of Titanium Dioxide.....	25
2.11.1	X-ray Powder Diffraction (XRD).....	25
2.11.2	Scanning Electron Microscope (SEM).....	26
2.11.3	Nitrogen Adsorption-Desorption Isotherm.....	27
2.11.4	Cyclic Voltammetry (CV).....	29
2.11.5	Electrochemical Impedance Spectroscopy (EIS).....	31
CHAPTER III EXPERIMENTAL.....		33
3.1	Instruments and Apparatus.....	33
3.2	Materials, Chemicals and Gases	35
3.3	Preparation of the Porous Carbon from Bamboo Waste as a Support.....	35
3.3.1	Preparation of the Carbon.....	35
3.3.2	Preparation of the Activated Carbon.....	35
3.4	Preparation of the TiO ₂ /C and TiO ₂ /AC Composites.....	37
3.4.1	Method A (The Novel Method): TTIP Impregnation Before Carbonization.....	37

3.4.2	Method B (The Conventional Method): TTIP Impregnation After Carbonization.....	37
3.5	Preparation of Bulk TiO ₂	39
3.6	Preparation of A1, A2, B1, B2 Composites with Various Amounts of TiO ₂ in Composite.....	39
3.7	Preparation of the Sample Electrodes.....	40
CHAPTER IV RESULTS AND DISCUSSION.....		41
4.1	Effect of Preparation Methods and Carbonization Temperature on Composite Properties.....	41
4.1.1	XRD Patterns.....	41
4.1.2	Nitrogen Adsorption.....	46
4.1.3	SEM Images.....	50
4.1.4	Electrochemical Properties.....	53
4.1.4.1	Cyclic Voltammograms.....	53
4.1.4.2	Electrochemical Impedance Spectra.....	63
4.2	Effect of TiO ₂ Contents in the Composite on Composite Properties.....	70
4.2.1	XRD Patterns.....	70
4.2.2	Nitrogen Adsorption.....	73
4.2.3	SEM Images.....	77
4.2.4	Electrochemical Properties	80
4.2.4.1	Cyclic Voltammograms.....	80
4.2.4.2	Electrochemical Impedance Spectra.....	86
CHAPTER V CONCLUSION.....		90
REFERENCES.....		92
APPENDICES.....		101
VITAE.....		107

LIST OF TABLES

Table	Page
2.1 Common electrical elements.....	22
2.2 Features of adsorption isotherms.....	28
2.3 IUPAC classification of pores.....	28
4.1 Relative peak width at half height for anatase crystals in the composites obtained from different preparation methods at various carbonization temperatures of 500, 600, and 700°C.....	45
4.2 Textural properties of composites obtained from different preparation methods at various carbonization temperatures of 500, 600, and 700°C.....	49
4.3 The average current from cyclic voltammetry of the sample electrodes obtained from different preparation methods at various carbonization temperatures of 500, 600, and 700°C.....	60
4.4 The specific capacitance calculated from cyclic voltammetry of the sample electrodes obtained from different preparation methods at various carbonization temperatures of 500, 600, and 700°C.....	61
4.5 The specific capacitance calculated from electrochemical impedance spectroscopy of the sample electrodes obtained from different preparation methods at carbonization temperatures of 500, 600, and 700°C.....	68
4.6 A comparison of the specific capacitance obtained from different techniques of the sample electrodes by different preparation methods at various carbonization temperatures of 500, 600, and 700°C.....	69
4.7 Relative peak width at half height for anatase crystals in the composites obtained from different preparation methods at the carbonization temperature of 500°C with various amounts of TiO ₂ at 10-40 wt% in the composite.....	73

Table	Page
4.8 Textural properties of TiO ₂ /C and TiO ₂ /AC composites obtained from different preparation methods at the carbonization temperature of 500°C at 10-40 wt% TiO ₂ contents in the composites.....	76
4.9 The average current calculated from cyclic voltammetry of the composite electrodes obtained from different preparation methods at the carbonization temperature of 500°C at 10-40 wt% TiO ₂ contents in the composites.....	80
4.10 The specific capacitance calculated from cyclic voltammetry of the composite electrodes obtained from different preparation methods at the carbonization temperature of 500°C at 10-40 wt% TiO ₂ contents in the composites.....	85
4.11 The specific capacitance calculated from electrochemical impedance spectroscopy of the composite electrodes obtained from different preparation methods at the carbonization temperature of 500°C at 10-40 wt% TiO ₂ contents in the composites.....	89
A-1 Specific capacitance of electrodes with effect of preparation methods and carbonization temperature calculated from cyclic voltammetric technique.....	102
A-2 Specific capacitance of electrodes with effect of TiO ₂ contents in the composite calculated from cyclic voltammetric technique.....	103
B-1 Specific capacitance of electrodes with effect of preparation methods and carbonization temperature calculated from electrochemical impedance spectroscopic technique.....	104
B-2 Specific capacitance of electrodes with effect of TiO ₂ contents in the composite calculated from electrochemical impedance spectroscopic technique.....	105

LIST OF FIGURES

Figure	Page
<p>2.1 The crystal structures of rutile and anatase. The tetragonal unit cell of rutile has the dimension, $a = b = 4.587 \text{ \AA}$, $c = 2.953 \text{ \AA}$, and the one of anatase $a = b = 3.782 \text{ \AA}$, $c = 9.502 \text{ \AA}$. In both structures, slightly distorted octahedral are the basic building units. The bond lengths and angles of the octahedrally coordinated Ti atoms are indicated and the stacking of the octahedral in both structures is shown on the right side.....</p>	12
<p>2.2 The crystal structure of brookite. The orthorhombic unit cell of brookite has the dimension, $a = 9.184 \text{ \AA}$, $b = 5.447 \text{ \AA}$, $c = 5.145 \text{ \AA}$.....</p>	13
<p>2.3 (a) A capacitor (b) Charging a capacitor with a battery.....</p>	19
<p>2.4 Diffraction of X-ray by regular planes of atoms.....</p>	25
<p>2.5 The IUPAC classification of adsorption isotherm.....</p>	27
<p>2.6 Some potential waveforms used in cyclic voltammetry.....</p>	29
<p>2.7 Cyclic voltammogram for a reversible.....</p>	30
<p>2.8 Equivalent circuit models with mixed kinetic and charge transfer control.....</p>	31
<p>2.9 Typical Nyquist plot for a cell with mixed kinetic and charge transfer.....</p>	32
<p>3.1 Drawing of the system used for thermal treatment.....</p>	33
<p>4.1 XRD patterns of TiO_2/C composites prepared by Method A1 at various carbonization temperatures of (a) 500°C, (b) 600°C, and (c) 700°C.....</p>	42
<p>4.2 XRD patterns of TiO_2/C composites prepared by Method A2 at various carbonization temperatures of (a) 500°C, (b) 600°C, and (c) 700°C.....</p>	42
<p>4.3 XRD patterns of TiO_2/C composites prepared by Method B1 at various carbonization temperatures of (a) 500°C, (b) 600°C, and (c) 700°C.....</p>	43
<p>4.4 XRD patterns of TiO_2/AC composites prepared by Method B2 at various carbonization temperatures of (a) 500°C, (b) 600°C, and (c) 700°C.....</p>	43
<p>4.5 XRD patterns of the unsupported TiO_2 (TiO_2 100%) prepared under N_2 at various calcination temperatures of (a) 500°C, (b) 600°C, and (c) 700°C.....</p>	44

Figure	Page
4.6 The N ₂ adsorption isotherms of TiO ₂ /C composites prepared by Method A1 at various carbonization temperatures of 500, 600, and 700°C.....	47
4.7 The N ₂ adsorption isotherms of TiO ₂ /C composites prepared by Method A2 at various carbonization temperatures of 500, 600, and 700°C.....	47
4.8 The N ₂ adsorption isotherms of TiO ₂ /C composites prepared by Method B1 at various carbonization temperatures of 500, 600, and 700°C.....	48
4.9 The N ₂ adsorption isotherms of TiO ₂ /AC composites prepared by Method B2 at various carbonization temperatures of 500, 600, and 700°C.....	48
4.10 SEM images of the unsupported TiO ₂ (TiO ₂ 100%) at various calcination temperatures of (a) 500°C, (b) 600°C, and (c) 700°C. All images are taken at a magnification of 500x.....	50
4.11 SEM images of TiO ₂ /C composites prepared by Method A1 at various carbonization temperatures of (a) 500°C, (b) 600°C at a magnification of 80,000x, and (c) 700°C at a magnification of 50,000x.....	51
4.12 SEM images of TiO ₂ /C composites prepared by Method A2 at various carbonization temperatures of (a) 500°C, (b) 600°C at a magnification of 80,000x, and (c) 700°C at a magnification of 20,000x.....	51
4.13 SEM images of TiO ₂ /C composites prepared by Method B1 at various carbonization temperatures of (a) 500°C, (b) 600°C (c) 700°C. All images are taken at a magnification of 10,000x.....	52
4.14 SEM images of TiO ₂ /AC composites prepared by Method B2 at various carbonization temperatures of (a) 500°C, (b) 600°C (c) 700°C. All images are taken at a magnification of 10,000x.....	53
4.15 Cyclic voltammograms of (a) carbon (b) activated carbon electrodes in 1 M H ₂ SO ₄	54
4.16 Cyclic voltammograms of TiO ₂ /C composite electrodes prepared by Method A1 at various carbonization temperatures of (a) 500°C, (b) 600°C, and (c) 700°C in 1 M H ₂ SO ₄	55
4.17 Cyclic voltammograms of TiO ₂ /C composite electrodes prepared by Method A2 at various carbonization temperatures of (a) 500°C, (b) 600°C, and (c) 700°C in 1 M H ₂ SO ₄	56

Figure	Page
4.18 Cyclic voltammograms of TiO ₂ /C composite electrodes prepared by Method B1 at various carbonization temperatures of (a) 500°C, (b) 600°C, and (c) 700°C in 1 M H ₂ SO ₄	57
4.19 Cyclic voltammograms of TiO ₂ /AC composite electrodes prepared by Method B2 at various carbonization temperatures of (a) 500°C, (b) 600°C, and (c) 700°C in 1 M H ₂ SO ₄	58
4.20 Cyclic voltammograms of the unsupported bulk TiO ₂ (TiO ₂ 100%) electrodes at various calcination temperatures of (a) 500°C, (b) 600°C, and (c) 700°C in 1 M H ₂ SO ₄	59
4.21 Complex-plane impedance spectra of electrochemical capacitors with electrode material made by (a) carbon (b) activated carbon.....	64
4.22 Complex-plane impedance spectra of electrochemical capacitors with electrode material made by Method A1 at various carbonization temperatures of (a) 500°C, (b) 600°C, and (c) 700°C.....	65
4.23 Complex-plane impedance spectra of electrochemical capacitors with electrode material made by Method A2 at various carbonization temperatures of (a) 500°C, (b) 600°C, and (c) 700°C.....	66
4.24 Complex-plane impedance spectra of electrochemical capacitors with electrode material made by Method B1 at various carbonization temperatures of (a) 500°C, (b) 600°C, and (c) 700°C.....	66
4.25 Complex-plane impedance spectra of electrochemical capacitors with electrode material made by Method B2 at various carbonization temperatures of (a) 500°C, (b) 600°C, and (c) 700°C.....	67
4.26 Complex-plane impedance spectra of electrochemical capacitors with electrode material made by the unsupported TiO ₂ (TiO ₂ 100%) at various calcination temperatures of (a) 500°C, (b) 600°C, and (c) 700°C.....	67
4.27 XRD patterns of TiO ₂ /C composites prepared by Method A1 at the carbonization temperature of 500°C at (a) 10%, (b) 20%, (c) 30%, and (d) 40% TiO ₂ contents in the composites.....	71

Figure	Page
4.28 XRD patterns of TiO ₂ /C composites prepared by Method A2 at the carbonization temperature of 500°C at (a) 10%, (b) 20%, (c) 30%, and (d) 40% TiO ₂ contents in the composites.....	71
4.29 XRD patterns of TiO ₂ /C composites prepared by Method B1 at the carbonization temperature of 500°C at (a) 10%, (b) 20%, (c) 30%, and (d) 40% TiO ₂ contents in the composites.....	72
4.30 XRD patterns of TiO ₂ /AC composites prepared by Method B2 at the carbonization temperature of 500°C at (a) 10%, (b) 20%, (c) 30%, and (d) 40% TiO ₂ contents in the composites.....	72
4.31 The N ₂ adsorption isotherms of TiO ₂ /C composites prepared by Method A1 at the carbonization temperature of 500°C at 10%, 20%, 30%, and 40% TiO ₂ contents in the composites.....	74
4.32 The N ₂ adsorption isotherms of TiO ₂ /C composites prepared by Method A2 at the carbonization temperature of 500°C at 10%, 20%, 30%, and 40% TiO ₂ contents in the composites.....	74
4.33 The N ₂ adsorption isotherms of TiO ₂ /C composites prepared by Method B1 at the carbonization temperature of 500°C at 10%, 20%, 30%, and 40% TiO ₂ contents in the composites.....	75
4.34 The N ₂ adsorption isotherms of TiO ₂ /AC composites prepared by Method B2 at the carbonization temperature of 500°C at 10%, 20%, 30%, and 40% TiO ₂ contents in the composites.....	75
4.35 SEM images of TiO ₂ /C composites prepared by Method A1 at the carbonization temperature of 500°C at (a) 10%, (b) 20%, (c) 30%, and (d) 40% TiO ₂ contents in the composites with magnification of 10,000x-40,000x, respectively.....	78
4.36 SEM images of TiO ₂ /C composites prepared by Method A2 at the carbonization temperature of 500°C at (a) 10%, (b) 20%, (c) 30%, and (d) 40% TiO ₂ contents in the composites with magnification of 10,000x.....	78

Figure	Page
4.37 SEM images of TiO ₂ /C composites prepared by Method B1 at the carbonization temperature of 500°C at (a) 10%, (b) 20%, (c) 30%, and (d) 40% TiO ₂ contents in the composites with magnification of 10,000x.....	79
4.38 SEM images of TiO ₂ /AC composites prepared by Method B2 at the carbonization temperature of 500°C at (a) 10%, (b) 20%, (c) 30%, and (d) 40% TiO ₂ contents in the composites with magnification of 10,000x.....	79
4.39 Cyclic voltammograms of TiO ₂ /C composites electrode prepared by Method A1 at carbonization temperature of 500°C at (a) 10%, (b) 20%, (c) 30%, and (d) 40% TiO ₂ contents in the composites in 1 M H ₂ SO ₄	81
4.40 Cyclic voltammograms of TiO ₂ /C composites electrode prepared by Method A2 at carbonization temperature of 500°C at (a) 10%, (b) 20%, (c) 30%, and (d) 40% TiO ₂ contents in the composites in 1 M H ₂ SO ₄	82
4.41 Cyclic voltammograms of TiO ₂ /C composites electrode prepared by Method B1 at carbonization temperature of 500°C at (a) 10%, (b) 20%, (c) 30%, and (d) 40% TiO ₂ contents in the composites in 1 M H ₂ SO ₄	83
4.42 Cyclic voltammograms of TiO ₂ /AC composites electrode prepared by Method B2 at carbonization temperature of 500°C at (a) 10%, (b) 20%, (c) 30%, and (d) 40% TiO ₂ contents in the composites in 1 M H ₂ SO ₄	84
4.43 Complex-plane impedance spectra of electrochemical capacitors with electrode material made by Method A1 at the carbonization temperature of 500°C at (a) 10%, (b) 20%, (c) 30%, and (d) 40% TiO ₂ contents in the composites.....	87
4.44 Complex-plane impedance spectra of electrochemical capacitors with electrode material made by Method A2 at the carbonization temperature of 500°C at (a) 10%, (b) 20%, (c) 30%, and (d) 40% TiO ₂ contents in the composites.....	87

Figure	Page
4.45 Complex-plane impedance spectra of electrochemical capacitors with electrode material made by Method B1 at the carbonization temperature of 500°C at (a) 10%, (b) 20%, (c) 30%, and (d) 40% TiO ₂ contents in the composites.....	88
4.46 Complex-plane impedance spectra of electrochemical capacitors with electrode material made by Method B2 at the carbonization temperature of 500°C at (a) 10%, (b) 20%, (c) 30%, and (d) 40% TiO ₂ contents in the composites.....	88
C-1 MP pore-size distribution of the TiO ₂ /C composite.....	106

LIST OF SCHEMES

Scheme	Page
3.1 A heating program of the preparation of activated carbon.....	36
3.2 Schematic diagram of the preparation of activated carbon.....	36
3.3 Schematic diagram of the synthesis procedure for Method A.....	38
3.4 Schematic diagram of the synthesis procedure for Method B.....	39
3.5 Schematic diagram of the preparation of the sample electrodes.....	40

LIST OF ABBREVIATIONS

C	Carbon
AC	Activated Carbon
TTIP	Titanium Tetraisopropoxide
PVDF	Polyvinylidene Fluoride
BET	Brunauer- Emmett-Teller
XRD	X-ray Diffraction
SEM	Scanning Electron Microscopy
CV	Cyclic Voltammetry
EIS	Electrochemical Impedance Spectroscopy
EDLC	Electrical Double Layer Capacitor
°C	degree Celsius
%	percent
cps	counts per second
g	gram (s)
mg	milligram (s)
ml	milliliter (s)
M	molar
h	hour (s)
min	minute (s)
s	second (s)
µm	micrometer
nm	nanometer
Å	Angstrom
<i>C</i>	the Capacitance
F	Farad
E	potential
V	Volt
<i>i</i>	current
A	Ampere
Hz	Hertz
Ag/AgCl	Silver/Silver Chloride Reference Electrode

RE	Reference Electrode
WE	Working Electrode
CPE	Constant Phase Element
Z	Impedance
R_p	Polarization Resistance or Charge Transfer Resistance
R_s	Solution Resistance
W	Warburg impedance

CHAPTER I

INTRODUCTION

1.1 Background

Biomass, as a renewable energy source, refers to living and recently dead biological material that can be used as fuel or for industrial production. In this context, biomass refers to plant matter grown to generate electricity or produce biofuel, and it also includes plant or animal matter used for production of fibers, chemicals or heat. Plant biomass is a natural renewable resource that can be converted into useful materials and energy [1]. The idea of using bamboo biomass to produce activated carbon rises in this context. In several countries in Asia including Thailand there is plenty of bamboo based chopsticks disposed as waste and it is worth converting such biomass towards the valued added material like TiO₂/carbon composite. The composite can be applied further as electrode material in electrochemistry, and as photocatalyst. In this work we report a novel method for preparation of the TiO₂/carbon nanocomposite with high thermal stability using bamboo chopsticks as carbon source for further application in an electric double layer capacitor.

In the last decade, the preparation of activated carbons from several agricultural by-products has been studied because of their availability at a low price. Researchers have studied the production of activated carbon from coconut shell [2], teak sawdust [3], rice husks [4], corn cobs [5], palm-tree cobs [6], plum kernels [7], cassava peel [8], bagasse [9], olive stones [10], date pits [11], fruit stones and nutshells [12]. The advantage of using agricultural by-products as raw materials for manufacturing activated carbon is that these raw materials are renewable and potentially less expensive to manufacture.

Bamboo is a grass, the most diverse group of plants in the grass family. It belongs to the sub-family Bambusoideae of the family Poaceae. It is an enduring, versatile, and highly renewable material, one that people and communities have known and utilized for thousands of years. Bamboo is the fastest growing woody plant

in the world. Their growth rate up to 1.2 meters/day is due to a unique rhizome-dependent system, but is highly dependent on local soil and climate conditions. There are more than 70 genera divided into about 1,000 species of bamboo. They are found in diverse climates, from cold mountains to hot tropical regions. They are of economic and high cultural significance in East Asia and South East Asia where they are used extensively in gardens, as a building material, furniture, chopsticks, and as a food source. Bamboo is an abundant natural resource in Thailand because it takes only several months to grow up. It has been traditionally used to construct various living facilities and tools [13]. Bamboo has been used as the structural material for steps at construction sites in China, Japan, Malaysia, Thailand and other countries because it is a strong, tough and low-cost material. Conversion of bamboo waste to a value-added product such as activated carbon will help to solve part of the problem of waste in Thailand. The bamboo chopsticks were used as a representative of bamboo waste.

Titanium dioxide (TiO_2) is generally chemically and biologically inert, photoactive and inexpensive, which are the underlying reasons for the fact that this material is probably one of the most extensively used photocatalytic supports for solving environmental problems, especially in what concerns the purification of wastewater [14-16]. TiO_2 is one of the important photocatalysts, especially for the detoxification of water and air because of its high activity, chemical stability, and robustness against photocorrosion, low toxicity and availability at low cost [17]. Many works were focused on the preparation as well as on the modification of TiO_2 [18-20] and some composites of $\text{SiO}_2/\text{TiO}_2$, $\text{ZrO}_2/\text{TiO}_2$ were also proposed [21-22]. A variety of methodologies for synthesizing nanosized TiO_2 have been investigated such as oxidation of titanium tetrachloride in a modified diffusion flame reactor [23], crystallization in reverse micelles [24-25] or in supercritical CO_2 [26], photoassisted sol-gel method [27], polymer templating method [28], and hydrothermal method [29,30]. The most widely used methods to synthesize titania composite nanoparticles are sol-gel method [31-32], co-precipitation [33] and chemical vapor deposition [34]. Some papers reported on preparation of the composites between TiO_2 and carbon [35-37]. It was confirmed that the introduction of active carbon to titania slurry could increase decomposition of some organic compounds in the photocatalytic process [38].

Carbon is a good support for preparing of metal oxide because it is inert in most reaction conditions and the metal precursor can easily be reduced to metal by carbon during the preparation. It provides high dispersion and inhibits sintering of metal

within its small pore structure. Porous materials of metal oxides with high surface areas have been attracting great attention regarding catalysts, sensors, batteries and electrochemical double layer capacitors. As nanosized TiO_2 and related compounds show interesting catalytic or dielectric properties, they have been widely studied as to the preparation of materials with high surface areas for electrodes. Many papers have been published on the modification of titanium dioxide by carbon. Carbon and titanium dioxide can form different composites. Preparation of TiO_2 loaded activated carbon was also reported such as carbonization of *n*-hexane deposited on TiO_2 [39], deposition of anatase on the surface of activated carbon [40], TiO_2 -coated active carbon composites with increased photocatalytic activity prepared by a properly controlled sol-gel method [41], synthesis of anatase TiO_2 supported on porous solids by chemical vapor deposition [42].

Although there are many studies in the literature relating to the preparation and characterization of TiO_2 /carbon as mentioned before, however, there is no information for the preparation of the TiO_2 /carbon nanocomposite using bamboo as the precursor by the novel method for further application in an electric double layer capacitor.

Electrical double-layer capacitor (EDLC) is an electrochemical energy storage device in which electric charges only accumulated by a pure electrostatic attraction force are stored on the electrolyte-electrode interface in a form of double layer and separated by the electrolyte. EDLC are used as power sources for camera flash equipment, lasers and as back-up power sources for computer memory [43]. The energy-storage in a supercapacitor is achieved either by Faradaic or non-Faradaic processes at the electrode-electrolyte interface. Since the reversibility of the double layer process at the surface of an electroactive material determines the capacitive performance, a high surface area is a key factor in achieving a high-capacitance.

The electric double layer capacitor using activated carbon as an electrode has been recognized as an efficient high power energy device in electric power storage because of its better rate capability and longer cycle life compared to secondary batteries [44]. Recently, new applications using such a performance have been attempted as an energy storage device for an electric vehicle or a pulse-current supply. In order to meet the needs of these new applications, it is necessary for the activated carbon to have a higher energy density per weight or volume than a conventional one. In the past years, many works have been focused on the application of activated carbons as the electrode material of double-layer capacitors because of their

accessibility, an easy processability and relatively low cost. It has been proven that activated carbon is able to perform in a wide range of temperatures due to its excellent stability against the electrolyte chemistry. Apart from these, activated carbon materials are environmentally friendly. Taking into account all the mentioned characteristics, activated carbon as a material for the storage of energy in electrochemical capacitors seems to be extremely attractive

Generally, activated carbon based capacitors have relatively low capacitance, which could limit their practical application. Some researcher reported that capacitance of the activated carbon based capacitors linearly enhanced with the surface area of activated carbon; many researchers have worked on increasing the surface area of activated carbon as an approach toward high capacitance [45]. It has been known that activated carbon electrode is rather polarizable and the resulted polarization adversely affect performance of the capacitors because polarization may reduce accumulation of the ions on double-layer. Therefore, reducing polarization of activated carbon has been considered to be an effective approach toward the improved capacitance of the double layer capacitors. It has been reported [46] that charges on the surface of TiO_2 are more than the other regions due to the attractive contribution of the positively charged depletion region. Based on this fact, we consider that the polarization of activated carbon can be reduced by incorporation of nanosized TiO_2 on the activated carbon surface. By this means, ion concentration on the double layer of activated carbon could be increased.

Some of the prominent studies and the modified TiO_2 are reviewed below.

N. Tatsuda et al. [47] investigated the penetration of titanium tetraisopropoxide (TTIP) dissolved in supercritical CO_2 into the nano-spaces of an activated carbon for the preparation of a TiO_2 -coated activated carbon. The conversion of TTIP to TiO_2 through thermal decomposition was confirmed by evolved gas analysis during heat treatment under a N_2 flow. Acetone was detected in the evolved gas, which suggested that some isopropoxide groups in TTIP reacted with the carbonyl groups on the activated carbon surface. This chemical reaction with carbon is expected to be advantageous for favorable attachment to the carbon surface. The crystallite size of anatase in the TiO_2 /carbon composites was 4.1 nm. As the size of the crystallite prepared by bulk condensation of TTIP was more than 15 nm, these results confirmed that the anatase crystals were present in the carbon pores. Also, it was suggested that the crystal growth of TiO_2 was influenced by the carbon nano-spaces.

S.X. Liu et al. [48] prepared a TiO₂/AC photocatalyst with high activity and easy separation using a hydrothermal method. Phenol, methyl orange (MO) and Cr(VI) were used as target pollutants to test the activity and decantability. Results showed that the activated carbon composite exhibited a significant effect on the TiO₂ activity. With suitable activated carbon content, the TiO₂/xAC catalysts prepared were much more active. The TiO₂/5AC catalyst exhibited easy separation and less deactivation after several runs, and was less sensitive to pH changes. UV/DRS revealed that no electronic bandgap change in TiO₂ occurred on addition of the activated carbon. SEM and XRD results suggest that better TiO₂ distribution was able to be achieved when optimal activated carbon content was used. A Ti–O–C bond was formed and a slight conjugation effect appeared between the activated carbon bulk and TiO₂. The advantages of the obtained TiO₂/5AC catalyst revealed its great practical potential in wastewater treatment.

A.H. El-Sheikh et al. [40] reported that titanium dioxide was deposited on the surface of active carbon. Three different techniques were used: chemical vapour deposition (CVD), direct air-hydrolysis (DAH) and high-temperature impregnation (HTI) techniques. The effect of each deposition procedure on surface area, porosity and thermal stability of the sample was studied by nitrogen adsorption, mercury intrusion, methylene blue (MB) adsorption and thermal gravimetric analysis. There was significant reduction, which may be due to TiO₂ deposition, in porosity and surface area. The reduction in MB adsorption was proportional to anatase TiO₂ but not to the total TiO₂ deposited. Chemical vapour deposition gave more anatase TiO₂ than the direct air-hydrolysis technique, which is thought to form the deposit within the micro-meso pores, and caused more porosity-surface area reduction. TiO₂ particles inside the pores have more opportunity to crystallize into the anatase form. The deposited layer of TiO₂ apparently catalyzed slight weight loss at low temperatures but generally gave more thermal stability for the support. Non-activated carbon was used and its thermal stability, porosity and surface area were not affected by TiO₂ deposition. The deposition, in non-activated carbon, is thought to occur on external surface, which may be due to absence of large micropores.

Z. Li et al. [49] prepared titania–silica composite nanoparticles by sol–gel-hydrothermal and sol–gel routes, respectively, and their physicochemical and photocatalytic properties were compared. The results of XRD, TEM and BET surface areas showed that sol–gel-hydrothermal route led to anatase titania–silica composite

nanoparticles with large specific surface area, but the sol–gel route tended to form mixture of anatase and rutile. The composite nanoparticles prepared by sol–gel-hydrothermal route had better thermal stability against phase transformation from anatase to rutile, agglomeration and particle growth than those prepared by sol–gel route. On the basis of XRD, FT-IR, XPS and NMR, a strong interaction was found between SiO_2 and TiO_2 , and Ti–O–Si bonds formed during both the two routes. But more Ti–O–Si bonds formed in the composite nanoparticles prepared by sol–gel-hydrothermal route than those prepared by sol–gel route. As a result, the titania–silica composite nanoparticles prepared by sol–gel-hydrothermal route exhibited higher photocatalytic activity in decomposition of methylene blue than that prepared by sol–gel route, and it had excellent photocatalytic activity even after calcined at 1000°C .

B. Jiang et al. [50] described the size-controlled synthesis of anatase TiO_2 nanoparticles by using metatitanic acid as a starting material and in the presence of carboxylic acid group-containing organics as modifiers. The average particle sizes and particle size distributions of the resulting anatase TiO_2 nanoparticles were significantly affected by the chemical structures of the organic modifiers. The presence of nonpolar group-containing carboxylic acids was beneficial to formation of small-sized and narrow size-distributed anatase TiO_2 nanoparticles.

L. Kőrösi and I. Dékány [51] prepared a series of high surface area titanium dioxide samples (P- TiO_2) with varying phosphate content by the sol–gel technique. The structural properties of the P- TiO_2 samples significantly changed with the phosphate content and calcination temperature. According to XRD data the presence of phosphate shifts the anatase rutile phase transition to higher temperatures, revealing that phosphate improves the thermal stability of the samples. The specific surface area and the semiconductor band gap energy increase with the phosphate content.

W. Qiao et al. [52] reported that coconut shell-based activated carbon was oxidized in aq. H_2SO_4 , HNO_3 and H_2O_2 to induce surface oxygen functional groups on its surface and to increase the mechanical strength of the resultant activated carbon artifact with PVB as a binder. Although the oxidation was confirmed to significantly increase the mechanical strength of activated carbon, aq. H_2O_2 was found to be the most effective, giving strength as high as 6000 kPa, which is believed to be sufficient for the electrode of an electric double layer capacitor (EDLC). The increase of CO_2 evolving groups induced on the surface of activated carbon appears to be

responsible for the increase in mechanical strength. There was an optimum extent of oxidation for the strength as well as the performance of the electrode. Too much oxidation reduces the electrical conductivity of the activated carbon. Facile oxidation by aq. H_2O_2 can be recommended as a practical modification of the surface since it takes place safely below 100°C without releasing any harmful gas.

M.S. Dandekar et al. [53] reported about the specific capacitance (F/g) of a composite electrode consisting of activated coconut-shell carbon and hydrous ruthenium oxide. The composite electrode shows an enhanced specific capacitance of 250 F/g in 1 M H_2SO_4 with 9 wt% ruthenium incorporated. Chemical and structural characterization of the composites reveals a homogeneous distribution of amorphous $\text{RuO}_x(\text{OH})_y$ throughout the porous network of the activated carbon. Electrochemical characterization indicates an almost linear dependence of capacitance on the amount of ruthenium owing to its pseudocapacitive nature.

H. Liang et al. [54] studied the energy storage of activated carbon modified with a semiconducting oxide TiO_2 . The composite was prepared by mixing nanosize TiO_2 and activated carbon through a means of ultrasonic vibration in ethanol solution for 30 min. It was found that with modification of TiO_2 , the specific capacitance of activated carbon measured at 0.65 mA/cm^2 was increased from 47.2 to 63.1 F/g. This method is unique in comparison the conventional method because it uses semiconducting TiO_2 other than electrochemically active materials such as RuO_2 . The later has been adopted to make electrochemical-double-layer hybrid supercapacitors, however, the former is attributed to a pure double-layer supercapacitor.

G.-h. Yuan et al. [55] reported that some nanometer-scale amorphous particles of nickel oxide were loaded into activated-carbon by suspending the activated-carbon in a $\text{Ni}(\text{NO}_3)_2$ solution followed by neutralization. A hybrid type electrochemical capacitor was made and tested, in which the activated-carbon loaded with nickel oxide was used as cathode material and activated-carbon was used as anode material. Although the BET surface area of the activated-carbon decreased upon nickel oxide loading compared to that of the starting material, its specific capacitance increased 10.84%, from 175.40 to 194.01 F/g and the potential of oxygen evolution on the composite material electrode was 0.076 V higher than that of the pure activated-carbon electrode, in the electrolyte of 6 mol/l KOH solution, so the hybrid capacitor had larger energy density. Similar to the pure activated-carbon electrode, no obvious

change appears on the specific capacitances of the composite material electrode at various discharge currents and the composite material electrode exhibiting good power characteristics.

In this work, we presented a novel process for fabrication of activated carbon semiconducting oxide composites and evaluated such composites as an electrode material of the double layer capacitors. The disposed bamboo chopsticks were employed as the carbon source in preparation of a composite of titanium dioxide and carbon for application in a capacitor because of plenty of bamboo chopsticks waste from restaurant in Thailand. A proposed preparation method contains 2 steps which are impregnation of the bamboo powder with a solution of titanium tetraisopropoxide in 2-propanol and subsequently carbonization at a required temperature. The carbonization temperatures were varied from 500 to 700°C and study the effect of TiO₂ content in the composite to enhance the specific capacitance value of the composite electrodes.

1.2 Objective

In this work we report a novel method for preparation of the TiO₂/carbon nanocomposite with high thermal stability using bamboo chopsticks as carbon source for further application in an electric double layer capacitor.

1.3 Scopes of This Work

1. Preparation of the porous carbon from bamboo waste.
2. Preparation and investigation of TiO₂/carbon nanocomposite from different methods and study the effect of carbonization temperature on formation of anatase structure.
3. Preparation of the TiO₂/carbon nanocomposite as electrode materials for electric double layer capacitors and study the effect of TiO₂ content in the composite to enhance the capacitive performance of the composite electrodes.

CHAPTER II

THEORY

2.1 Carbon

Carbon is used extensively in one form or another in a variety of electrochemical systems. Carbon is selected for many electrochemical applications because of its good electrical and thermal conductivities, low density, adequate corrosion resistance, low thermal expansion, low elasticity, and high purity. In addition, carbon material can be produced in a variety of structures, such as powders, fibers, large blocks, and thin solid and porous sheets. Furthermore, carbon materials are readily available and generally low-cost. In particular, renewed interest in carbon for use in electrode material for fabricating supercapacitor electrodes has emerged.

Different types of specially-designed electrode materials have been intensely investigated in the past decade for fabricating supercapacitor electrodes. Some of the well-known materials include carbon nanotubes (CNTs) [56-58], carbon aerogels [59], activated carbon [60, 61], and conducting polymer-based nanocomposites [62, 63]. Although CNTs are potential candidates for supercapacitors, commercial application is yet to be realized because of difficulties in mass production and purification. Furthermore, the properties of CNTs depend on their prehistory and hence their reproducibility is difficult with respect to their diameter and conductivity distribution. Carbon aerogels can also be used as electrode materials for supercapacitors, but the critical drying step involved in the synthesis of this material is hazardous and expensive for practical application. A comparison of these different materials shows that activated carbon is one of the most promising materials for fabricating supercapacitors, because of its low cost, inherent high surface area, structural stability, and electrochemical inertness within a wide potential window (up to 1 V in aqueous and 3.5 V in non-aqueous media) [54,64].

Generally, activated carbon based capacitors have relatively low capacitance, which could limit their practical application. Since Watanabe [65] reported that capacitance of the activated carbon based capacitors linearly enhanced with

the surface area of activated carbon, many researchers have worked on increasing the surface area of activated carbon as an approach toward high capacitance. Activated carbons can be produced from carbonaceous materials, such as wood, sawdust, coconut shells, anthracite, bituminous coal, etc., by physical or chemical activation. Activated carbons are high surface area, high porosity carbons that are produced by two principal methods.

1. Physical activation

Physical activation involves heating a previously charred material at high temperature using oxidants such as steam [66], carbon dioxide [67]. Physical activation is generally carried out at elevated temperatures between 750 and 1100°C.

2. Chemical activation

Chemical activation involves heating a mixture of the raw material and a dehydrating agent to temperatures from 200 to 650°C. After carbonization the dehydrating agent is leached out and reused. The three dehydrating agents that are most commonly used are H_3PO_4 [68], $ZnCl_2$ [9], and H_2SO_4 .

The specific capacitance of activated carbon is promoted by mixing it with various metal oxides, which causes a significant improvement in intra and inter-particle electronic conduction. The supercapacitive behaviour of several transition metal oxides, such as RuO_2 [69], NiO_x [70] and manganese oxide [71] has already been evaluated. Based on this fact, we consider that the polarization of active carbon can be reduced by modifying activated carbon with semiconducting TiO_2 , especially these with nanosize. By this means, ion concentration on the double-layer of activated carbon could be increased.

2.2 Titanium Dioxide

Inorganic n-type semiconductor titanium dioxide (TiO_2) particles have good biocompatibility, stability and environmental safety. Titanium dioxide has been widely used in many areas such as the paint industry, biomedicine, electronics and environmental engineering. Titanium dioxide nanocrystallites can be used as a photocatalyst for the degradation of a variety of toxic chemicals and as a promising electrode material in dye-sensitized solar cells. The crystal structures, morphology and chemical species on the surface that are derived from the starting materials play important roles in the photophysical and photochemical performances of the nanocrystallites. It is found that photoelectron transfer at the interface between

TiO₂ nanocrystallites and substrates is strongly affected by the crystal surface and surface morphology. For comparison of the characteristics of phase-pure TiO₂ nanocrystallites with comparable morphology, facile and novel syntheses of nano-sized anatase and rutile TiO₂ are worth investigation [72].

Titanium dioxide was first produced commercially in 1923 and accounts for approximately 70% of the total volume of pigment production. Relatively small quantities of titanium dioxide are used for non-pigmentary purposes. In 2004, worldwide production of titanium dioxide was 4.4 million tonnes. Titanium dioxide is obtained from a variety of ores that contain ilmenite, rutile, anatase and leucoxene, which are mined from deposits located throughout the world. The primary particles are typically between 0.2 and 0.3 μm in diameter, although larger aggregates and agglomerates are formed. Ultrafine grades of titanium dioxide have a primary particle size of 10–50 nm and are used predominantly as ultraviolet blockers in sunscreens and plastics, and in catalysts. Most commercial titanium dioxide products are coated with inorganic (e.g. alumina, zirconia, silica) and organic (e.g. polyols, esters, siloxanes, silanes) compounds to control and improve surface properties.

2.3 Structure of Titanium Dioxide [73]

Titanium dioxide (TiO₂) has three most commonly encountered crystalline polymorphs: anatase, brookite, and rutile. All the three crystal structures are made up of distorted TiO₆ octahedra, but in different ways. Rutile adopts a tetragonal structure, in which two opposing edges of each octahedron are shared to form linear chains along the [001] direction and the TiO₆ chains are then linked together via corner connection. Anatase (tetragonal) has no corner sharing but has four edges shared per octahedron. The crystal structure of anatase can be viewed as zigzag chains of the octahedral linked together through edge sharing.

As for brookite (orthorhombic), the octahedra share three edges and also corners, and the dominant structural feature is a chain of edge sharing: the distorted TiO₆ octahedra are arranged parallel to the c-axis and are cross-linked by shared edges. The crystal built-up (in terms of the number of shared edges) and some known physical properties of brookite seem to go between those of anatase and rutile. For example the refractive index of anatase, brookite, and rutile increases in the order 2.52, 2.63, and 2.72, while the theoretical density 3.84, 4.11, and 4.26 g/cm³.

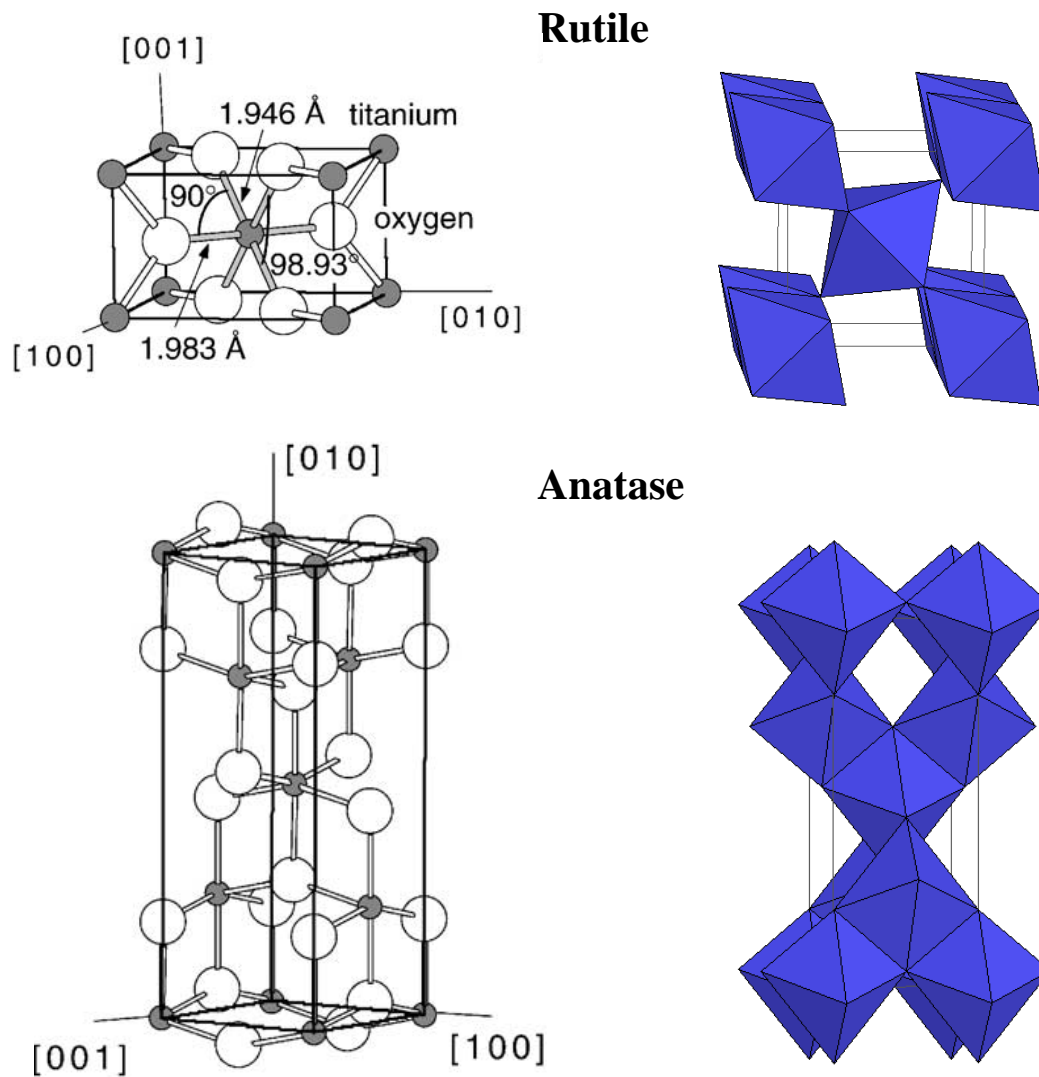


Figure 2.1 The crystal structures of rutile and anatase. The tetragonal unit cell of rutile has the dimension, $a = b = 4.587 \text{ \AA}$, $c = 2.953 \text{ \AA}$, and the one of anatase $a = b = 3.782 \text{ \AA}$, $c = 9.502 \text{ \AA}$. In both structures, slightly distorted octahedral are the basic building units. The bond lengths and angles of the octahedrally coordinated Ti atoms are indicated and the stacking of the octahedral in both structures is shown on the right side.

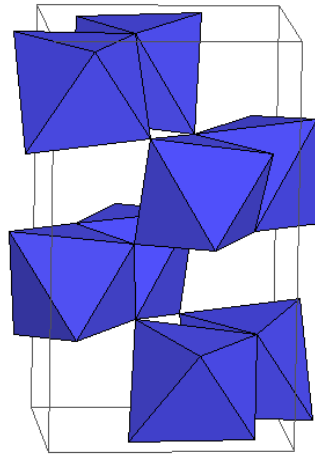
**Brookite**

Figure 2.2 The crystal structure of brookite. The orthorhombic unit cell of brookite has the dimension, $a = 9.184 \text{ \AA}$, $b = 5.447 \text{ \AA}$, $c = 5.145 \text{ \AA}$.

2.4 Synthesis Methods for Titanium Dioxide Nanostructures [74]

2.4.1 Sol-Gel Method

The sol-gel method is a versatile process used in making various ceramic materials. In a typical sol-gel process, a colloidal suspension, or a sol, is formed from the hydrolysis and polymerization reactions of the precursors, which are usually inorganic metal salts or metal organic compounds such as metal alkoxides. Complete polymerization and loss of solvent leads to the transition from the liquid sol into a solid gel phase. Thin films can be produced on a piece of substrate by spin-coating or dip-coating. A wet gel will form when the sol is cast into a mold, and the wet gel is converted into a dense ceramic with further drying and heat treatment. A highly porous and extremely low-density material called an aerogel is obtained if the solvent in a wet gel is removed under a supercritical condition. Ceramic fibers can be drawn from the sol when the viscosity of a sol is adjusted into a proper viscosity range. Ultrafine and uniform ceramic powders are formed by precipitation, spray pyrolysis, or emulsion techniques. Under proper conditions, nanomaterials can be obtained.

2.4.2 Hydrothermal Method

Hydrothermal synthesis is normally conducted in steel pressure vessels called autoclaves with or without Teflon liners under controlled temperature and/or pressure

with the reaction in aqueous solutions. The temperature can be elevated above the boiling point of water, reaching the pressure of vapor saturation. The temperature and the amount of solution added to the autoclave largely determine the internal pressure produced. It is a method that is widely used for the production of small particles in the ceramics industry. Many groups have used the hydrothermal method to prepare TiO₂ nanoparticles.

2.4.3 Solvothermal Method

The solvothermal method is almost identical to the hydrothermal method except that the solvent used here is nonaqueous. However, the temperature can be elevated much higher than that in hydrothermal method, since a variety of organic solvents with high boiling points can be chosen. The solvothermal method normally has better control than hydrothermal methods of the size and shape distributions and the crystallinity of the TiO₂ nanoparticles. The solvothermal method has been found to be a versatile method for the synthesis of a variety of nanoparticles with narrow size distribution and dispersity. The solvothermal method has been employed to synthesize TiO₂ nanoparticles and nanorods with/without the aid of surfactants.

2.4.4 Chemical Vapor Deposition

Vapor deposition refers to any process in which materials in a vapor state are condensed to form a solid-phase material. These processes are normally used to form coatings to alter the mechanical, electrical, thermal, optical, corrosion resistance, and wear resistance properties of various substrates. They are also used to form free-standing bodies, films, and fibers and to infiltrate fabric to form composite materials. Recently, they have been widely explored to fabricate various nanomaterials. Vapor deposition processes usually take place within a vacuum chamber. If no chemical reaction occurs, this process is called physical vapor deposition (PVD); otherwise, it is called chemical vapor deposition (CVD). In CVD processes, thermal energy heats the gases in the coating chamber and drives the deposition reaction.

2.4.5 Sonochemical Method

Ultrasound has been very useful in the synthesis of a wide range of nanostructured materials, including high-surfacearea transition metals, alloys,

carbides, oxides, and colloids. The chemical effects of ultrasound do not come from a direct interaction with molecular species. Instead, sonochemistry arises from acoustic cavitation: the formation, growth, and implosive collapse of bubbles in a liquid.

2.4.6 Microwave Method

A dielectric material can be processed with energy in the form of high-frequency electromagnetic waves. The principal frequencies of microwave heating are between 900 and 2,450 MHz. At lower microwave frequencies, conductive currents flowing within the material due to the movement of ionic constituents can transfer energy from the microwave field to the material. At higher frequencies, the energy absorption is primarily due to molecules with a permanent dipole which tend to reorientate under the influence of a microwave electric field. This reorientation loss mechanism originates from the inability of the polarization to follow extremely rapid reversals of the electric field, so the polarization phasor lags the applied electric field. This ensures that the resulting current density has a component in phase with the field, and therefore power is dissipated in the dielectric material. The major advantages of using microwaves for industrial processing are rapid heat transfer, and volumetric and selective heating.

2.4.7 TiO₂ Aerogels

The study of TiO₂ aerogels is worthy of special mention. The combination of sol-gel processing with supercritical drying offers the synthesis of TiO₂ aerogels with morphological and chemical properties that are not easily achieved by other preparation methods with high surface area.

2.5 Modifications of Titanium Dioxide Nanomaterials

Many applications of TiO₂ nanomaterials are closely related to its optical properties. However, the highly efficient use of TiO₂ nanomaterials is sometimes prevented by its wide band gap. The band gap of bulk TiO₂ lies in the UV regime (3.0 eV for the rutile phase and 3.2 eV for the anatase phase). Thus, one of the goals for improvement of the performance of TiO₂ nanomaterials is to increase their optical activity by shifting the onset of the response from the UV to the visible region.

There are several ways to achieve this goal. First, doping TiO₂ nanomaterials with other elements can narrow the electronic properties and, thus, alter the optical properties of TiO₂ nanomaterials. Second, sensitizing TiO₂ with other colorful inorganic or organic compounds can improve its optical activity in the visible light region. Third, coupling collective oscillations of the electrons in the conduction band of metal nanoparticle surfaces to those in the conduction band of TiO₂ nanomaterials in metal-TiO₂ nanocomposites can improve the performance. In addition, the modification of the TiO₂ nanomaterials surface with other semiconductors can alter the charge-transfer properties between TiO₂ and the surrounding environment, thus improving the performance of TiO₂ nanomaterials-based devices.

2.5.1 Metal-Doped TiO₂ Nanomaterials

Different metals have been doped into TiO₂ nanomaterials. The preparation methods of metal-doped TiO₂ nanomaterials can be divided into three types: wet chemistry, high temperature treatment, and ion implantation on TiO₂ nanomaterials. Wet chemistry methods usually involve hydrolysis of a titanium precursor in a mixture of water and other reagents, followed by heating.

Li et al. [75] developed La³⁺ doped TiO₂ by the sol-gel process and found that the lanthanum doping could inhibit the phase transformation of TiO₂, enhance the thermal stability of the TiO₂, reduce the crystallite size, and increase the Ti³⁺ content on the surface. Nagaveni et al. [76] prepared W, V, Ce, Zr, Fe, and Cu ion-doped anatase TiO₂ nanoparticles by a solution combustion method and found that the solid solution formation was limited to a narrow range of concentrations of the dopant ions.

2.5.2 Nonmetal-Doped TiO₂ Nanomaterials

Various nonmetal elements, such as B, C, N, F, S, Cl, and Br, have been successfully doped into TiO₂ nanomaterials. C-doped TiO₂ nanomaterials have been obtained by heating titanium carbide [77] or by direct burning of a titanium metal sheet in a natural gas flame [78].

2.6 Applications of TiO₂ Nanomaterials

The existing and promising applications of TiO₂ nanomaterials include paint, toothpaste, UV protection, photocatalysis, photovoltaics and sensing. TiO₂ nanomaterials normally have electronic band gaps larger than 3.0 eV and high absorption in the UV region. TiO₂ nanomaterials are very stable, nontoxic, and cheap. Their optical and biologically benign properties allow them to be suitable for UV protection applications.

2.6.1 Photocatalytic Applications

TiO₂ is regarded as the most efficient and environmentally benign photocatalyst, and it has been most widely used for photodegradation of various pollutants. The photocatalytic reaction mechanisms are widely studied. The principle of the semiconductor photocatalytic reaction is straightforward. Upon absorption of photons with energy larger than the band gap of TiO₂, electrons are excited from the valence band to the conduction band, creating electron-hole pairs. These charge carriers migrate to the surface and react with the chemicals adsorbed on the surface to decompose these chemicals. This photodecomposition process usually involves one or more radicals or intermediate species such as •OH, O²⁻, H₂O₂, or O₂, which play important roles in the photocatalytic reaction mechanisms. The photocatalytic activity of a semiconductor is largely controlled by (i) the light absorption properties, e.g., light absorption spectrum and coefficient, (ii) reduction and oxidation rates on the surface by the electron and hole, (iii) and the electron-hole recombination rate. A large surface area with a constant surface density of adsorbents leads to faster surface photocatalytic reaction rates. In this sense, the larger the specific surface area, the higher the photocatalytic activity is. On the other hand, the surface is a defective site; therefore, the larger the surface area, the faster the recombination. The higher the crystallinity, the fewer the bulk defects, and the higher the photocatalytic activity are. Hightemperature treatment usually improves the crystallinity of TiO₂ nanomaterials, which in turn can induce the aggregation of small nanoparticles and decrease the surface area. Judging from the above general conclusions, the relation between the physical properties and the photocatalytic activities is complicated. Optimal conditions are sought by taking these considerations into account and may vary from case to case [79].

2.6.2 Photovoltaic Applications

Photovoltaics based on TiO₂ nanocrystalline electrodes have been widely studied. At the heart of the system is a nanocrystalline mesoporous TiO₂ film with a monolayer of the charge-transfer dye attached to its surface. The film is placed in contact with a redox electrolyte or an organic hole conductor. Photoexcitation of the dye injects an electron into the conduction band of TiO₂. The electron can be conducted to the outer circuit to drive the load and make electric power.

2.7 Faradaic and Nonfaradaic Processes [80]

Two types of processes occur at electrodes. One kind comprises reactions like those just discussed in which charges (e.g., electrons) are transferred across the metal-solution interface. Electron transfer caused oxidation or reduction to occur. Since such reactions are governed by Faraday's law (i.e., the amount of chemical reaction caused by the flow of current is proportional to the amount of electricity passed), they are called *faradaic processes*. Electrodes at which faradaic processes occur are sometimes called *charge-transfer electrodes*. Under some conditions, a given electrode-solution interface will show a range of potentials where no charge-transfer reactions occur because such reactions are thermodynamically or kinetically unfavorable. However, processes such as adsorption and desorption can occur, and the structure of the electrode-solution interface can change with charging potential or solution composition. These processes are called *nonfaradaic processes*. Although charge does not cross the interface, external currents can flow when the potential, electrode area, or solution composition changes. Both faradaic and nonfaradaic processes occur when electrode reaction take place. Although the faradaic processes are usually of primary interest in the investigation of an electrode reaction, the effects of the nonfaradaic processes must be taken into account in using electrochemical data to obtain information about the charge transfer and associated reactions.

2.8 Nonfaradaic Processes and the Nature of the Electrode-Solution Interface

2.8.1 The ideal Polarized Electrode

An electrode at which no charge transfer can occur across the metal-solution interface, regardless of the potential imposed by and outside source of voltage, is called an *ideal polarized* (or *ideal polarizable*) *electrode* (IPE). While no real

electrode can behave as an IPE over the whole potential range available in a solution, some electrode-solution systems can approach ideal polarizability over limited potential ranges.

2.8.2 Capacitance and Charge of an Electrode

Since charge cannot cross the IPE interface when the potential across it is changed, the behavior of the electrode-solution interface is analogous to that of a capacitor. A capacitor is an electrical circuit element composed of two metal sheets separated by a dielectric material (Figure 2.3a). Its behavior is governed by the equation

$$\frac{q}{E} = C$$

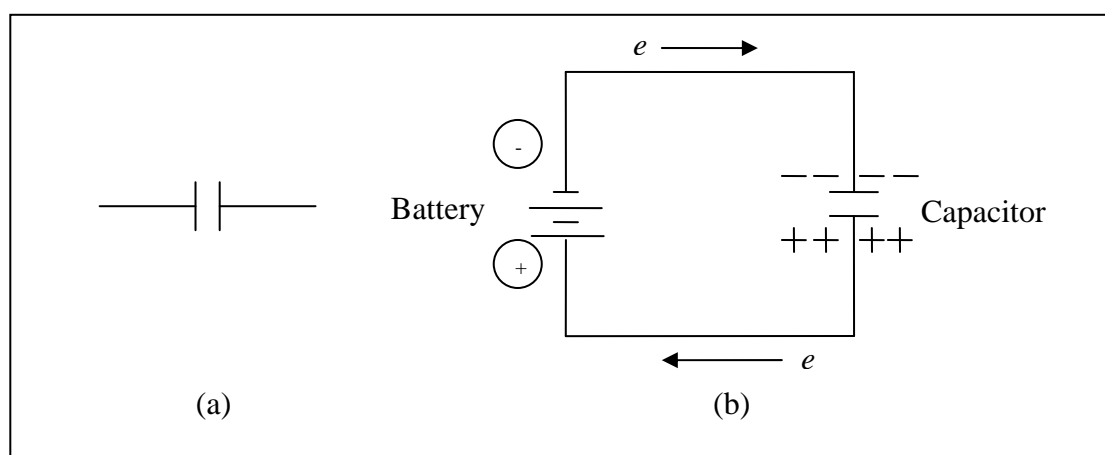


Figure 2.3 (a) A capacitor (b) Charging a capacitor with a battery [80].

where q is the charge stored on the capacitor (in coulombs, C), E is the potential across the capacitor (in Volts, V), and C is the capacitance (in farads, F). When a potential is applied across a capacitor, charge will accumulate on its metal plates until q satisfies equation. During this charging process, a current (called the *charging current*) will flow. The charge on the capacitor consists of an excess of electrons on one plate and a deficiency of electron on the other (Figure 2.3b).

2.9 Electric Double Layer Capacitors (EDCLs)

Electric double-layer capacitors, also known as supercapacitors, electrochemical double layer capacitors (EDLCs) or ultracapacitors are electrochemical capacitors that have an unusually high energy density when compared to common capacitors. Electric

double layer capacitors are attractive energy-storage devices, particularly for applications that involve high-power requirements, such as electric vehicles and hybrid electric vehicle systems [81]. In addition, electric double layer capacitors are used as power sources for camera flash equipment, lasers and as back-up power sources for computer memory.

In general, electric double layer capacitors improve storage density through the use of a nanoporous material, typically activated carbon, in place of the conventional insulating barrier. Activated carbon is a powder made up of extremely small and very "rough" particles, which in bulk form a low-density volume of particles with holes between them that resembles a sponge. The overall surface area of even a thin layer of such a material is many times greater than a traditional material like aluminum, allowing many more charge carriers (ions or radicals from the electrolyte) to be stored in any given volume. The downside is that the charcoal is taking the place of the improved insulators used in conventional devices. Activated carbon is not the "perfect" material for this application. The charge carriers are actually (in effect) quite large especially when surrounded by solvent molecules and are often larger than the holes left in the carbon, which are too small to accept them, limiting the storage. Recent research in electric double-layer capacitors has generally focused on improved materials that offer even higher usable surface areas. The specific capacitance of activated carbon is promoted by mixing it with various metal oxides, which causes a significant improvement in intra and inter-particle electronic conduction.

In the discussion of electron transfer reactions so far there has been no mention of the nature of the electrode/electrolyte interface. It is clear that any interface will disrupt the electrolyte solution since the interactions between the solid and the electrolyte will be considerably different to those in solution. For electrodes which are under potentiostatic control there will also be the additional influence of the charge held at the electrode. These different factors result in strong interactions occurring between the ions/molecules in solution and the electrode surface. This gives rise to a region called the electrical double layer. Many models have been put forward to explain the behaviour observed when electrochemical measurements are performed in electrolyte solutions.

2.10 Electrochemical Impedance Spectroscopy (EIS) [82]

Electrochemical Impedance Spectroscopy (EIS) is an experimental method of characterizing electrochemical systems. This technique measures the impedance of a system over a range of frequencies, and therefore the frequency response of the system, including the energy storage and dissipation properties, is revealed. Often, data obtained by EIS is expressed graphically in a Bode plot or a Nyquist plot. Impedance is the opposition to the flow of alternating current (AC) in a complex system. A passive complex electrical system comprises both energy dissipater (resistor) and energy storage (capacitor) elements. If the system is purely resistive, then the opposition to AC or direct current (DC) is simply resistance.

2.10.1 Definition of Impedance

Almost everyone knows about the concept of electrical resistance. It is the ability of a circuit element to resist the flow of electrical current. Ohm's law defines resistance in terms of the ratio between voltage E and current I .

$$R = \frac{E}{I}$$

An ideal resistor has several simplifying properties:

- 1) It follows Ohm's Law at all current and voltage levels.
- 2) It's resistance value is independent of frequency.
- 3) AC current and voltage signals through a resistor is in phase with each other.

The real world contains circuit elements that exhibit much more complex behavior. These elements force us to abandon the simple concept of resistance. In its place we use impedance, which is a more general circuit parameter. Like resistance, impedance is a measure of the ability of a circuit to resist the flow of electrical current. Unlike resistance, impedance is not limited by the simplifying properties listed above. Electrochemical impedance is usually measured by applying an AC potential to an electrochemical cell and measuring the current through the cell.

2.10.2 Electrical Circuit Elements

EIS data is commonly analyzed by fitting it to an equivalent electrical circuit model. Most of the circuit elements in the model are common electrical elements such as resistors, inductors, and capacitors. To be useful, the elements in the model should have a basis in the physical electrochemistry of the system. Table 2.1 lists the common circuit elements, the equation for their current versus voltage relationship, and their impedance.

Table 2.1 Common electrical elements

Component	Current Vs Voltage	Impedance
Resistor, R	$E = IR$	$Z = R$
Inductor, L	$E = L \frac{di}{dt}$	$Z = j\omega L$
Capacitor, C	$I = C \frac{dE}{dt}$	$Z = \frac{1}{j\omega C}$

Notice that the impedance of a resistor is independent of frequency and has only a real component. Because there is no imaginary impedance, the current through a resistor is always in phase with the voltage. The impedance of an inductor increases as frequency increases. Inductors have only an imaginary impedance component. As a result, an inductor's current is phase shifted 90 degrees with respect to the voltage. The impedance versus frequency behavior of a capacitor is opposite to that of an inductor. A capacitor's impedance decreases as the frequency is raised. Capacitors also have only an imaginary impedance component. The current through a capacitor is phase shifted -90 degrees with respect to the voltage.

2.10.3 Charge Transfer Resistance, R_{ct} (or Polarization Resistance, R_p)

A similar resistance is formed by a single kinetically controlled electrochemical reaction. In this case we do not have a mixed potential, but rather a single reaction at

equilibrium. Consider a metal substrate in contact with an electrolyte. The metal molecules can electrolytically dissolve into the electrolyte, according to:



or more generally:



In the forward reaction in the first equation, electrons enter the metal and metal ions diffuse into the electrolyte. Charge is being transferred. This charge transfer reaction has a certain speed. The speed depends on the kind of reaction, the temperature, the concentration of the reaction products and the potential. When the overpotential is very small and the electrochemical system is at equilibrium, the expression for the charge transfer resistance changes into:

$$R_{ct} = \frac{RT}{nFi_0}$$

R = Gas constant

T = Temperature

n = Number of electrons involved

F = Faradays constant

i_0 = Exchange current density

From this equation the exchange current density can be calculated when R_{ct} is known. Whenever the potential of an electrode is forced away from its value at open circuit is referred to as polarizing the electrode. When an electrode is polarized, it can cause current to flow via electrochemical reactions that occur at the electrode surface. The amount of current is controlled by the kinetics of the reactions and the diffusion of reactants both towards and away from the electrode.

2.10.4 Double Layer Capacitance, C_{dl}

An electrical double layer exists at the interface between an electrode and its surrounding electrolyte. This double layer is formed as ions from the solution stick on the electrode surface. Charges in the electrode are separated from the charges of these ions. The separation is very small, on the order of angstroms. Charges separated by an insulator form a capacitor. The value of the double layer capacitance depends on

many variables including electrode potential, temperature, ionic concentrations, types of ions, oxide layers, electrode roughness, impurity adsorption, etc.

2.10.5 Constant Phase Element (CPE)

Capacitors in EIS experiments often do not behave ideally. Instead, they act like a constant phase element (CPE) as defined below. The impedance of a capacitor has the form:

$$Z = \frac{1}{(j\omega C)^\alpha}$$

Where, ω is the angle frequency ($\omega = 2\pi f$, f being the frequency). When this equation describes a capacitor, the exponent $\alpha = 1$. For a CPE, the exponent α is an empirical constant less than one. The double layer capacitor on real cells often behaves like a CPE instead of like a capacitor.

2.10.6 Warburg Impedance (Z_w)

Diffusion can create impedance known as the Warburg impedance. This impedance depends on the frequency of the potential perturbation. At high frequencies the Warburg impedance is small since diffusing reactants don't have to move very far. At low frequencies the reactants have to diffuse farther, thereby increasing the Warburg impedance. If the diffusion layer is bounded within a thin slice of solution or a thin slice of material, the Warburg impedance is the Bounded Warburg, having the form (Common examples are electric double layer capacitors):

$$Z_w = Z_0 (j\omega)^{-1/2} \coth [B(j\omega)^{1/2}]$$

$$Z = \frac{RT}{n^2 F^2 A C_s \sqrt{D}}, B = \frac{\sigma}{\sqrt{D}}$$

Where B and Z_0 are the Warburg factors, D is the diffusion coefficient of the ion in the electrolyte, σ is the Nernst diffuse layer thickness, n is the valency of the ion, F is the Faraday constant, A is the area of the electrode and C_s is the concentration of the electrolyte on the surface of the electrode, which can be replaced by the bulk concentration of the electrolyte, because of the reversible formation process of the electric double layer.

2.11 Characterization of Titanium Dioxide

2.11.1 X-ray Powder Diffraction (XRD)

X-ray powder diffraction (XRD) is an instrumental technique used to identify minerals, as well as other crystalline materials. XRD is a technique in which a collimated beams of nearly monochromatic. X-rays is directed onto the flat surface of a relatively thin layer of finely ground material. XRD can provide additional information beyond basic identification. If the sample is a mixture, XRD data can be analyzed to determine the proportion of the different minerals present. Other information obtained can include the degree of crystallinity of the minerals present, possible deviations of the minerals from their ideal compositions, the structural state of the minerals and the degree of hydration for minerals that contain water in their structure. Figure 2.4 shows a monochromatic beam of X-ray incident on the surface of crystal at an angle θ . The scattered intensity can be measured as a function of scattering angle 2θ . The resulting XRD pattern efficiently determines the different phases present in the sample.

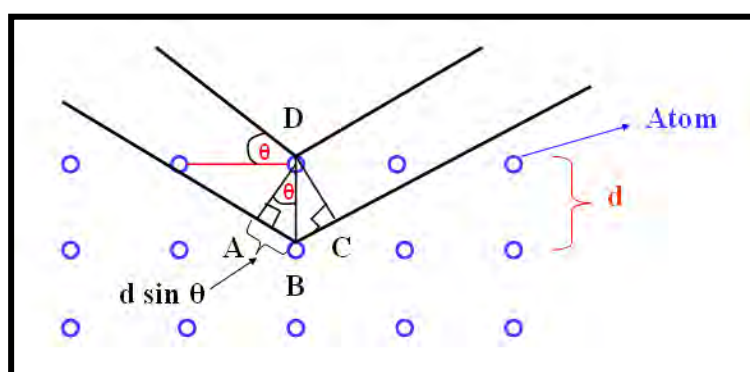


Figure 2.4 Diffraction of X-ray by regular planes of atoms.

Using this method, Bragg's law is able to determine the interplanar spacing of the samples, from diffraction peak according to Bragg angle.

$$AB = BC = d \sin\theta$$

$$AB+BC = 2d \sin\theta$$

$$n\lambda = 2 d \sin\theta$$

Where the integer n is the order of the diffracted beam, λ is the wavelength; d is the distance between adjacent planes of atoms (the d -spacings) and θ is the angle of between the incident beam and these planes.

2.11.2 Scanning Electron Microscope (SEM)

The scanning electron microscope (SEM) has unique capabilities for analyzing surfaces and morphology of materials. It is analogous to the reflected light microscope, although different radiation sources serve to produce the required illumination. Whereas the reflected light microscope forms an image from light reflected from a sample surface, the SEM uses electrons for image formation. The different wavelength of these radiation sources result in different resolution levels: electron have much shorter wavelength than light photons, and shorter wavelength are capable of generating the higher resolution information. Enhanced resolution in turn permits higher magnification without loss of detail. The maximum magnification of the light microscope is about 2,000 times; beyond this level is “empty magnification”, or the point where increased magnification does not provide additional information. This upper magnification limit is a function of the wavelength of visible light, 2000 Å, which equal the theoretical maximum resolution of conventional light microscope. In comparison, the wavelength of electron is less than 0.5 Å, and theoretically the maximum magnification of electron beam instrument is beyond 800,000 times. Because of instrumental parameters, practical magnification and resolution limits are about 75,000 times and 40 Å in a conventional SEM. The SEM consists basically of four systems:

1. The *illuminating/imaging system* produces the electron beam and directs it onto the sample.
2. The *information system* includes the data released by the sample during electron bombardment and detectors which discriminate among analyze these information signals.
3. The *display system* consists of one or two cathode-ray tubes for observing and photographing the surface of interest.
4. The *vacuum system* removes gases from the microscope column which increase the mean free path of electron, hence the better image quality.

2.11.3 Nitrogen Adsorption-Desorption Isotherm [83]

The N₂ adsorption technique is used to determine the physical properties of mesoporous molecular sieves, such as the surface area, pore volume, pore diameter and pore-size distribution of porous materials.

Adsorption of gas by a porous material is described by an adsorption isotherm, the amount of adsorbed gas by the material at a fixed temperature as a function of pressure. Porous materials are frequently characterized in terms of pore sizes derived from gas sorption data. IUPAC conventions have been proposed for classifying pore sizes and gas sorption isotherms that reflect the relationship between porosity and sorption. The IUPAC classification of adsorption isotherms is illustrated in Figure 2.5. Six types of isotherms are characteristic of adsorbents that are microporous (type I), nonporous or macroporous (types II, III, and VI) or mesoporous (types IV and V).

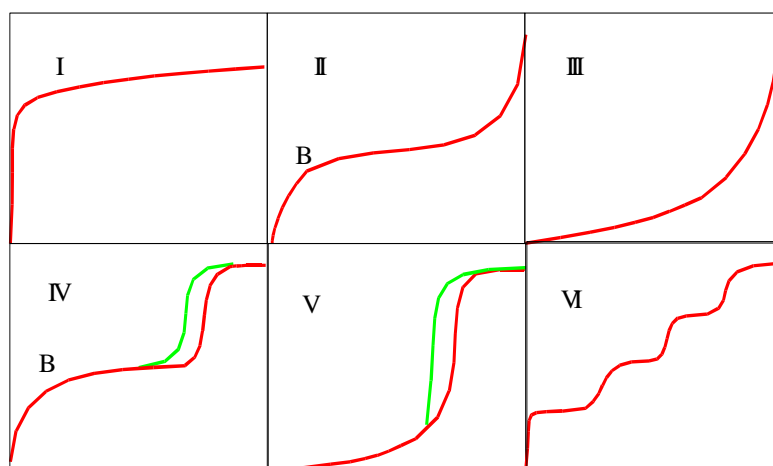


Figure 2.5 The IUPAC classification of adsorption isotherm.

Adsorption isotherms are described as shown in Table 2.2 based on the strength of the interaction between the sample surface and gas adsorbate, and the existence or absence of pores. Pore types are classified as shown in Table 2.3.

Pore size distribution is measured by the use of nitrogen adsorption/desorption isotherm at liquid nitrogen temperature and relative pressures (P/P_0) ranging from 0.05-0.1. The large uptake of nitrogen at low P/P_0 indicates filling of the micropores ($<20 \text{ \AA}$) in the adsorbent. The linear portion of the curve represents multilayer adsorption of nitrogen on the surface of the sample, and the concave upward portion of the curve represents filling of mesopores and macropores.

Table 2.2 Features of adsorption isotherms

Type	Features	
	Interaction between sample surface and gas adsorbate	Porosity
I	Relatively strong	Micropores
II	Relatively strong	Nonporous
III	Weak	Nonporous
IV	Relatively strong	Mesopore
V	Weak	Micropores or Mesopore
VI	Relatively strong sample surface has an even distribution of energy	Nonporous

Table 2.3 IUPAC classification of pores

Pore Type	Pore diameter (nm)
Micropore	Up to 2
Mesopore	2 to 50
Macropore	50 to up

The multipoint Brunauer, Emmett and Teller (BET) method is commonly used to measure total surface area.

$$\frac{1}{W[(P_o/P)-1]} = \frac{1}{W_m C} + \frac{C-1}{W_m C} (P/P_o)$$

Where W is the weight of nitrogen adsorbed at a given P/P_o, and W_m is the weight of gas to give monolayer coverage, and C is a constant that is related to the heat of adsorption. A linear relationship between 1/W [(P_o/P)-1] and P/P_o is required to obtain the quantity of nitrogen adsorbed. This linear portion of the curve is restricted to a limited portion of the isotherm, generally between 0.05-0.30. The slope and intercept are used to determine the quantity of nitrogen adsorbed in the monolayer and calculate the surface area. For a single point method, the intercept is taken as zero or a small positive value, and the slope from the BET plot is used to calculate the surface area. The surface area reported depends upon the method used, as well as the partial pressures at which the data are collected.

2.11.4 Cyclic Voltammetry (CV) [84-86]

Cyclic voltammetry (CV) is very useful electroanalytical technique in many areas of chemistry. It is rarely used for quantitative determinations, but it is widely used for studying the mechanisms and reversibility of electrode processes. This technique is based on varying the applied potential at a working electrode in both forward and reverse direction while monitoring the current. For example, the initial scan could be in the negative direction to the switching potential. At that point the scan would be reversed and run in the positive direction. Depending on the analysis, one full cycle, a partial cycle, or a series of cycles can be performed. Some potential waveforms used in cyclic voltammetry are illustrated in Figure 2.6.

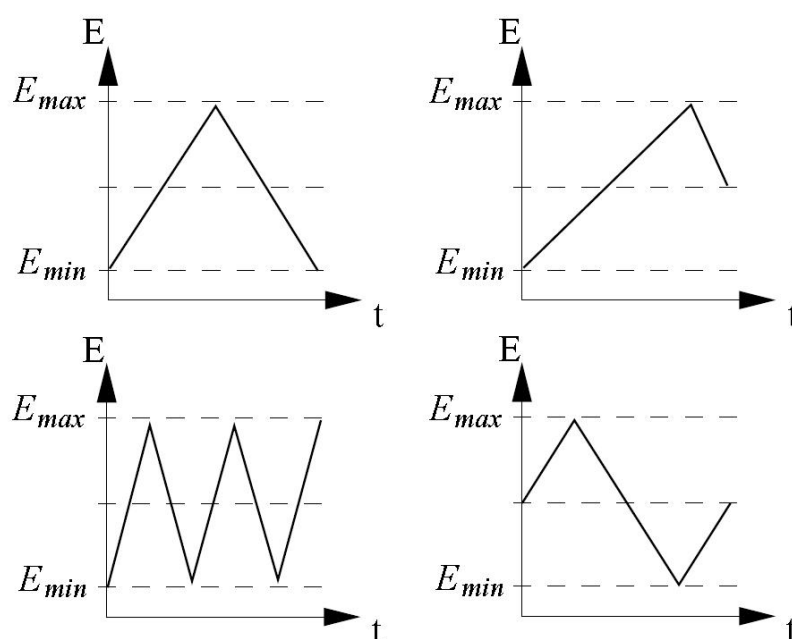


Figure 2.6 Some potential waveforms used in cyclic voltammetry.

The resulting plot of current vs. potential is termed a cyclic voltammogram. The cyclic voltammogram can be very simple as shown in Figure 2.7 for the reversible redox system. The important parameters in a cyclic voltammogram are the peak potentials (E_{pc} , E_{pa}) and peak currents (i_{pc} , i_{pa}) of the cathodic and anodic peaks, respectively. If the electron transfer process is fast compared with other processes (such as diffusion), the reaction is said to be electrochemically reversible. The current-voltage cycle illustrated in figure 2.7 for the reversible electrode process is obtained when the reaction products, formed during the forward scan as a result of

the electrode reaction that gives rise to the peak at E_{pc} , are oxidized on the reverse scan as shown by the peak at E_{pa} .

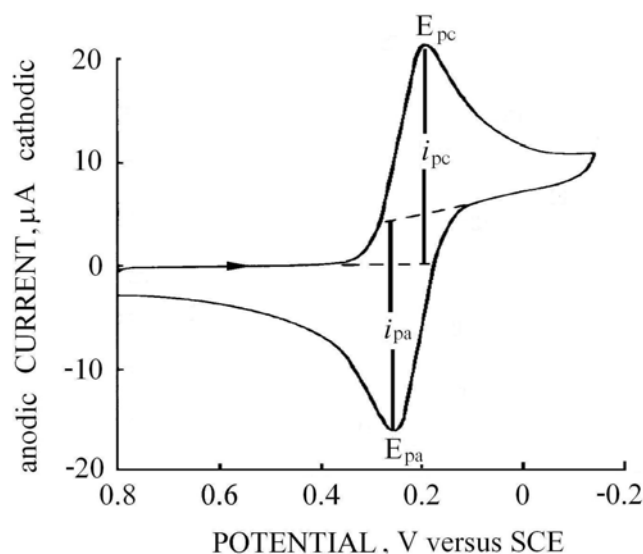


Figure 2.7 Cyclic voltammogram for a reversible.

The peak current for a reversible couple (at 25 °C) is given by the Randles–Sevcik equation:

$$i_p = 2.686 \times 10^5 n^{3/2} A c D^{1/2} \nu^{1/2}$$

where i_p is the peak current (amps), n is the number of electrons, A is the electrode area (cm^2), c is the concentration (mol cm^{-3}), D is the diffusion coefficient ($\text{cm}^2 \text{s}^{-1}$), and ν is the potential scan rate (V s^{-1})

The separation between the peak potential is given by

$$\Delta E_p = |E_{pa} - E_{pc}| = 2.303 RT / nF$$

Thus, for a reversible reaction at 25 °C with n electrons, ΔE_p should be $0.0592/n$ V or about 60 mV for one electron. In practice this value is difficult to attain because of such factors as cell resistance. Irreversibility due to a slow electron transfer rate results in $\Delta E_p > 0.0592/n$ V.

For a totally irreversible process, that is one in which the electrode reaction products cannot be oxidized back to the initial analyte because k_{ox} is extremely small or because they have undergone a subsequent irreversible chemical change to compounds that are not electroactive, no anodic current peak is observed. Because of

the dynamic nature of voltage-sweep voltammetry, irreversible processes give an expression for the peak current distinctly different from those of reversible systems:

$$i_p = 2.99 \times 10^5 n (\alpha n_a)^{1/2} A c D^{1/2} v^{1/2} \quad \text{at } 25^\circ\text{C}$$

where n_a represents the number of electrons in the rate-controlling step and α is the transfer coefficient (normally with a value between 0.3 and 0.7). The latter two quantities can be evaluated by taking the difference between the peak potential and half-peak potential:

$$E_p - E_{p/2} = -0.048 / (\alpha n_a) \quad \text{at } 25^\circ\text{C}$$

An alternative approach is to scan the voltammogram at two different rates. Under these conditions α and n_a may be evaluated by the expression

$$(E_p)_2 - (E_p)_1 = \frac{RT}{\alpha n_a F} \ln \sqrt{\frac{v_1}{v_2}} \quad \text{at } 25^\circ\text{C}$$

2.11.5 Electrochemical Impedance Spectroscopy (EIS) [87]

An equivalent circuit model with mixed kinetic and charge transfer control is assumed as shown in Figure 2.8, where R_s is the series solution resistance, R_p is the polarization impedance, W is the Bounded Warburg impedance, and the constant phase element (CPE) is used instead of a double layer capacitor, as capacitors in EIS experiments often do not behave ideally.

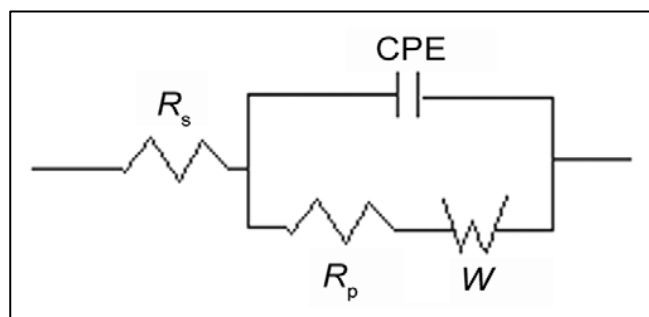


Figure 2.8 Equivalent circuit models with mixed kinetic and charge transfer control.

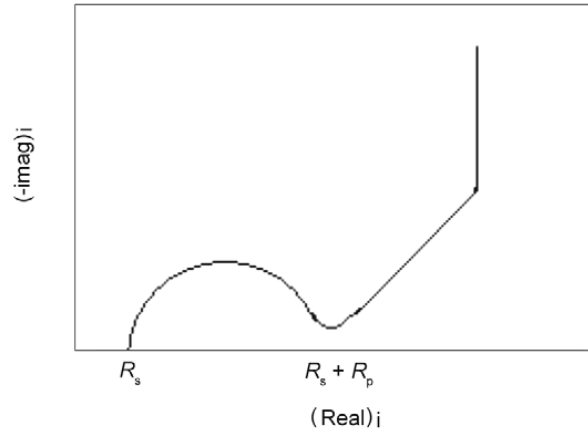


Figure 2.9 Typical Nyquist plot for a cell with mixed kinetic and charge transfer.

The Nyquist plot for such a model is shown in Figure 2.9, for a cell with mixed kinetic and charge transfer control, the Nyquist plot can be divided into three parts, in terms of frequencies. The semicircle is related to charge transfer resistance or polarization resistance (R_p). The intercept of the semicircle at the left of the real axis is the solution resistance (R_s), and the intercept at the right of the real axis is the sum of the polarization resistance and the solution resistance. The diameter of the semicircle is therefore equal to the polarization resistance. The straight line with a slope of 45° is related to the Warburg impedance created by the diffusion of electrolyte ions within pores of electrochemical capacitor electrodes. The vertical line to the real axis is caused by purely capacitive behavior.

CHAPTER III

EXPERIMENTAL

3.1 Instruments and Apparatus

Rotary Evaporator

After the bamboo powder or carbon was impregnated with a solution of titanium tetraisopropoxide in 2-propanol, the alcohol was removed from the solid sample using a BUCHI R-114 rotary evaporator above room temperature.

Ovens and Tube Furnaces

TiO₂ impregnated samples were normally dried at the temperature of 105°C in a Memmert UM-500 oven. Thermal treatment of the dried impregnated samples were carried out in a 15 cm long quartz boat and put into a 72 cm long quartz tube reactor (2 cm in inner diameter) with a temperature-programmable controller.

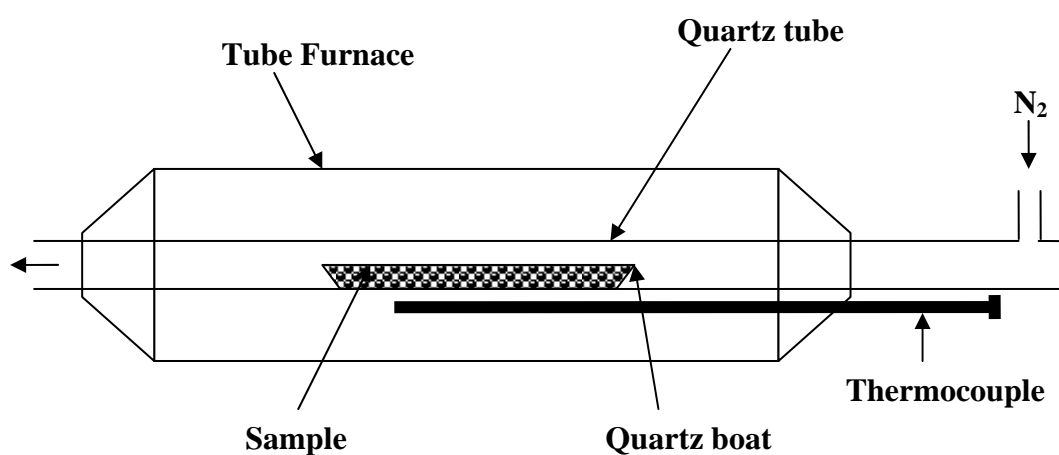


Figure 3.1 Drawing of the system used for thermal treatment.

X-ray Powder Diffractometer (XRD)

The X-ray powder diffractometer was used for investigation of the structure and crystal size of TiO₂. X-ray diffraction (XRD) patterns of the TiO₂/C and TiO₂/AC composites were obtained with a Rigaku Dmax 2200 Ultima Plus X-ray powder diffractometer with a monochromator and Cu K_α radiation (40 kV, 30 mA). The 2-theta angle was ranged from 20 to 60 degree with scan speed of 3 degree/min and sampling width of 0.02 degree. The scattering slit, divergent slit and receiving slit were fixed at 0.5 degree, 0.5 degree, and 0.3 mm, respectively. The measured diffractograms were analyzed using MDI software (Jade6.5) and the TiO₂ crystal size was calculated from the Scherrer equation.

Nitrogen Adsorptometer

Characterization of sample porosity in terms of nitrogen adsorption-desorption isotherms, BET specific surface area, and pore size distribution of the composite was carried out using a BEL Japan, BELSORP-mini instrument. The samples were outgassed at 400°C for 3 h before the surface area measurements.

Scanning Electron Microscope (SEM)

JEOL JSM-6480LV scanning electron microscope was used for the identification of the surface morphology and particle size of the synthesized TiO₂/C and TiO₂/AC composites. All samples were coated with sputtering gold under vacuum prior to the SEM measurements.

Cyclic Voltammetry (CV) and Electrochemical Impedance Spectroscopy (EIS)

Electrochemical characterization by cyclic voltammetry and impedance spectroscopy were used in order to understand the electrochemical behavior of the composite electrodes performed with a computer-controlled potentiostat (Autolab PGSTAT 30) using a conventional three-electrode cell, including a composite electrode as the working electrode, 3 M KCl-Ag/AgCl as the reference electrode, and platinum wire as the counter electrode. Cyclic voltammetric measurements were carried out in the potential range of 0.5 to 1 V at scan rate 0.01 V/s. Electrochemical impedance analysis was performed by an impedance analyzer (Autolab PGSTAT 30 with FRA

software) in the frequency range of 10 kHz to 0.1 Hz with an AC signal of 10 mV amplitude. All the electrochemical measurements were performed in 1 M H₂SO₄ aqueous solution as electrolyte.

3.2 Materials, Chemicals and Gases

1. Waste bamboo based chopsticks (100 mesh, <150 μm)
2. Titanium tetraisopropoxide, TTIP (Fluka)
3. 2-Propanol, C₃H₇OH (Carlo Erba reagents)
4. Phosphoric acid, H₃PO₄ (Merck)
5. Ethanol, C₂H₅OH (Merck)
6. Sulfuric acid 95-97%, H₂SO₄ (Merck)
7. Nitrogen gas, N₂ (Thai Industrial Gases (TIG), highly pure grade)

3.3 Preparation of the Porous Carbon from Bamboo Waste as a Support

The carbon precursor used in the study was waste bamboo based chopsticks, a bio-waste product procured from the restaurant. The waste chopsticks were washed thoroughly and dried in sunshine before chopped and blended into powder before sifted through a 100 mesh sieve. The bamboo powder was dried at 100°C to reduce the moisture.

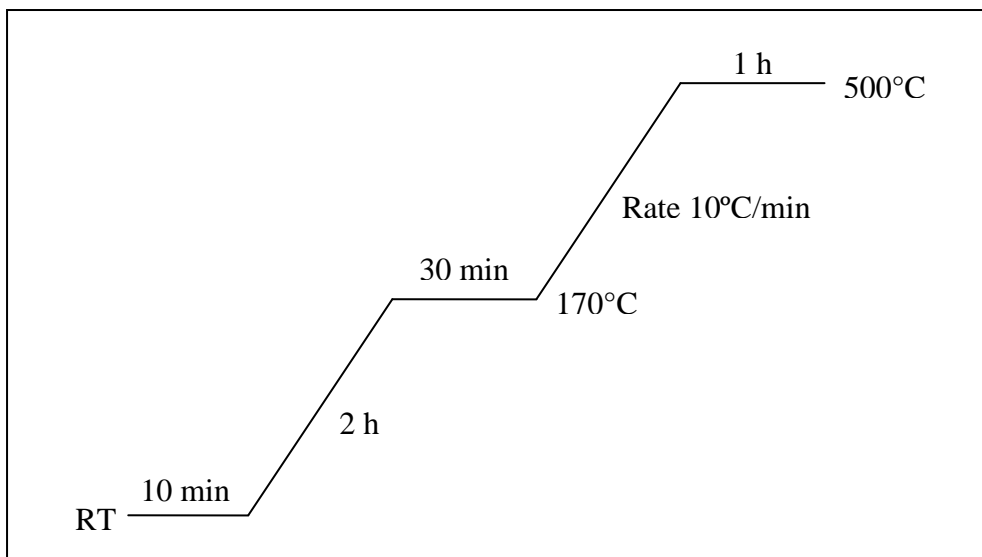
3.3.1 Preparation of the Carbon

The bamboo powder was carbonized at 500°C for 2 h with the heating rate of 10°C/min in a quartz tube reactor and this reactor was flowed with 500 ml/min of nitrogen. The bamboo powder was carbonized in the tube furnace. Then the carbon was obtained.

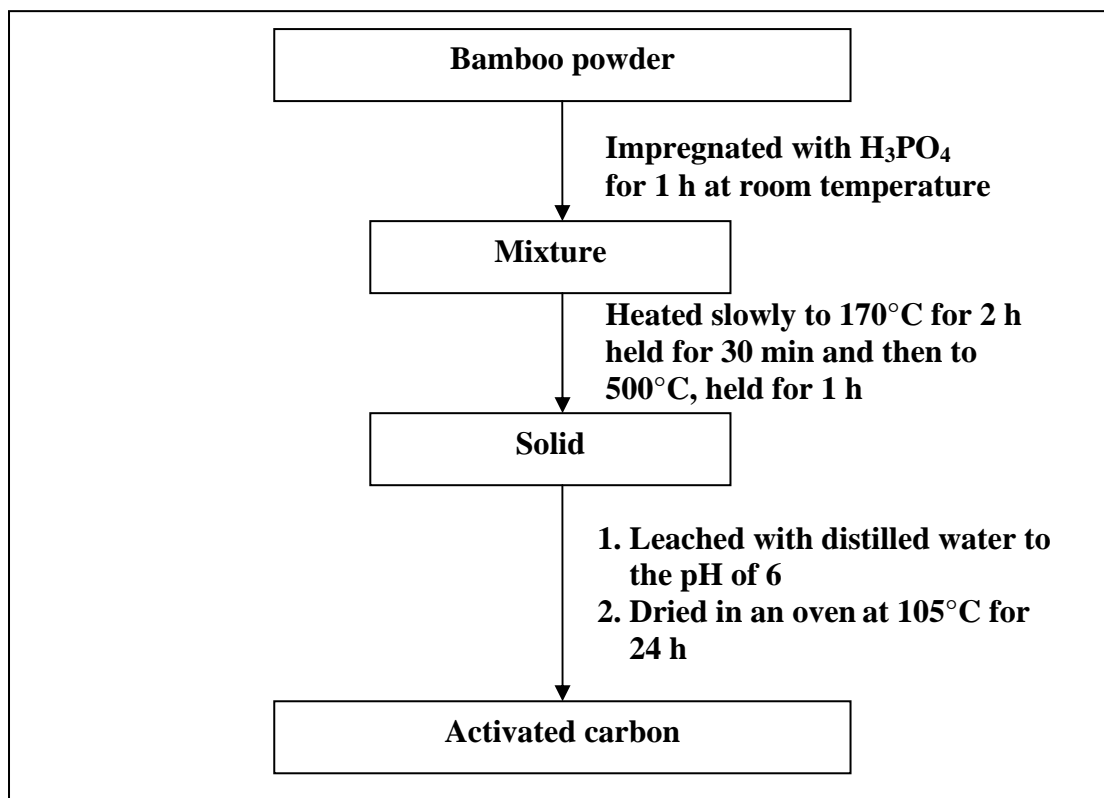
3.3.2 Preparation of the Activated Carbon

The activation of carbon was carried out from a procedure reported in the literature [68]. The bamboo powder was impregnated with a phosphoric acid solution for 1 h at room temperature to allow penetration of acid into the wood structure. The weight ratio of H₃PO₄ to bamboo powder on an as-received basis was 1.45 (1.45 g phosphoric acid: 1 g bamboo powder). At this ratio of reagent to bamboo powder, the amount of reagent is considered to be in excess. The mixture was heated slowly to

170°C for 2 h in a quartz tube reactor, under flowing nitrogen, held for 30 min, and then to a final temperature of 500°C and held for 1 h. The heating program is illustrated in scheme 3.1. The solid product was leached with distilled water to the pH of 6 and dried in an oven at 105°C for 24 h. Then the activated carbon was obtained. The whole procedure was summarized in scheme 3.2.



Scheme 3.1 A heating program of the preparation of activated carbon.



Scheme 3.2 Schematic diagram of the preparation of activated carbon.

3.4 Preparation of the TiO₂/C and TiO₂/AC Composites

We are proposing a novel method for preparing the TiO₂/carbon and TiO₂/activated carbon composite. A novel method (Method A) was compared with a conventional method (Method B) [47] and effect of carbonization temperature on formation of anatase structure was studied. In the present work, titanium tetraisopropoxide (TTIP) was used as titanium source.

3.4.1 Method A (The Novel Method): TTIP Impregnation Before Carbonization (Using Bamboo Powder)

► *Synthesis of TiO₂/C (Sample Notation: A1)*

The bamboo powder was impregnated with a solution of titanium tetraisopropoxide in 2-propanol for 15 h. The alcohol was evaporated from the solid sample using a rotary evaporator above room temperature and dried in an oven at 105°C for 8 h in air. The impregnated sample was carbonized in a quartz tube reactor under N₂ flow at different temperatures of 500, 600, and 700°C for 2 h with the heating rate of 10°C/min. The TiO₂/C composites obtained were denoted as A1.

► *Synthesis of TiO₂/AC (Sample Notation: A2)*

The composite A1 was impregnated with phosphoric acid solution for 1 h at room temperature. The mixture was activated by heating at 500°C and the solid products were leached with distilled water to the pH of 6 and dried in an oven at 105°C for 24 h before further characterization. The TiO₂/AC composites obtained were denoted as A2.

3.4.2 Method B (The Conventional Method): TTIP Impregnation After Carbonization (Using Bamboo Based Carbon)

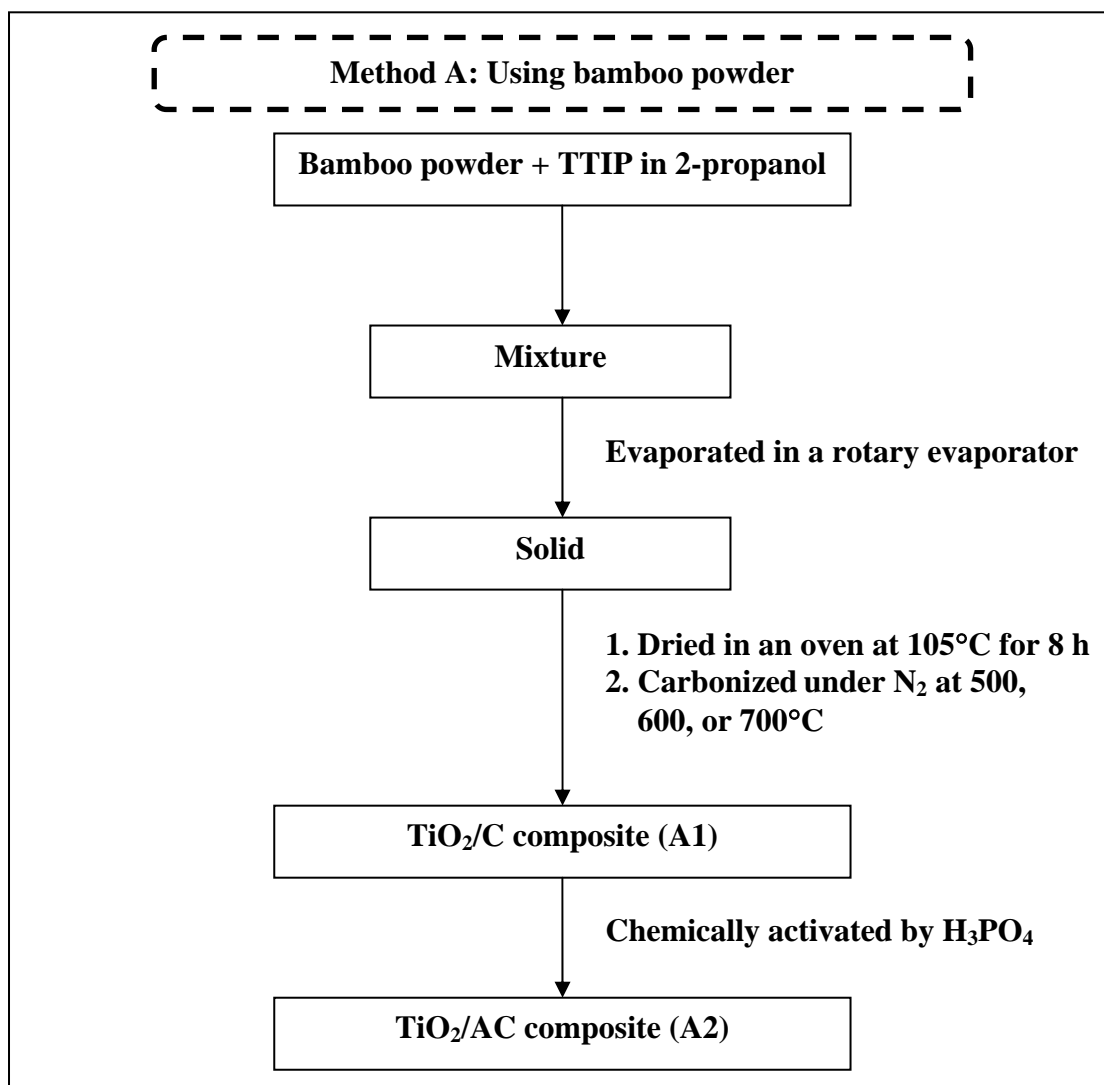
► *Synthesis of TiO₂/C (Sample Notation: B1)*

The carbon was first prepared following the procedure in section 3.3.1 and impregnated with a solution of titanium tetraisopropoxide in 2-propanol for 15 h. The alcohol was evaporated from the solid sample using a rotary evaporator above room temperature and dried in an oven at 105°C for 8 h in air. Finally, the impregnated sample was calcined in a quartz tube reactor under N₂ flow at different temperatures of 500, 600, and 700°C for 2 h with the heating rate of 10°C/min to convert TTIP to TiO₂. The TiO₂/C composites obtained were denoted as B1.

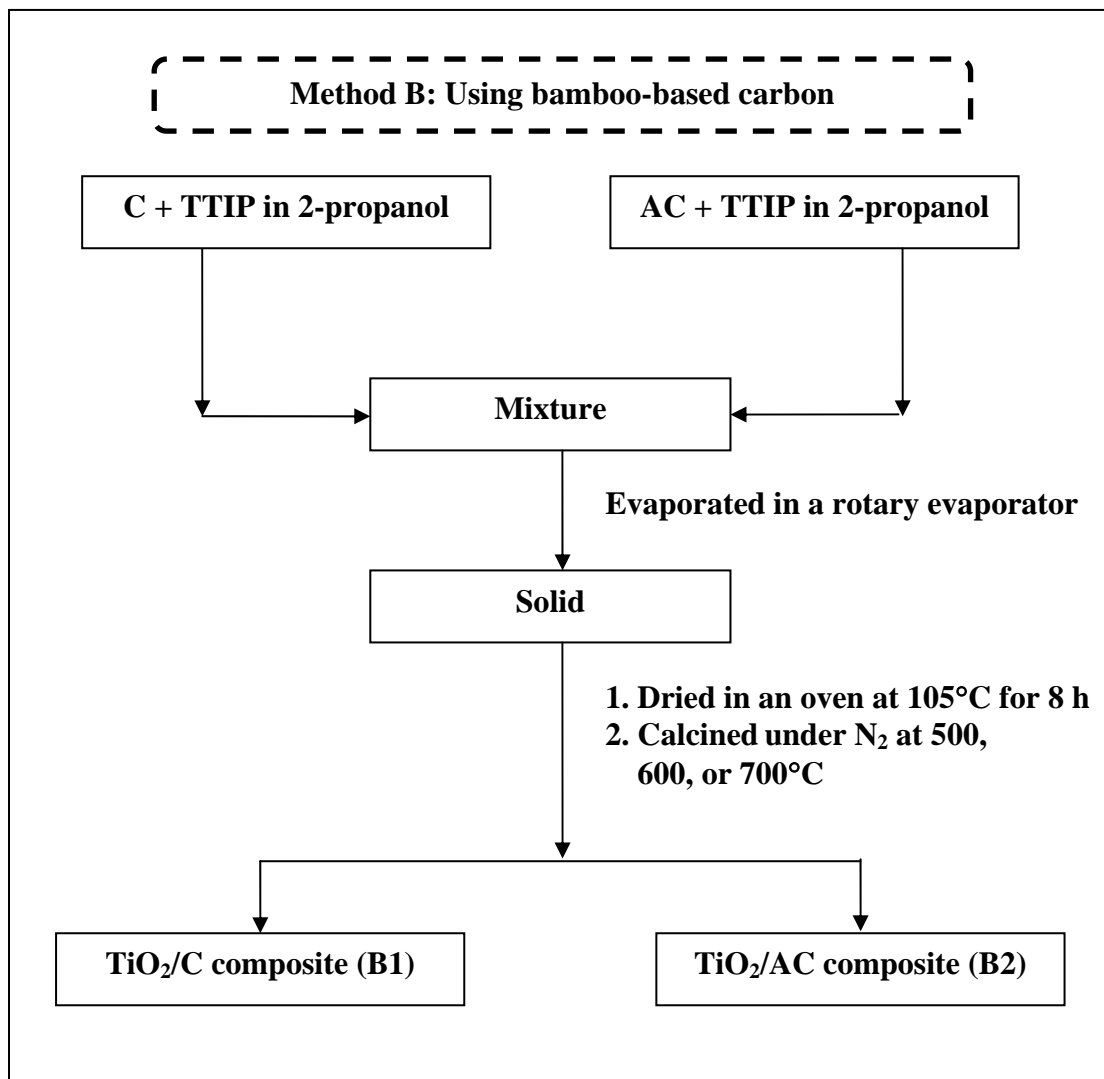
► *Synthesis of TiO₂/AC (Sample Notation: B2)*

The activated carbon was first prepared following the procedure in section 3.3.2 and impregnated with a solution of titanium tetraisopropoxide in 2-propanol for 15 h. The alcohol was evaporated from the solid sample using a rotary evaporator above room temperature and dried in an oven at 105°C for 8 h in air. Finally, the impregnated sample was calcined in a quartz tube reactor under N₂ flow at different temperatures of 500, 600, and 700°C for 2 h with the heating rate of 10°C/min to convert TTIP to TiO₂. The TiO₂/AC composites obtained were denoted as B2.

All prepared composites were grinded and stored in a desiccator before use.



Scheme 3.3 Schematic diagram of the synthesis procedure for Method A.



Scheme 3.4 Schematic diagram of the synthesis procedure for Method B.

3.5 Preparation of Bulk TiO₂

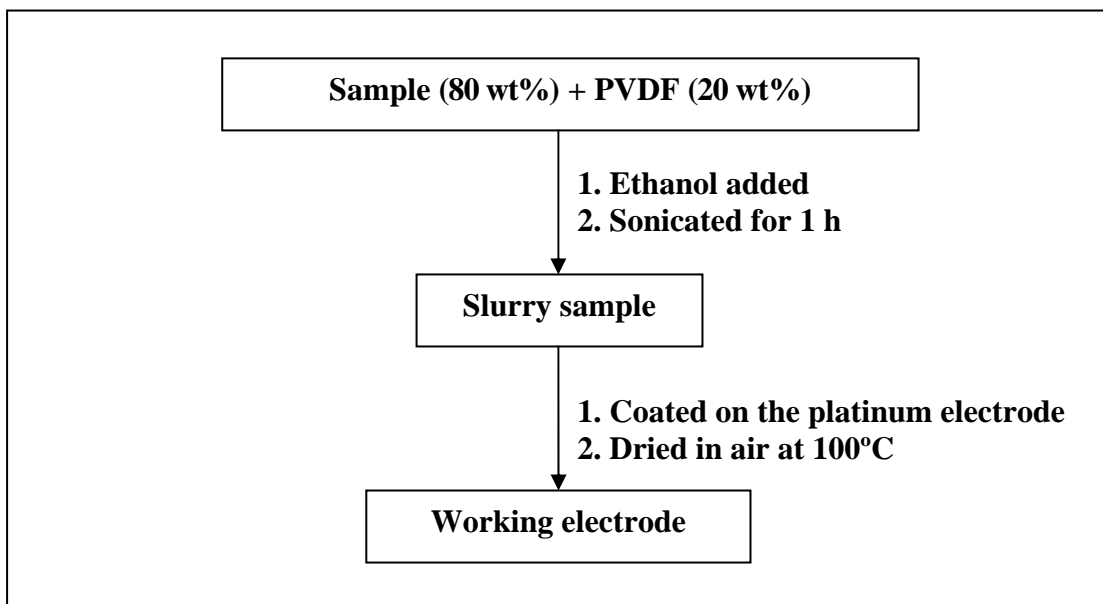
For a reference, non-loaded carbon was also prepared. The unsupported bulk TiO₂ was prepared as a reference under N₂ similar to the preparation of the composite but without bamboo powder or carbon or activated carbon.

3.6 Preparation of A1, A2, B1, B2 Composites with Various Amounts of TiO₂ in Composite

In order to study the effect of TiO₂ amounts in the composite on the capacitive performance of the composite electrode, all the composite samples were synthesized in similar way as described in Section 3.4 with various amounts of TiO₂ of 10, 20, 30, 40 wt% in the composite. The carbonization temperature of 500°C was used.

3.7 Preparation of the Sample Electrodes

The sample electrodes were prepared by mixing 80 wt% composite samples with 20 wt% binder (polyvinylidene fluoride, PVDF) and then sonicated in ethanol for 1 h to form homogenous slurries. Finally, the platinum electrodes were coated with the slurries and dried in the air at 100°C. The sample electrodes were used as the working electrode.



Scheme 3.5 Schematic diagram of the preparation of the sample electrodes.

CHAPTER IV

RESULTS AND DISCUSSION

4.1 Effect of Preparation Methods and Carbonization Temperature on Composite Properties

4.1.1 XRD Patterns

XRD patterns of TiO₂/C composites prepared by Methods A1 and A2 at various carbonization temperatures of 500, 600, and 700°C are shown in Figures 4.1 and 4.2, respectively. They are similar to the typical XRD pattern of anatase with the characteristic peaks at 2θ of 25.3, 37.0, 37.8, 38.5, 48.0, 53.9, and 55.0 degrees. XRD patterns of TiO₂/C composites (B1) and TiO₂/AC composites (B2) prepared by Method B are shown in Figures 4.3 and 4.4, respectively. The broadening of XRD peaks of A1 and A2 are due to the extremely small crystals compared to those of B1 and B2 samples. Anatase-type TiO₂ was readily formed in all composites. The anatase phase obtained was very stable even at 700°C and no rutile phase was observed for all preparation methods. This is different from anatase prepared by other methods [41, 49] that TiO₂ normally undergoes anatase-to-rutile phase transformation in the temperature range between 600 and 700°C and anatase is completely converted to rutile above 700°C.

It indicates that carbon can obviously stabilize the nano-anatase phase up to 700°C. Thus, the unsupported bulk anatase prepared by sol-gel method which was the conventional method is not thermally stable and it can be transformed easily to rutile upon heating. The nanocrystals of anatase prepared by sol-gel method were found much less stable, only up to about 300°C [51]. The crystal titanium pyrophosphate (TiP₂O₇) phase was found in the composites synthesized by Method A2 because this method was performed through phosphoric acid treatment followed by heating. Some researchers *Z. Shi et al.* [88] reported preparation of titanium pyrophosphate at the carbonization temperature as high as 800°C and this phase has excellent thermal stability and good cyclic voltammetric performance. This is a reason why the H₃PO₄ treatment was also attempted in this work.

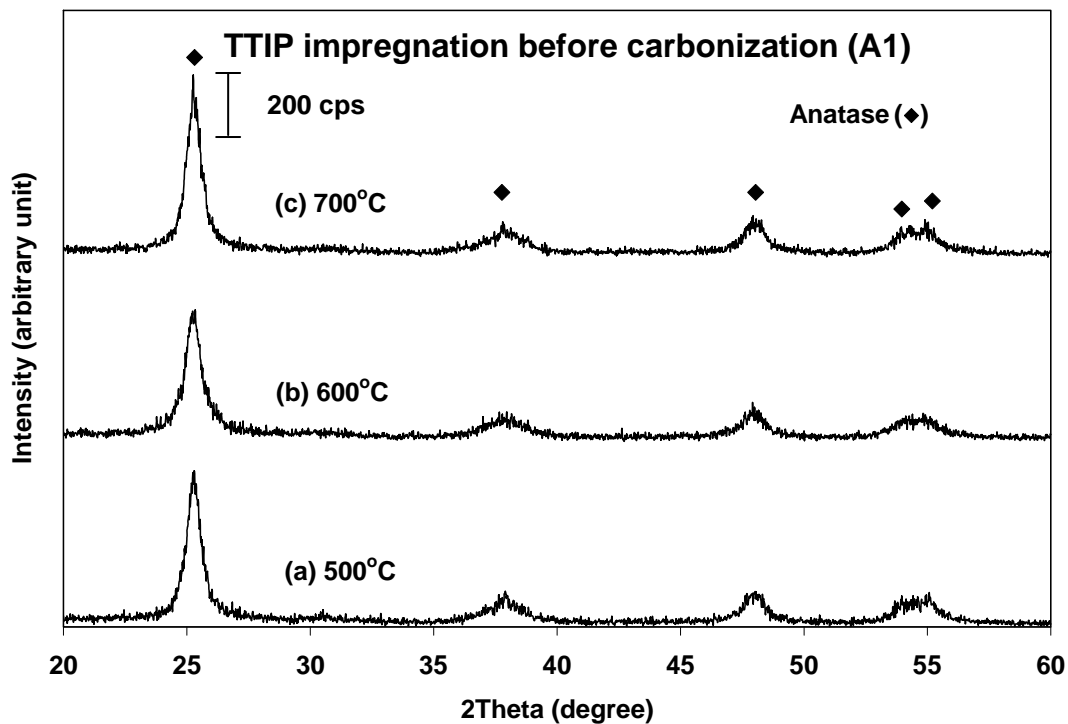


Figure 4.1 XRD patterns of TiO₂/C composites prepared by Method A1 at various carbonization temperatures of (a) 500°C, (b) 600°C, and (c) 700°C.

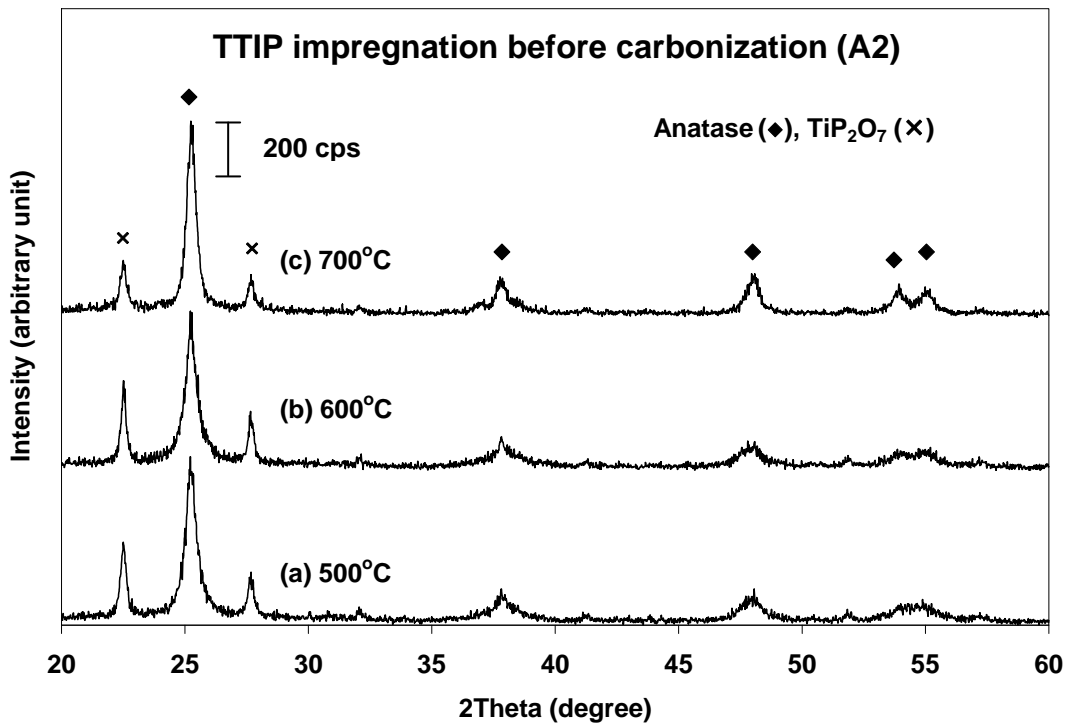


Figure 4.2 XRD patterns of TiO₂/C composites prepared by Method A2 at various carbonization temperatures of (a) 500°C, (b) 600°C, and (c) 700°C.

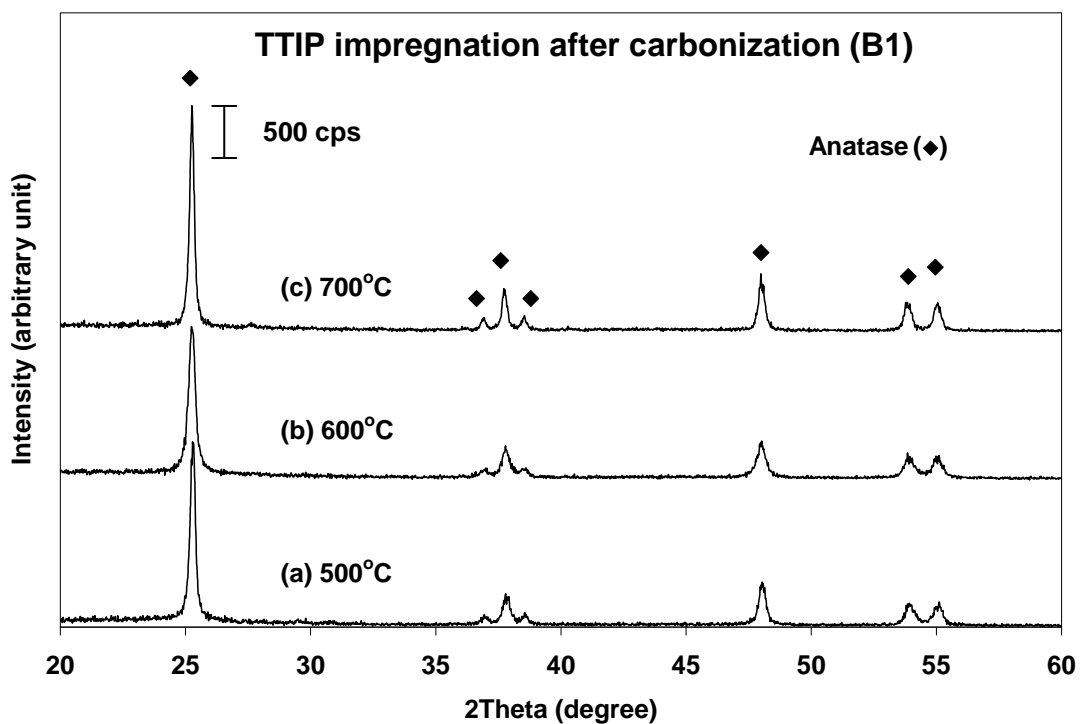


Figure 4.3 XRD patterns of TiO₂/C composites prepared by Method B1 at various carbonization temperatures of (a) 500°C, (b) 600°C, and (c) 700°C.

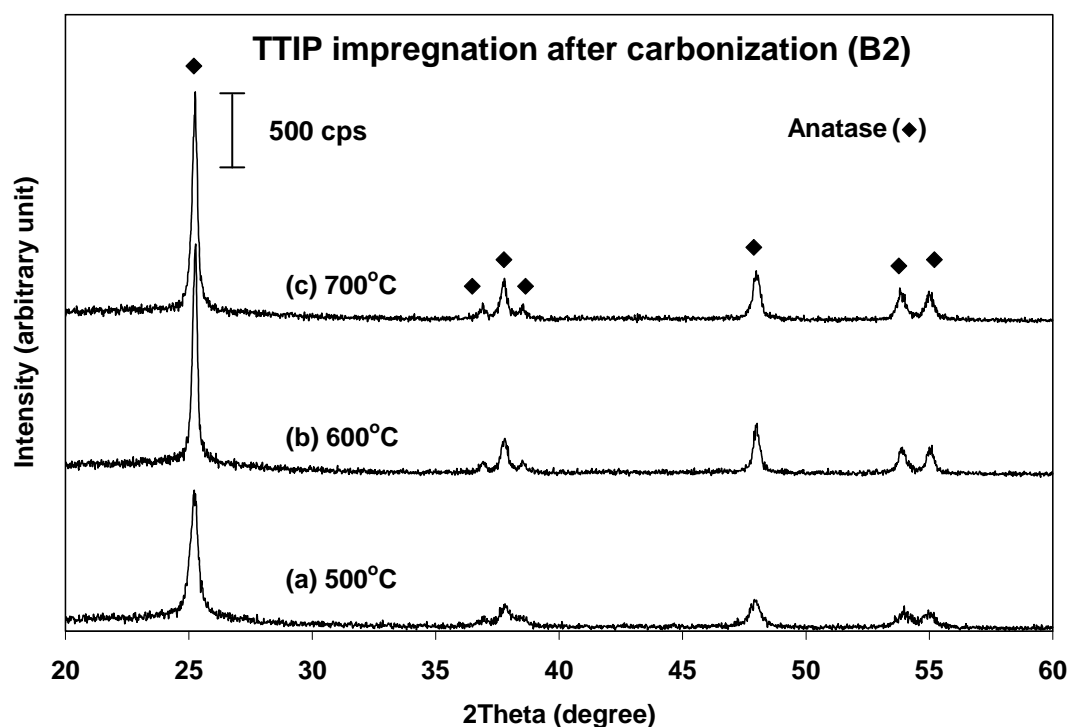


Figure 4.4 XRD patterns of TiO₂/AC composites prepared by Method B2 at various carbonization temperatures of (a) 500°C, (b) 600°C, and (c) 700°C.

Figure 4.5 shows the XRD patterns of the unsupported bulk TiO₂ prepared under N₂ similar to the preparation of the composites but without carbon or activated carbon as a support. All unsupported TiO₂ samples calcined at 500, 600, and 700°C are crystalline and at all calcination temperatures both anatase and rutile phase were found. The characteristic XRD peaks of rutile phase at 2θ are 27.4, 36.0, 39.2, 41.2, 54.3 and 56.6 degrees. At the lowest calcination temperature of 500°C, the rutile phase of TiO₂ was still found. At higher calcination temperatures than 500°C, the amount of rutile formed was larger. It reveals that the unsupported bulk anatase TiO₂ was found low thermally stable and readily to convert to rutile TiO₂.

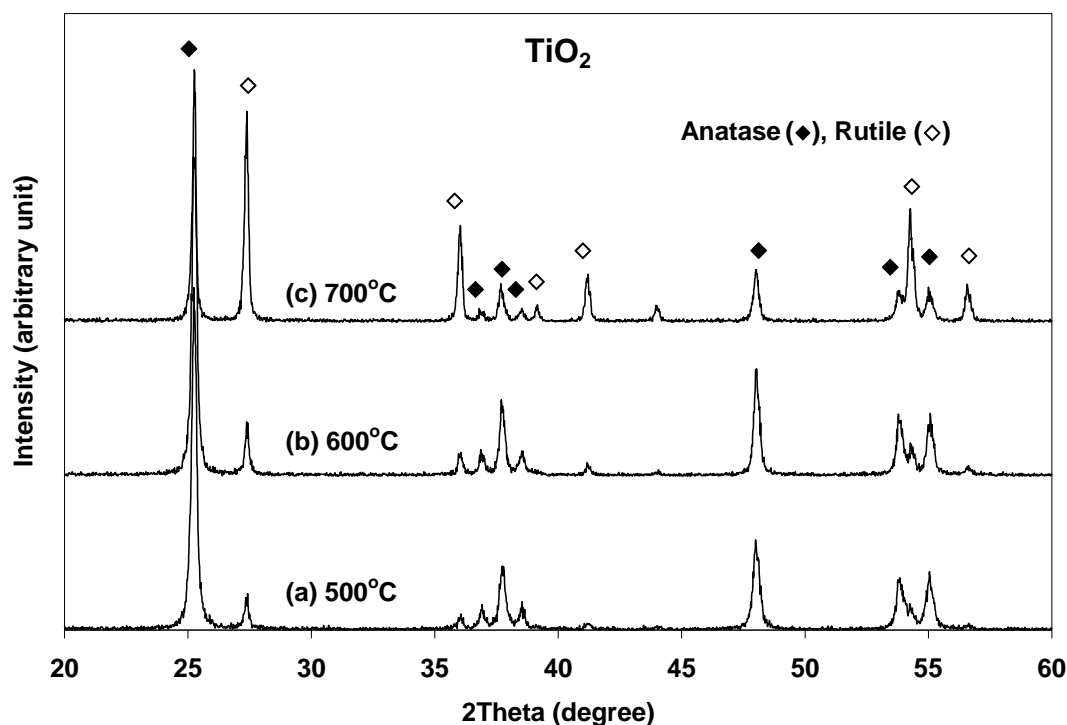


Figure 4.5 XRD patterns of the unsupported TiO₂ (TiO₂ 100%) prepared under N₂ at various calcination temperatures of (a) 500°C, (b) 600°C, and (c) 700°C.

In addition, *L. Kőrösi and I. Dékány* [51] studied the effect of phosphates on improving thermal stability of TiO₂ but rutile phase in the composite was still observed at 700°C. All composites prepared by our proposed method are very stable even at 700°C with no observation of rutile phase. Thus, carbon from bamboo can obviously stabilize the anatase phase up to 700°C and increase thermal stability of anatase phase. This novel method A can reduce the preparation steps because during carbonization of bamboo powder, crystalline anatase structure was developed

simultaneously with formation of porous structure of carbon from bamboo powder. Thus, carbon formed during carbonization of bamboo powder seemed to suppress the phase transformation from anatase to rutile and increased thermal stability.

The relative peak width of anatase in the composites was summarized in Table 4.1. Based on the XRD results, the crystallite grain size was estimated according to Scherrer formula:

$$L = \frac{K\lambda}{\beta \cos \theta}$$

Where L is the crystal size, K is a constant taken as 0.89, λ is the wavelength of the X-ray radiation, β is the difference in line width at half-maximum height of the sample peak and the reference peak, θ is the diffracting angle [48]. Thus, the crystal size is inversely proportional to a width at half height of a sample peak.

Table 4.1 Relative peak width at half height for anatase crystals in the composites obtained from different preparation methods at various carbonization temperatures of 500, 600, and 700°C

Conditions	Relative peak width at half height*(degree)		
	500°C	600°C	700°C
Carbonization temperature			
Method A: TTIP impregnation before carbonization			
- TiO ₂ /C (A1)	0.66	0.58	0.67
- TiO ₂ /C (A2)	0.42	0.43	0.51
Method B: TTIP impregnation after carbonization			
- TiO ₂ /C (B1)	0.25	0.33	0.23
- TiO ₂ /AC (B2)	0.23	0.53	0.28
Bulk TiO ₂	0.25	0.22	0.23

*Based on the most intense characteristic peak at 2θ of 25.3°

The novel method A provides the most broadened peak that implies the smallest crystals size which is almost one half of those prepared by the conventional method B. For the unsupported anatase prepared by sol-gel method, the crystal size of anatase is also larger than those from Method A but as large as those from Method B. It indicates that our proposed method A, TTIP impregnation before carbonization, provides much smaller crystal size range than the conventional method B, TTIP impregnation after

carbonization and the sol-gel method. For the composites from Method A2 treated by phosphoric acid, the crystal sizes slightly increased. This may be resulted by a chemical activation inside the composite during calcination, thus leading to the agglomeration of TiO_2 and the increase in the crystal size.

4.1.2 Nitrogen Adsorption

The nitrogen adsorption isotherms of the TiO_2/C and TiO_2/AC composites prepared by the novel method A and the conventional method B at various carbonization temperatures of 500, 600, and 700°C are illustrated in Figures 4.6-4.9. All samples exhibit the type I adsorption isotherm which is the typical isotherm of a microporous material [83]. Each isotherm exhibits three different adsorption zones which are typical of microporosity of carbon. The first zone, adsorption at very low pressure corresponds to the nitrogen adsorption in the micropore system. At the medium partial pressure, the second zone is created by the saturation of nitrogen adsorption in the micropores or so-called internal surface. At high relative pressure ($P/P_0 > 0.8$), the third one rises steeply due to the nitrogen adsorption on the external surface.

Figure 4.6 presents the adsorption isotherms of the TiO_2/C composites prepared by Method A1 and all isotherms are not superimposed with each other. There are some differences in nitrogen isotherms of the three samples obtained from the three temperatures. The isotherm of the composite sample at the carbonization temperature of 700 °C shows little higher absorbed amount of nitrogen than other samples while the isotherms of the samples at carbonization temperatures of 600 and 500°C give smaller absorbed amounts of nitrogen, respectively. The adsorption isotherms of the TiO_2/C composites prepared by Method A2 are shown in Figure 4.7 and also presented the typical isotherm type of micropore. The adsorption isotherms from the three temperatures are slightly different and the isotherm of the composite sample at the carbonization temperature of 600 °C shows relatively higher absorbed amount of nitrogen than 700 and 500°C, respectively. It is similar to the adsorption isotherms of the composites prepared by Method B1 in Figure 4.8. However, the adsorption isotherms for those methods are not significantly different. In contrast, the adsorption isotherm for Method B2 in Figure 4.9 is obviously different from those for other three methods. The plateau shows larger absorbed amount of nitrogen than other methods. It is due to extremely high surface area of the composite prepared by Method B2.

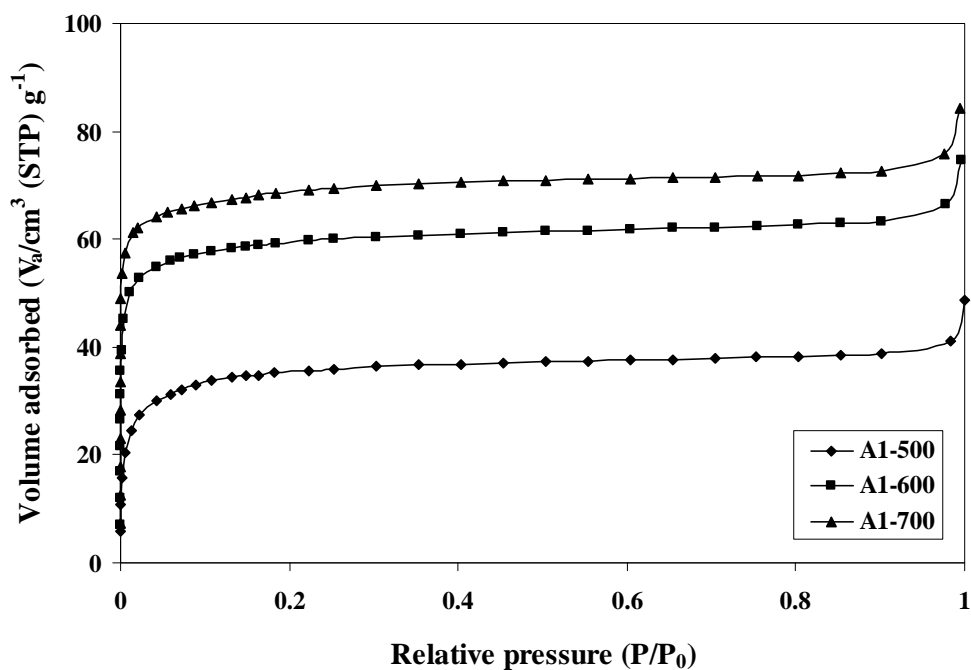


Figure 4.6 The N₂ adsorption isotherms of TiO₂/C composites prepared by Method A1 at various carbonization temperatures of 500, 600, and 700°C.

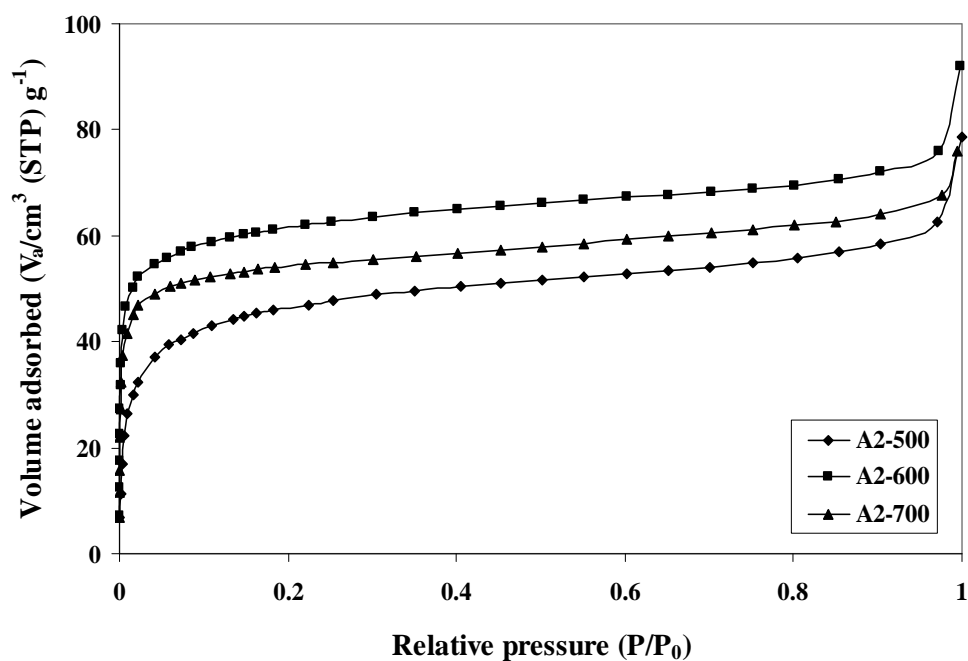


Figure 4.7 The N₂ adsorption isotherms of TiO₂/C composites prepared by Method A2 at various carbonization temperatures of 500, 600, and 700°C.

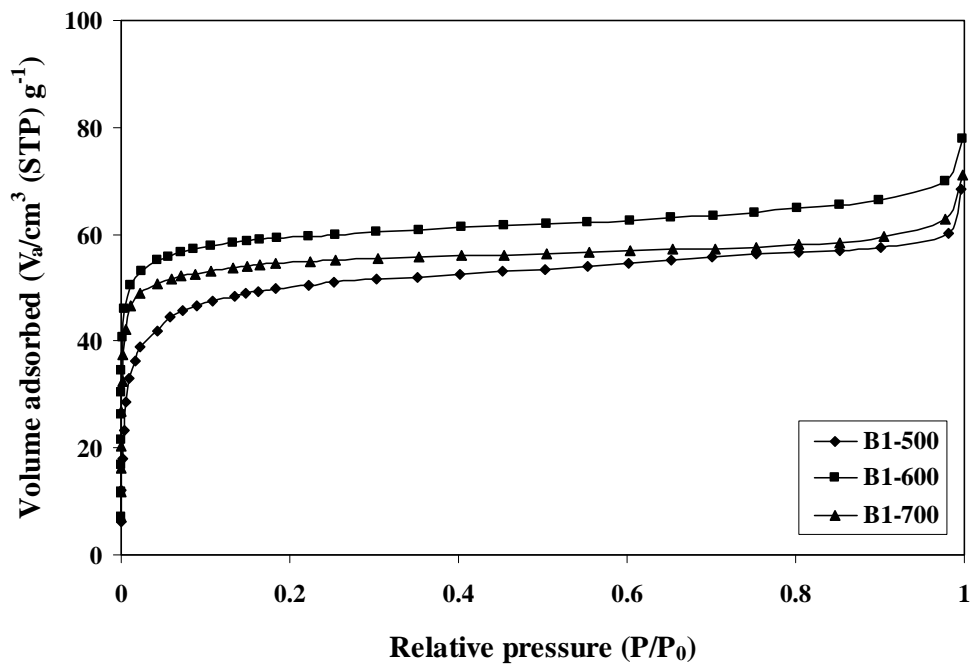


Figure 4.8 The N_2 adsorption isotherms of TiO_2/C composites prepared by Method B1 at various carbonization temperatures of 500, 600, and 700°C.

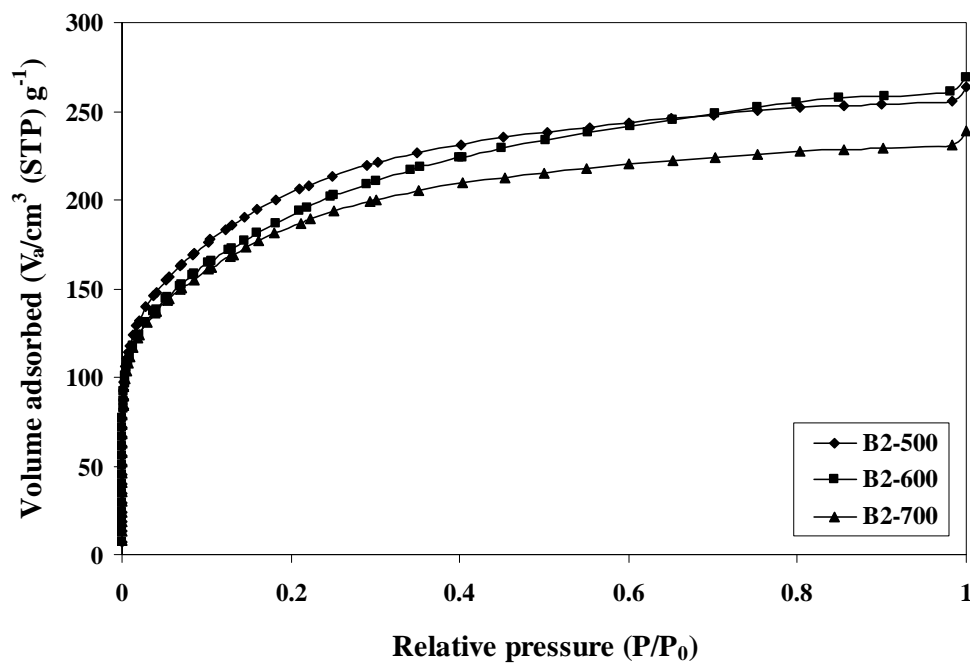


Figure 4.9 The N_2 adsorption isotherms of TiO_2/AC composites prepared by Method B2 at various carbonization temperatures of 500, 600, and 700°C.

Table 4.2 shows textural properties of TiO₂/C and TiO₂/AC composites obtained from different preparation methods at various carbonization temperatures. There is no significant difference among them in either BET specific surface area or external specific surface area except for the B2 Method providing extremely high specific surface areas at all temperatures. It is resulted from the activated carbon readily formed by Methods B2. It indicated that the chemical activation of carbon in the presence of TiO₂ is more difficult than the chemical activation of carbon without TiO₂. For methods A1, A2 and B1, the carbon was still not activated.

In addition, the formation of TiP₂O₇ must consume some H₃PO₄ especially at 700°C, thus this composite reduce the chance of carbon to react with H₃PO₄ to yield activated carbon. This is in agreement with the XRD result. Considering the effect of carbonization temperature on the specific surface area, it is obvious that the higher carbonization temperature the higher BET specific surface area was obtained. After H₃PO₄ treatment, the specific surface area was increased especially for the sample carbonized at 500°C. Surprisingly the BET specific surface area of the sample carbonized at 700°C decreased due to the formation of TiP₂O₇ have larger particle than TiO₂, and resulted in less space in the porous composite.

Table 4.2 Textural properties of composites obtained from different preparation methods at various carbonization temperatures of 500, 600, and 700°C

Samples	S _{BET} ^a (m ² /g)	d _p ^b (nm)	S _{ext} ^c (m ² /g)	V _{micro} ^c (cm ³ /g)
A1-500	135	0.8	9	0.0521
A1-600	227	0.6	11	0.0880
A1-700	259	0.6	13	0.1016
A2-500	174	0.7	35	0.0584
A2-600	231	0.6	29	0.0848
A2-700	208	0.6	30	0.0715
B1-500	190	0.6	22	0.0689
B1-600	229	0.6	18	0.0844
B1-700	212	0.6	12	0.0799
B2-500	711	1.0	174	0.2610
B2-600	680	1.0	170	0.2565
B2-700	661	1.0	134	0.2504

^a Specific surface area determined by application of the BET-plot method

^b Micropore size determined by application of the MP-plot method

^c External surface area and micropore volume determined by application of the t-plot method

4.1.3 SEM Images

SEM images of the unsupported TiO_2 (TiO_2 100%) prepared under N_2 at the calcination temperatures of 500, 600, and 700°C are shown in Figure 4.10. For bulk TiO_2 , the aggregation of TiO_2 crystallites was significant and SEM images exhibit the aggregation of TiO_2 crystallites with a large size of approximately 10-40 μm . Both particle size and shape are not uniform. It is obvious that the properties of TiO_2 samples synthesized without carbon at the three carbonization temperatures are not different in terms of crystal morphology.

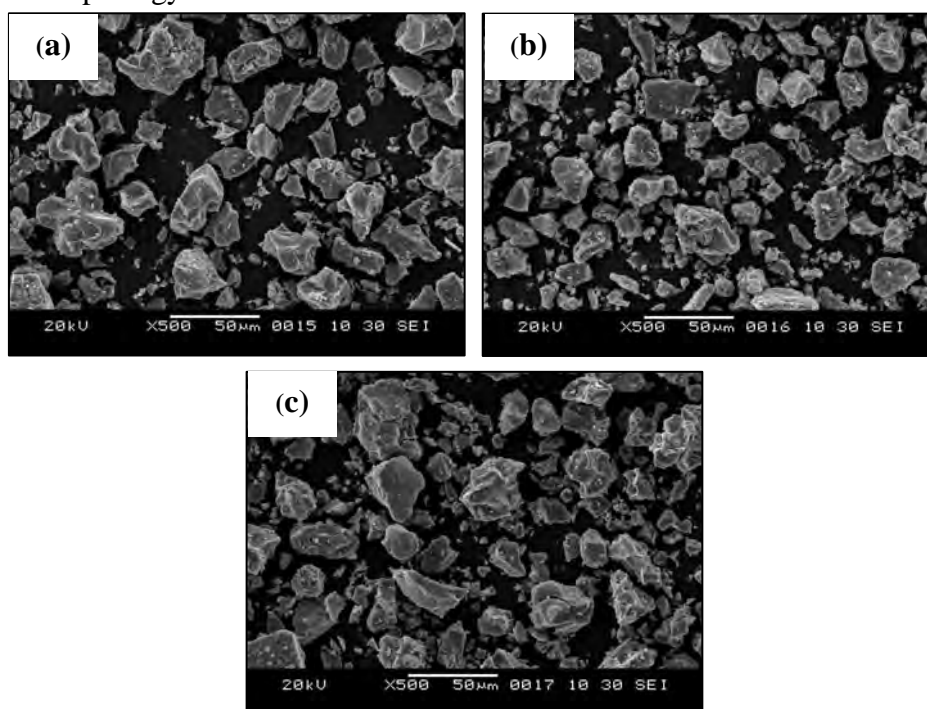


Figure 4.10 SEM images of the unsupported TiO_2 (TiO_2 100%) at various calcination temperatures of (a) 500°C, (b) 600°C, and (c) 700°C. All images are taken at a magnification of 500x.

SEM images of TiO_2/C composite prepared by Method A1 at carbonization temperatures of 500, 600, and 700°C show very small particles in Figure 4.11. It was observed that the TiO_2/C composites contain fine TiO_2 particles of approximately 70-100 nm distributed uniformly on the supported carbon surface. It agrees with XRD results that our proposed method, TTIP impregnation before carbonization, provides much small particle size because crystal growth was restricted by the microporous structures of carbon. For the TiO_2/C composite from Method A2 treated by

phosphoric acid, the particle sizes were not well distributed as obtained from method A1 and agglomeration was obviously observed as shown in Figure 4.12.

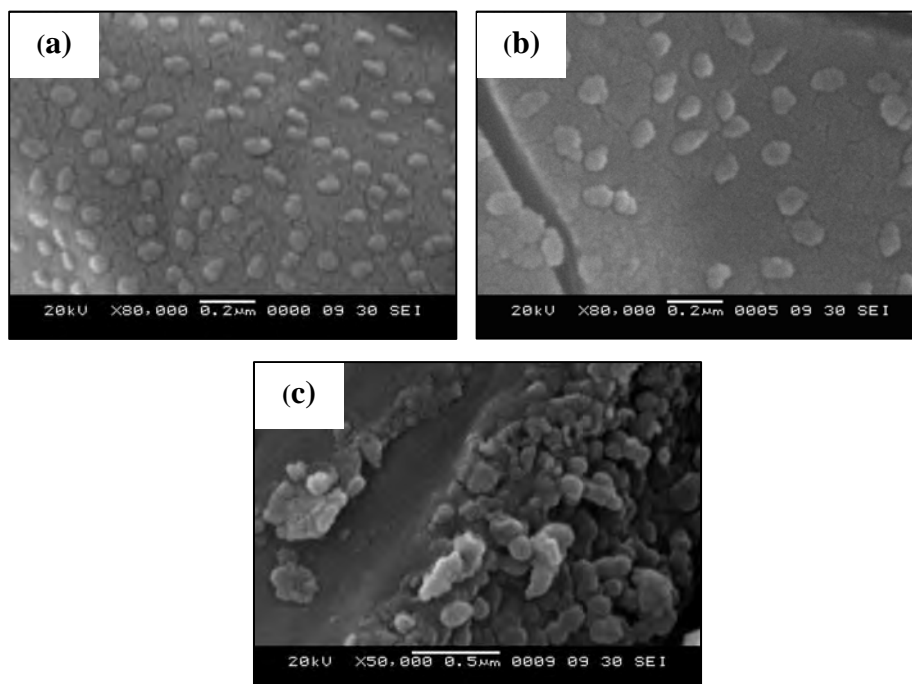


Figure 4.11 SEM images of TiO_2/C composites prepared by Method A1 at various carbonization temperatures of (a) 500°C, (b) 600°C at a magnification of 80,000x, and (c) 700°C at a magnification of 50,000x.

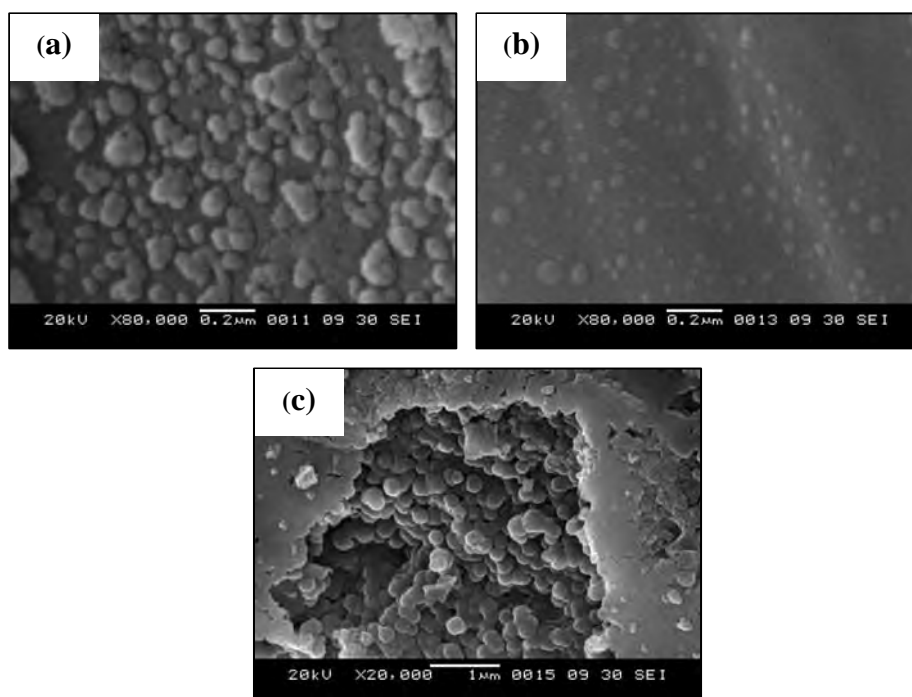


Figure 4.12 SEM images of TiO_2/C composites prepared by Method A2 at various carbonization temperatures of (a) 500°C, (b) 600°C at a magnification of 80,000x, and (c) 700°C at a magnification of 20,000x.

Figures 4.13 and 4.14 show TiO_2/C and TiO_2/AC composites at various carbonization temperatures of 500, 600, and 700°C prepared by Methods B1 and B2, respectively. It is clear that for the composites by the conventional method present significantly larger particles than those with the novel method and show non-uniform distribution of TiO_2 . SEM images indicated uneven distribution of TiO_2 like a bulk on the carbon surface. It is revealed that TiO_2 particles from the conventional method B preferred the location outside or on the carbon surface while TiO_2 particles from the novel method A preferred the site underneath the carbon surface.

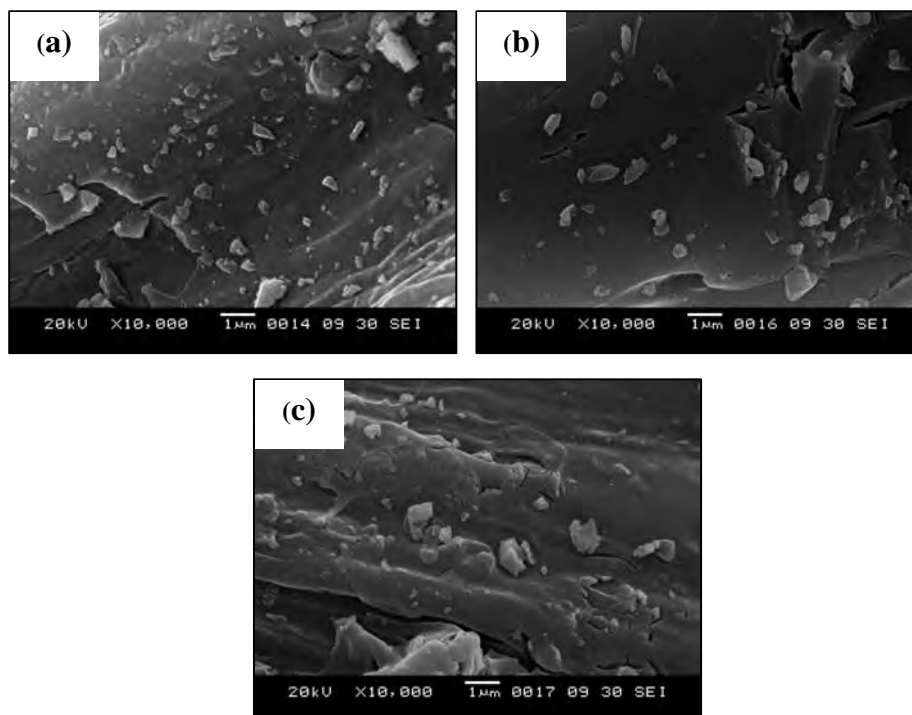


Figure 4.13 SEM images of TiO_2/C composites prepared by Method B1 at various carbonization temperatures of (a) 500°C, (b) 600°C (c) 700°C. All images are taken at a magnification of 10,000x.

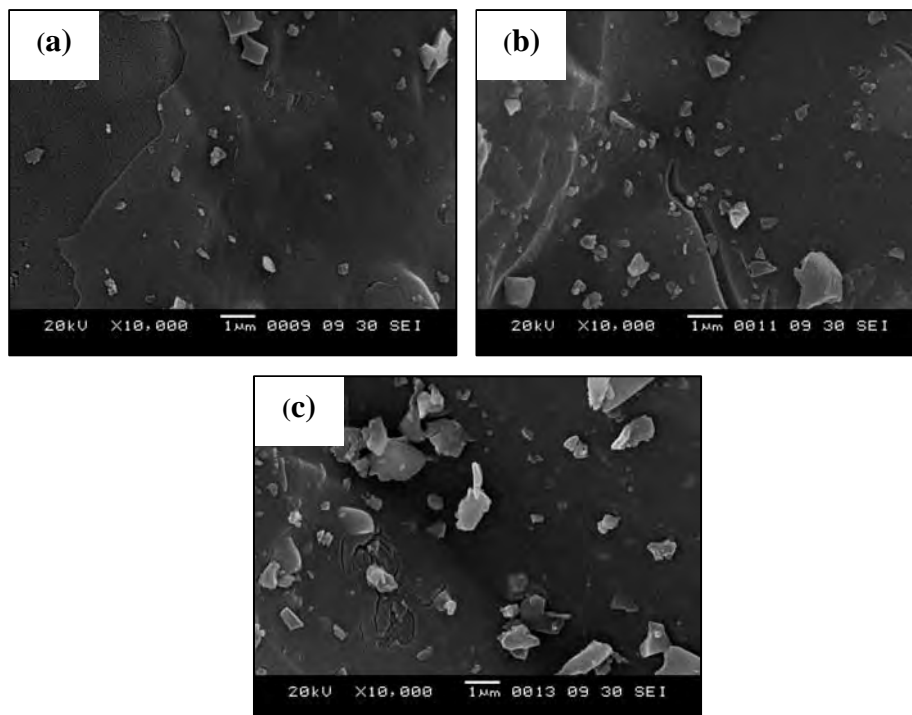


Figure 4.14 SEM images of TiO_2/AC composites prepared by Method B2 at various carbonization temperatures of (a) 500°C , (b) 600°C (c) 700°C . All images are taken at a magnification of 10,000x.

4.1.4 Electrochemical Properties

The capacitive behavior of these nanocrystalline composite electrodes has been studied using cyclic voltammetry, and electrochemical impedance spectroscopy measurements, and the results have been compared with those of carbon, activated carbon, and pure TiO_2 electrodes.

4.1.4.1 Cyclic Voltammograms

The cyclic voltammograms of the different electrode materials at a scan rate of 0.01 V/s are shown in Figures 4.15-4.20. Voltammetric testing was carried out at potentials between 0.5 and 1.0 V. The cyclic voltammograms of the carbon and the activated carbon electrode in Figures 4.15(a) and 4.15(b) present the typical rectangular like curve, expected for an ideal capacitor. This appearance shows the capacitive behavior of the electric double layer capacitor electrodes. Curves are symmetric for both carbon and activated carbon electrodes, which may be due to the capacitance arising solely due to the double layer. For porous carbon electrodes, it

is well known that the capacitance and the non-Faradaic current of carbon electrode increase by activation of the carbon. The activated carbon electrode has better conductivity than the unactivated carbon electrode because higher surface area of the activated carbon promotes the electric double layer capacitor or supercapacitor that can store high energy, so-called high energy density.

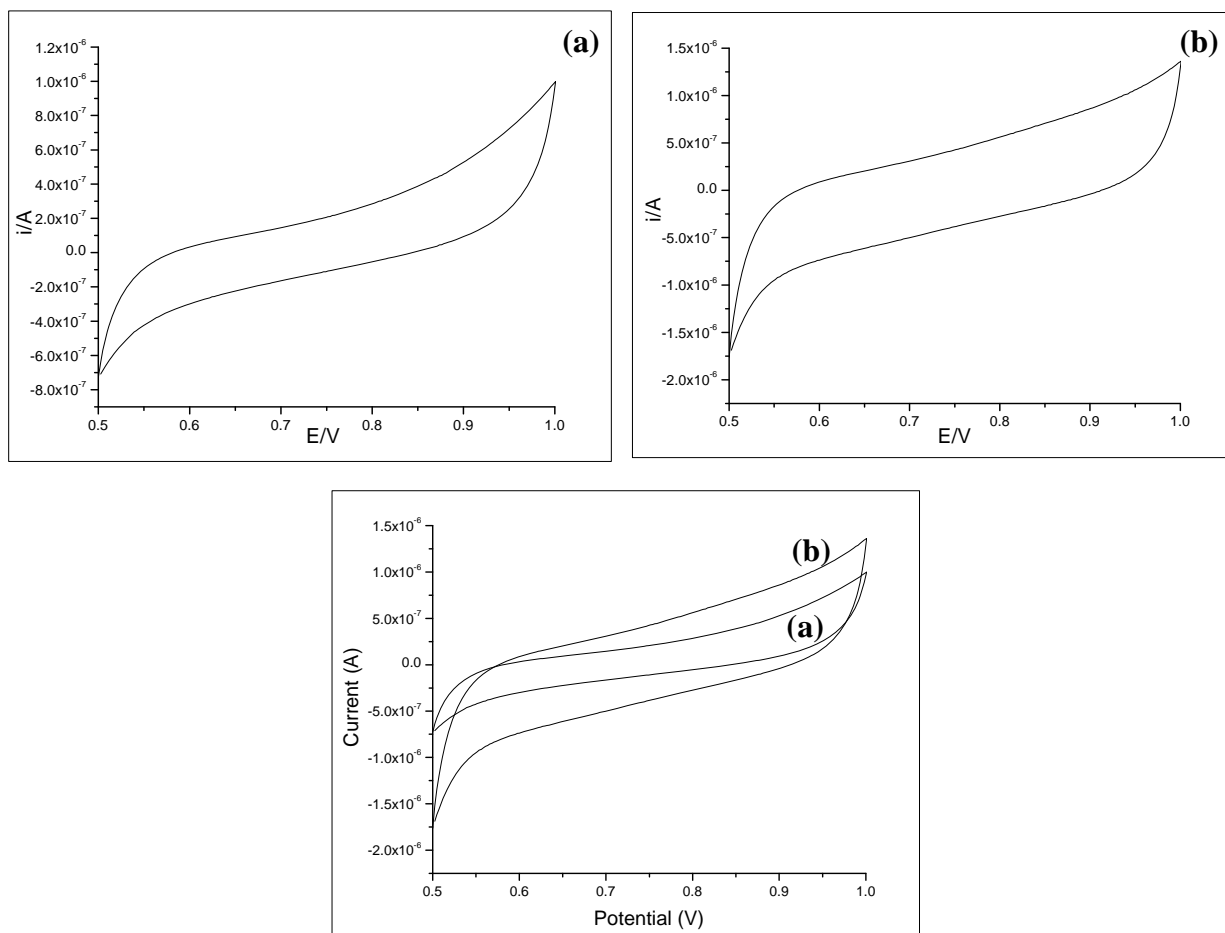


Figure 4.15 Cyclic voltammograms of (a) carbon (b) activated carbon electrodes in 1 M H_2SO_4 .

Metal oxide/carbon electrodes such as TiO_2/C or TiO_2/AC electrodes as shown in Figures 4.16-4.19 provided the lack of symmetry to the curves due to combination of double layer and pseudo capacitances contributing to the total capacitance. The area of these curves also increased with TiO_2 functionalization, indicating an enhancement of the specific capacitance for those electrodes. Figure 4.20 shows cyclic voltammograms of the unsupported bulk TiO_2 (pure TiO_2) electrodes at a scan rate of 0.01 V/s which presents the typical rectangular similar to those of the composites. However, the average current is

rather lower than others. For all sample electrodes obtained from different preparation methods, the average current at the carbonization temperature of 500°C is higher than those at 600 and 700°C, respectively as shown in the Table 4.3.

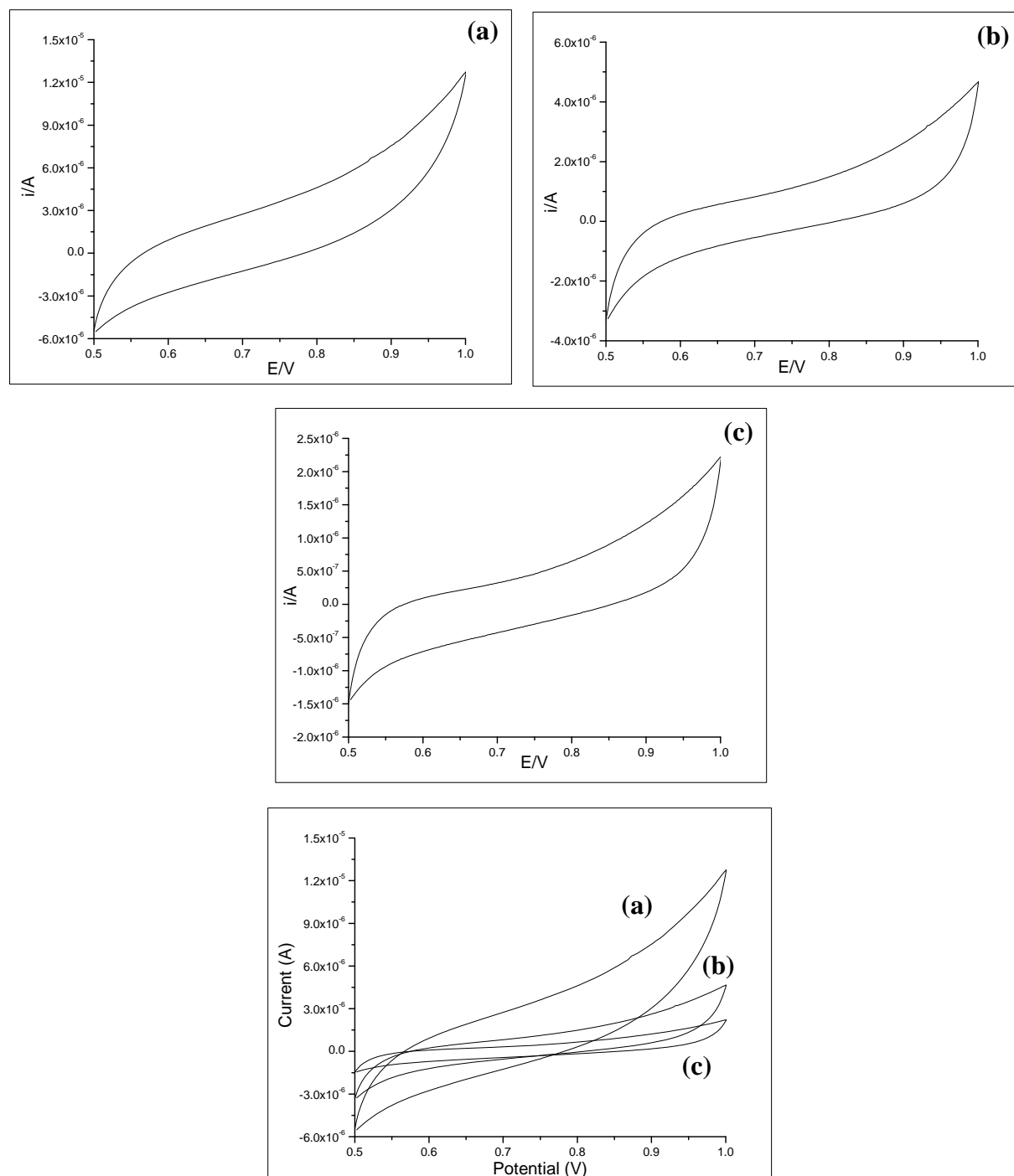


Figure 4.16 Cyclic voltammograms of TiO_2/C composite electrodes prepared by Method A1 at various carbonization temperatures of (a) 500°C, (b) 600°C, and (c) 700°C in 1 M H_2SO_4 .

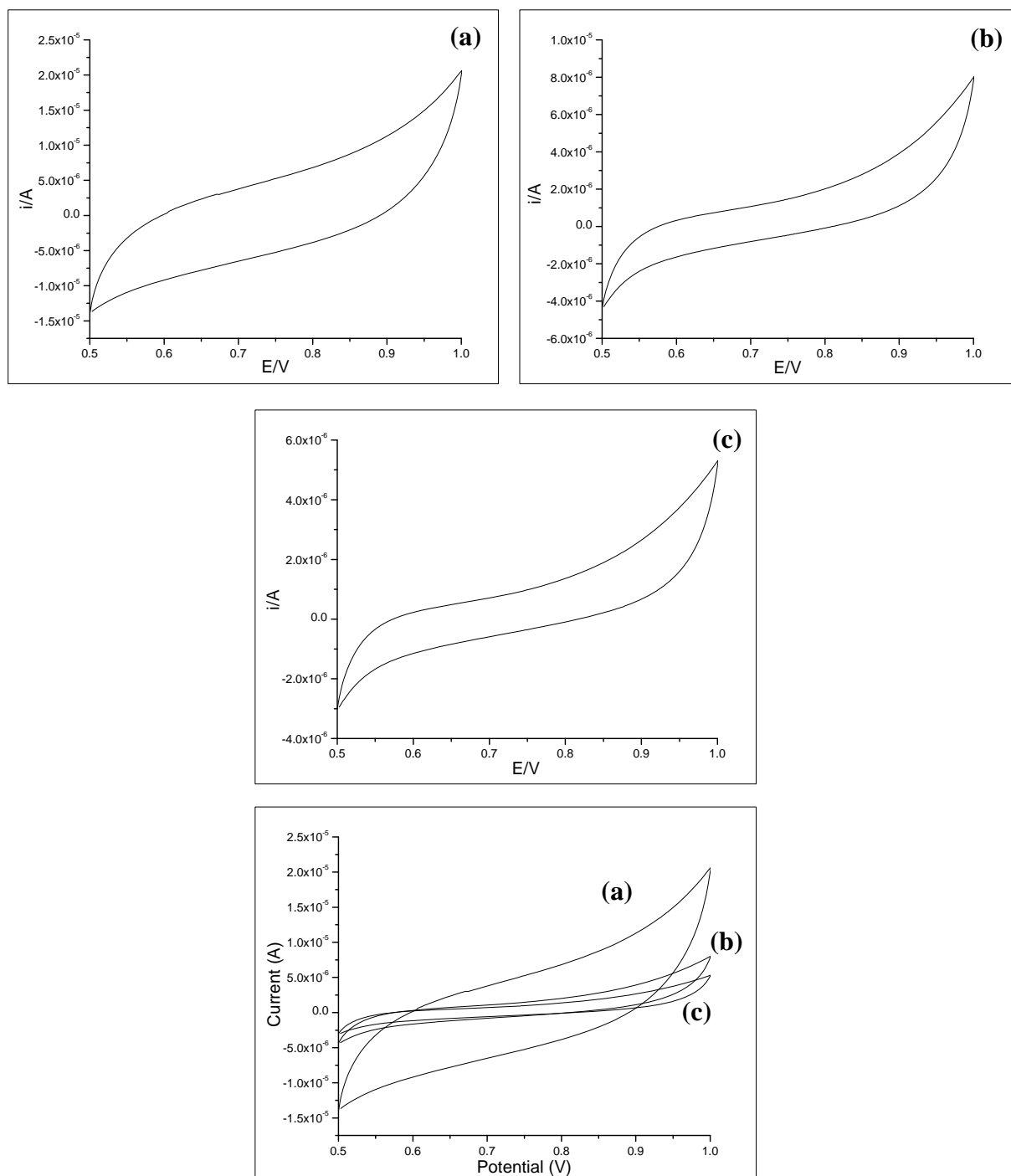


Figure 4.17 Cyclic voltammograms of TiO₂/C composite electrodes prepared by Method A2 at various carbonization temperatures of (a) 500°C, (b) 600°C, and (c) 700°C in 1 M H₂SO₄.

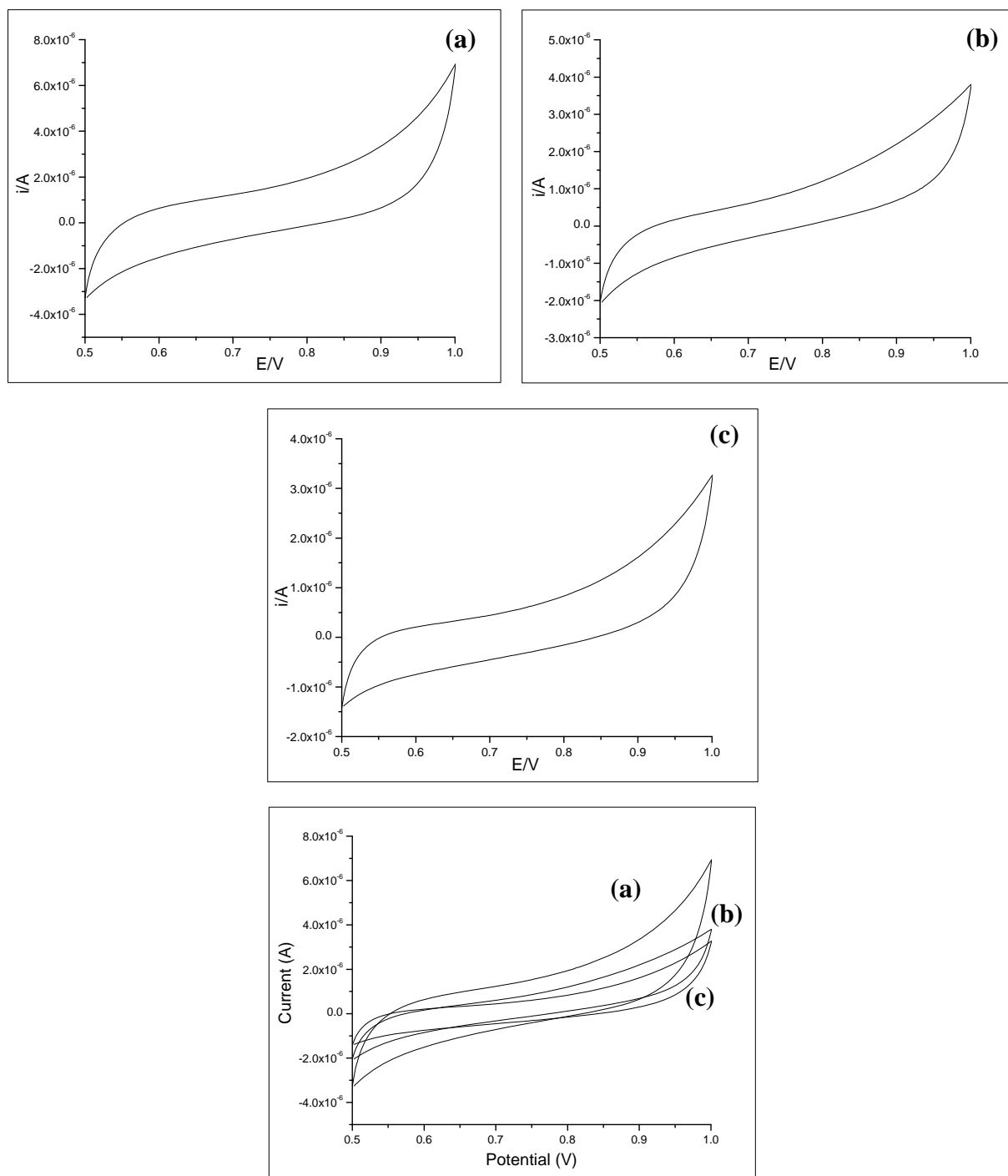


Figure 4.18 Cyclic voltammograms of TiO_2/C composite electrodes prepared by Method B1 at various carbonization temperatures of (a) 500°C , (b) 600°C , and (c) 700°C in $1\text{ M H}_2\text{SO}_4$.

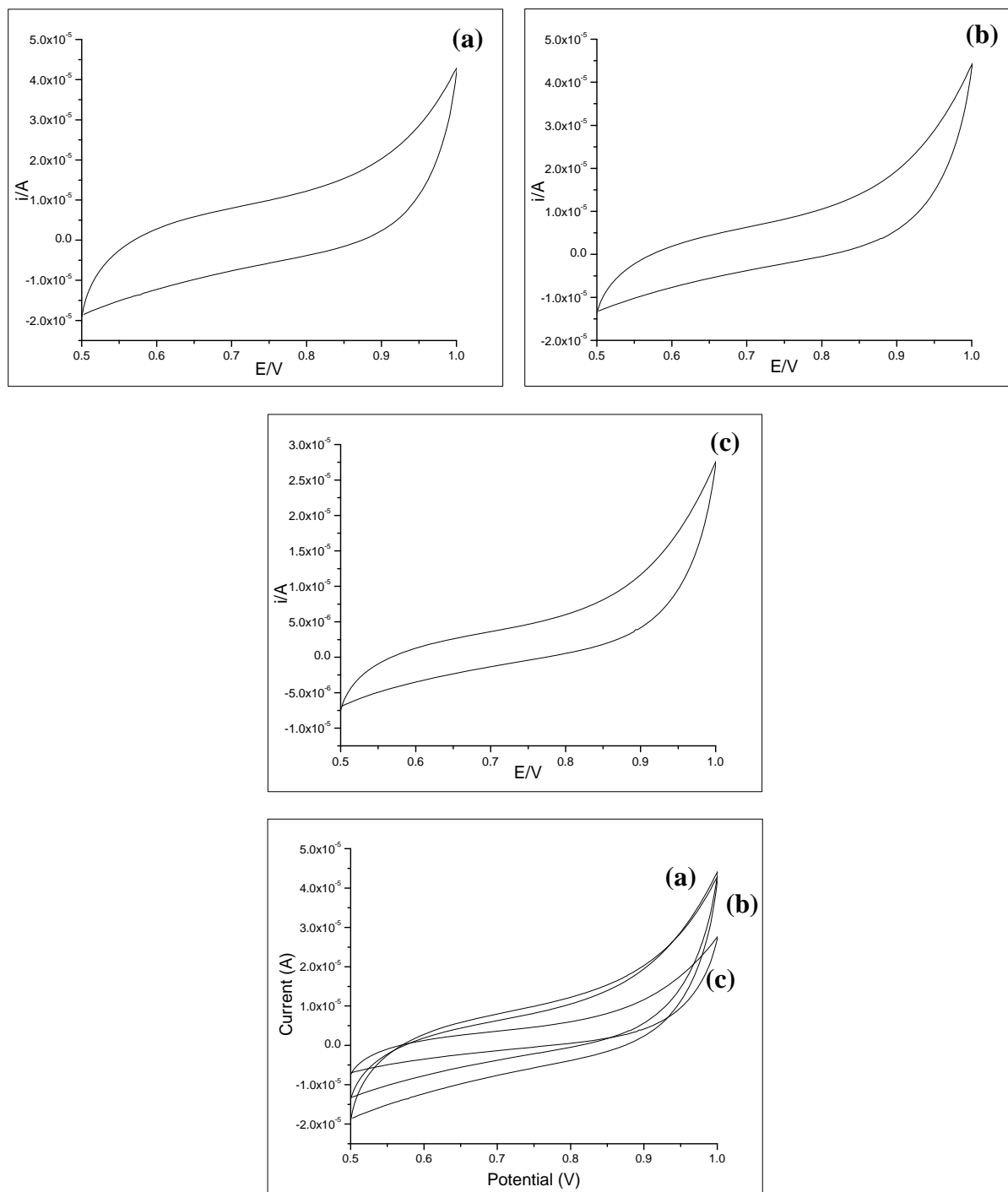


Figure 4.19 Cyclic voltammograms of TiO_2/AC composite electrodes prepared by Method B2 at various carbonization temperatures of (a) 500°C, (b) 600°C, and (c) 700°C in 1 M H_2SO_4 .

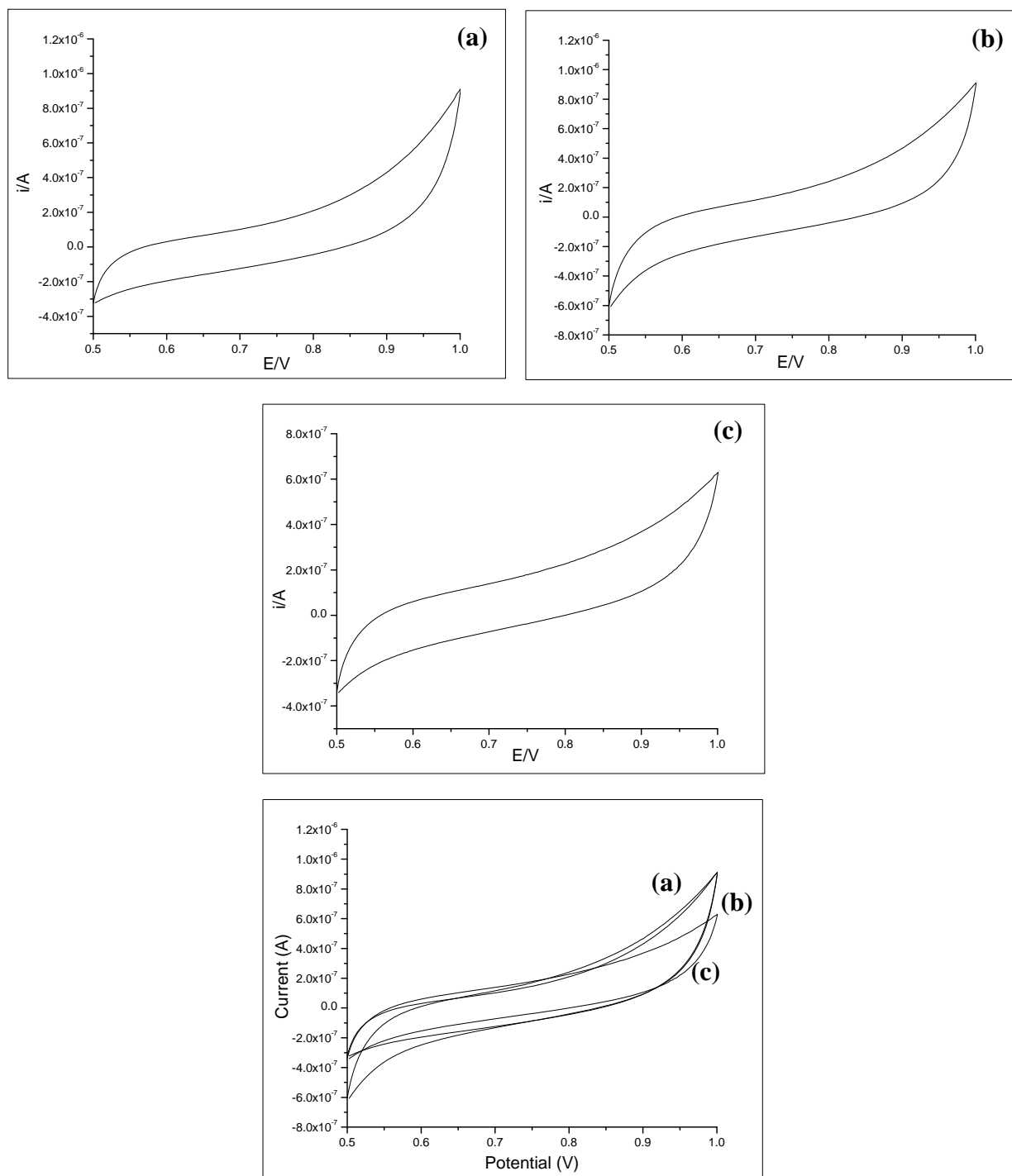


Figure 4.20 Cyclic voltammograms of the unsupported bulk TiO_2 (TiO_2 100%) electrodes at various calcination temperatures of (a) 500°C, (b) 600°C, and (c) 700°C in 1 M H_2SO_4 .

From the cyclic voltammetric curve in Figures 4.15-4.20, the average current was obtained and listed in Table 4.3. It is shown that the values of average current of carbon and activated carbon electrodes are very low. For the unsupported anatase electrode prepared by sol-gel method, the average current is similar to those values for carbon and activated carbon. It is exhibited that loading of TiO₂ on the supporting carbon increases the electric capacitance although TiO₂ itself has low electric capacitance. It can be seen that the average current of bulk TiO₂ is low. The average current tends to increase with phosphoric acid treatment in Method A2 and B2 because this performance provides the extremely porous material to enhance the electric capacitance. The average current of the composite electrodes at the carbonization temperature of 500°C is significantly higher than those at other temperatures. This agreed with the significant increase of the specific surface area of those samples.

Table 4.3 The average current from cyclic voltammetry of the sample electrodes obtained from different preparation methods at various carbonization temperatures of 500, 600, and 700°C

Conditions	The average current (Ampere, A)		
	500°C	600°C	700°C
Carbonization temperature			
Method A: TTIP impregnation before carbonization			
- TiO ₂ /C (A1)	2.31×10 ⁻⁶	7.82×10 ⁻⁷	5.25×10 ⁻⁷
- TiO ₂ /C (A2)	4.66×10 ⁻⁶	1.10×10 ⁻⁶	7.53×10 ⁻⁷
Method B: TTIP impregnation after carbonization			
- TiO ₂ /C (B1)	1.12×10 ⁻⁶	6.51×10 ⁻⁷	4.13×10 ⁻⁷
- TiO ₂ /AC (B2)	7.96×10 ⁻⁶	6.73×10 ⁻⁶	4.66×10 ⁻⁶
Bulk TiO ₂	1.30×10 ⁻⁷	1.20×10 ⁻⁷	1.10×10 ⁻⁷
Carbon	1.76×10 ⁻⁷		
Activated carbon	3.98×10 ⁻⁷		

The specific capacitance can be obtained from the cyclic voltammetric curve according to the following equation:

$$C = \frac{i}{sm}$$

Where C represents the total specific capacitance of sample electrode, i is the average current of anodic and cathodic process obtained from the positive and negative sweeps of cyclic voltammogram, s is the potential sweep rate, and m is the mass of each composite electrode [89].

Table 4.4 summarized the specific capacitance of carbon, activated carbon, bulk TiO_2 and their composites, which were calculated from the cyclic voltammogram by the equation above. The specific capacitance value of the pure carbon electrode is 35 mF/g enhanced to 80 mF/g of pure activated carbon electrode because the performance through phosphoric acid treatment provides the higher specific surface areas which lead to the more charging current of the electric double layer capacitor electrode. The novel method A, TTIP impregnation before carbonization, provides the specific capacitance in the range of 105-932 mF/g while the conventional method B, TTIP impregnation after carbonization, provides the specific capacitance in the range of 83-1,592 mF/g. It can be seen that the poor performance of pure TiO_2 electrodes exhibit very low capacitance in the range of 22-26 mF/g.

Table 4.4 The specific capacitance calculated from cyclic voltammetry of the sample electrodes obtained from different preparation methods at various carbonization temperatures of 500, 600, and 700°C

Conditions	Specific capacitance from cyclic voltammetry (mF/g)		
	500°C	600°C	700°C
Carbonization temperature			
Method A: TTIP impregnation before carbonization			
- TiO_2/C (A1)	462	156	105
- TiO_2/C (A2)	932	220	151
Method B: TTIP impregnation after carbonization			
- TiO_2/C (B1)	224	130	83
- TiO_2/AC (B2)	1,592	1,346	932
Bulk TiO_2	26	24	22
Carbon	35		
Activated carbon	80		

The specific capacitance of carbon is enhanced by modification of TiO₂. It can be explained that this is due to the interaction between carbon and TiO₂, namely, the electric effect of semiconducting TiO₂ nanoparticles. It has been known that carbon electrode is rather polarizable and the resulted polarization adversely affect performance of the capacitors because polarization may reduce the accumulation of the ions on double-layer. Therefore, reducing polarization of carbon has been considered to be an effective approach toward the improved capacitance of the double layer capacitors. *H. Liang et al.* [54] has been reported that charges on the surface of TiO₂ (an n-type semiconductor) are more than the other regions due to the attractive contribution of the positively charged depletion region. So the polarization of carbon can be reduced by modifying carbon with semiconducting TiO₂, especially these with nanosize from our proposed method. For all sample electrodes obtained from different preparation methods, the specific capacitance value at carbonization temperature of 500°C is the highest and the method with phosphoric acid treatment exhibits the increase of the capacitance of double layer capacitors.

In comparison of Method A1 with B1, which is not treated by phosphoric acid, the specific capacitance of the composites by the novel method A1 is significantly higher than the conventional method B1, especially at the carbonization temperature of 500°C. It can be explained by the smaller crystal size of TiO₂ which is almost one half of that prepared by the conventional method (see Table 4.1). Therefore, the small anatase crystal sizes are expected to improve capacitive behavior.

At all carbonization temperatures, the conventional method B2 provides significantly higher specific capacitance than the novel method A2 although the crystal size of TiO₂ from the novel method is smaller. It indicated that the extremely high surface areas of the conventional method B2 much influenced on capacitive behavior and at the carbonization temperature of 500°C, the highest surface areas is up to 711 m²/g (see Table 4.2) so this method provides the highest capacitance of 1,592 mF/g.

It is found that the performance through phosphoric acid treatment in Method A2 provides the higher specific capacitance than that without phosphoric acid treatment in Method A1. Such surface functional groups may play essential roles in the improvement and curing on the surface of the composite. Especially, the carbonization temperature of 500°C which is the effective carbonization temperature when treated by phosphoric

acid in Method A2 increases the specific capacitance value almost twice of Method A1 (increases from 462 mF/g to 932 mF/g). It is likely that the effect of higher surface area after phosphoric acid treatment of the sample enhancing the capacitance of the electrode. The capacitance value slightly increases at others carbonization temperatures.

For Methods B1 and B2, it was found that the specific capacitance value of Method B2 is higher than Method B1. This is a result from an effective activation to obtain the extremely high surface area that causes the high capacitance. In conclusion, the specific capacitance value at the carbonization temperature of 500°C is the highest among those from other. The specific capacitance values at this carbonization temperature are 932 and 1,592 mF/g for the novel method and the conventional method, respectively.

However, both of the specific surface area and the crystal size of TiO₂ influences the capacitance of the capacitive electrode. A high surface area of the composite and the small crystal size of TiO₂ are a key factor to increase the electric double layer at the surface of electrode in achieving a high capacitance. The performance through phosphoric acid treatment in the preparation steps leads to an increase in the electric conductivity and a decrease in resistance for supporting the capacitive behavior of electrode. The suitable TiO₂ contents in the composite may play essential roles in the improvement on the total specific capacitance that will be discussed in next section.

4.1.4.2 Electrochemical Impedance Spectra

The impedance plot consists of the real part (Z') at the horizontal axis, the imaginary part (Z'') at the vertical axis and the measurements carried out from high frequencies to low frequencies. The charge-transfer process at the electrode electrolyte interface is determined by the region represented by a semicircle at higher frequencies, whereas the straight line inclined at an angle of around 45° to the real part axis (Z') represents the diffusion-controlled electrode kinetics in the lower frequency region and known as the Warburg impedance. The impedance plot should theoretically be a vertical line, parallel to the imaginary axis. In fact, a difference between this theoretical behavior and experimental can be observed.

The complex plane impedance spectra for carbon and activated carbon electrodes are presented in Figures 4.21(a) and 4.21(b). The presence of a small semicircular loop for each electrode is due to the double layer charging capacitance of the electrodes. It was found that the values read from the intercepts of the semicircle at the left of the real part axis were similar, indicating the similar solution resistance of the electrochemical capacitor electrodes. The semicircle diameter of the activated carbon is slightly increased but the capacitance value is not different and shown in Table 4.5. It was observed that the impedance (Z') is very high cause by the large polarization resistance of the carbon electrode.

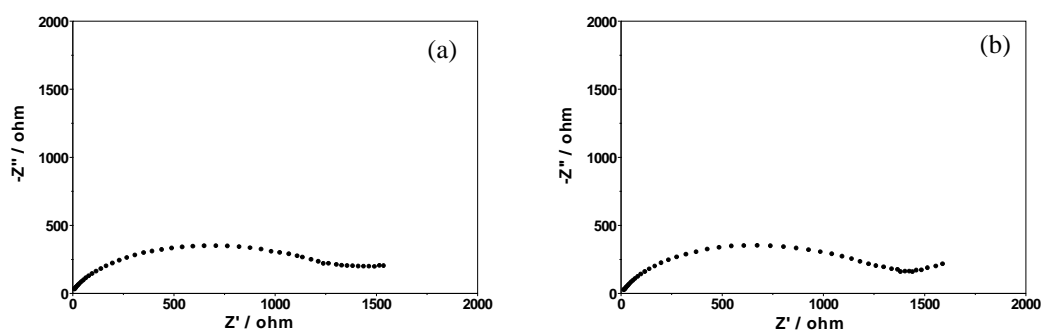


Figure 4.21 Complex-plane impedance spectra of electrochemical capacitors with electrode material made by (a) carbon (b) activated carbon.

Figure 4.22 presents complex plane impedance plots for the TiO_2/C composite by Method A1. The semicircle diameter of impedance spectra at three carbonization temperatures is not significantly different but it is obviously different from those carbon and activated carbon electrode. The impedance (Z') is lower it indicates that the polarization resistance is decrease and increasing in the capacitance. Those of reason cause by modification carbon with anatase TiO_2 . However, the TiO_2/C composite of Method A1 prepared at carbonization temperature of 500°C exhibits the lowest Warburg impedance indicating that the preparation at this temperature could enhance the diffusion of ion within pores of electrochemical electrodes. Complex plane impedance plots for TiO_2/C composite prepared by Method A2 shown in Figure 4.23. The semicircular loop of impedance spectra at carbonization temperatures of 600 and 700°C is not obviously different but the carbonization temperature of 500°C is rather different from others.

The complex plane impedance spectra for TiO_2/C composite prepared by Method B1 are presented in Figure 4.24 and the semicircular loop is similar to the result from Method A1. The difference is the length of Warburg impedance from Method B1 is rather increased so the diffusion of ions within pore of electrode will be decreased. It is caused that why the capacitance from the conventional method B1 is lower than the novel method A1. The results from AC impedance agree with those obtained from cyclic voltammetric technique. It suggests that our proposed method is better than the conventional method in case which is not performed through phosphoric acid treatment. Figure 4.25 presented complex plane impedance plots for the TiO_2/AC composite by Method B2 and the impedance plot is similar to Method B1. The impedance spectra of bulk TiO_2 are shown in Figure 4.26. The impedance values (Z') are rather high like those from carbon and activated carbon electrode cause by the high resistance of the pure TiO_2 .

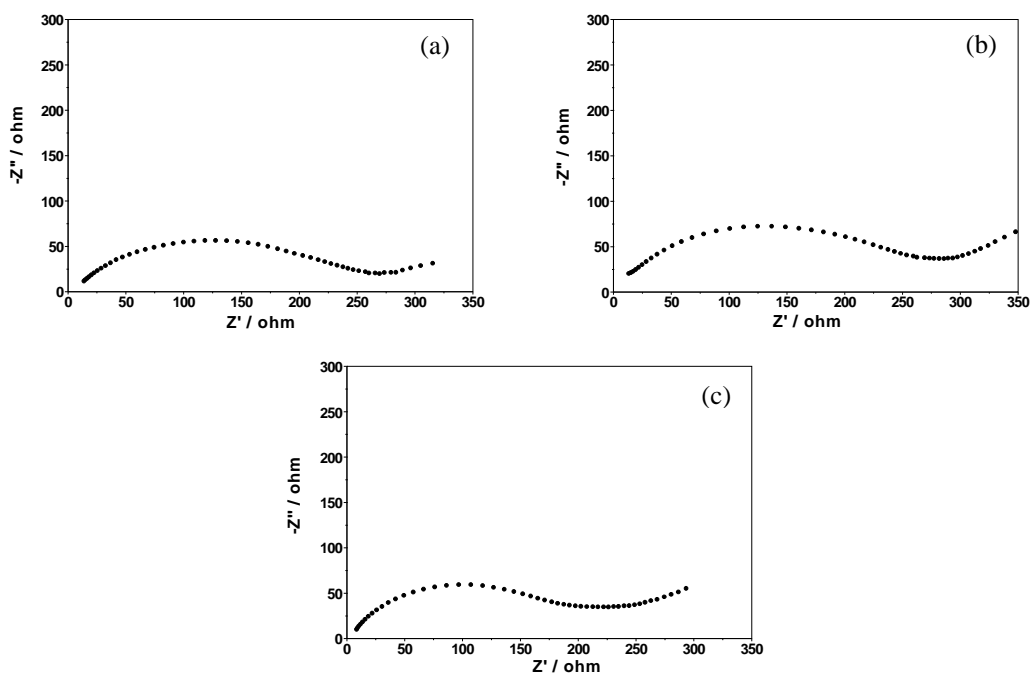


Figure 4.22 Complex-plane impedance spectra of electrochemical capacitors with electrode material made by Method A1 at various carbonization temperatures of (a) 500°C, (b) 600°C, and (c) 700°C.

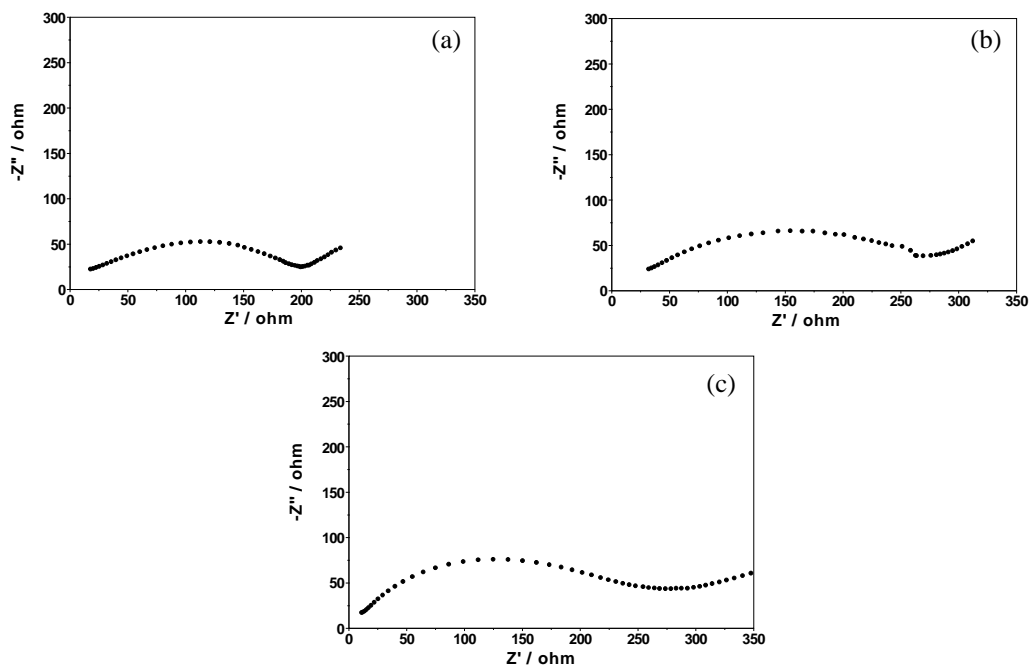


Figure 4.23 Complex-plane impedance spectra of electrochemical capacitors with electrode material made by Method A2 at various carbonization temperatures of (a) 500°C, (b) 600°C, and (c) 700°C.

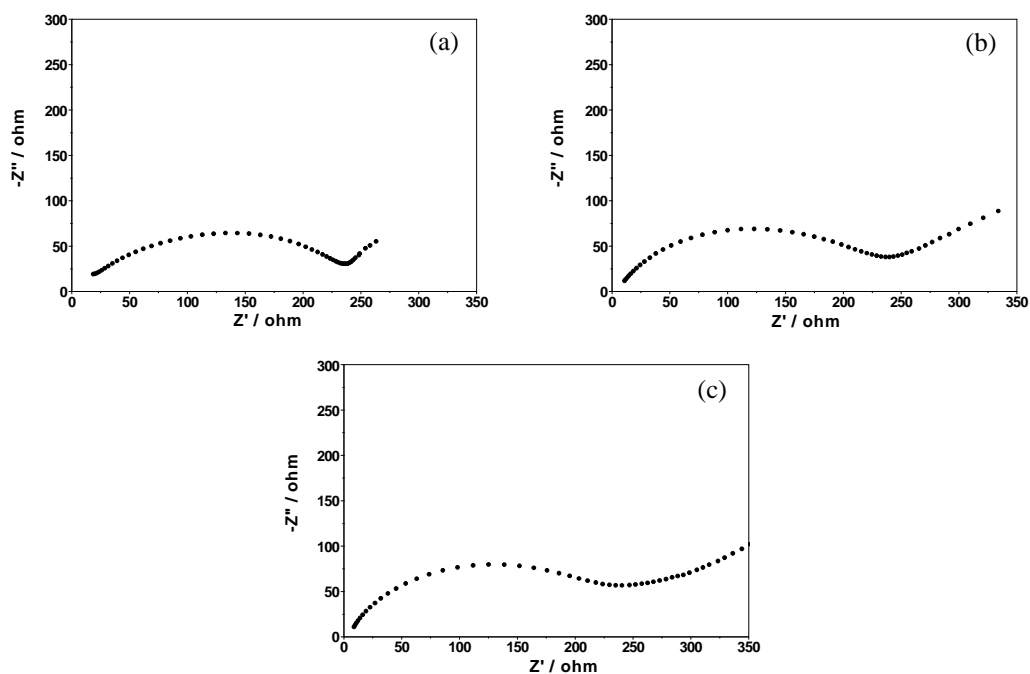


Figure 4.24 Complex-plane impedance spectra of electrochemical capacitors with electrode material made by Method B1 at various carbonization temperatures of (a) 500°C, (b) 600°C, and (c) 700°C.

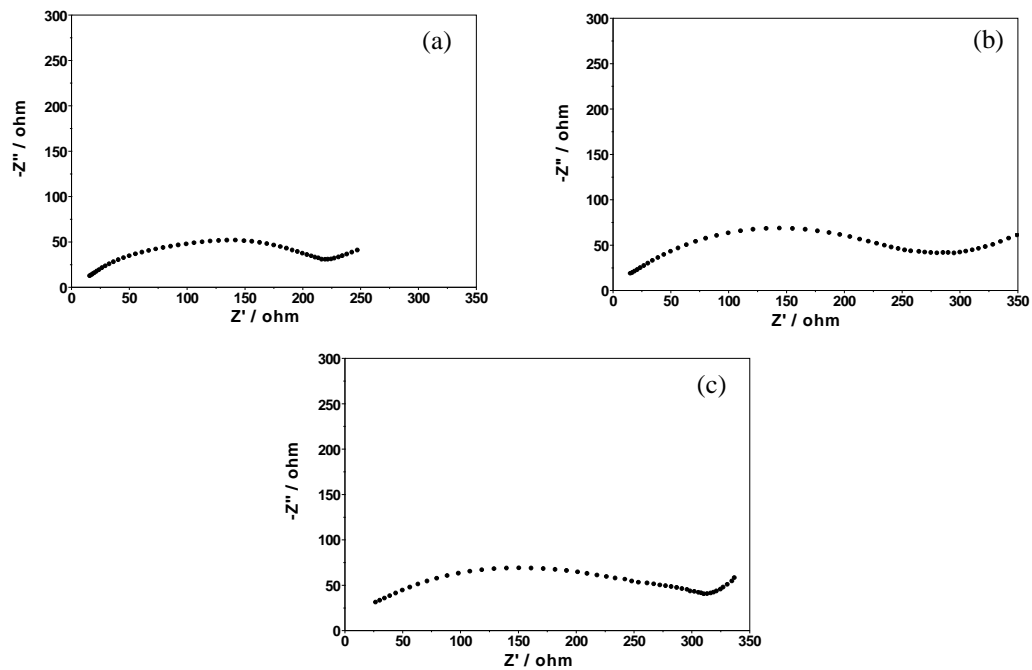


Figure 4.25 Complex-plane impedance spectra of electrochemical capacitors with electrode material made by Method B2 at various carbonization temperatures of (a) 500°C, (b) 600°C, and (c) 700°C.

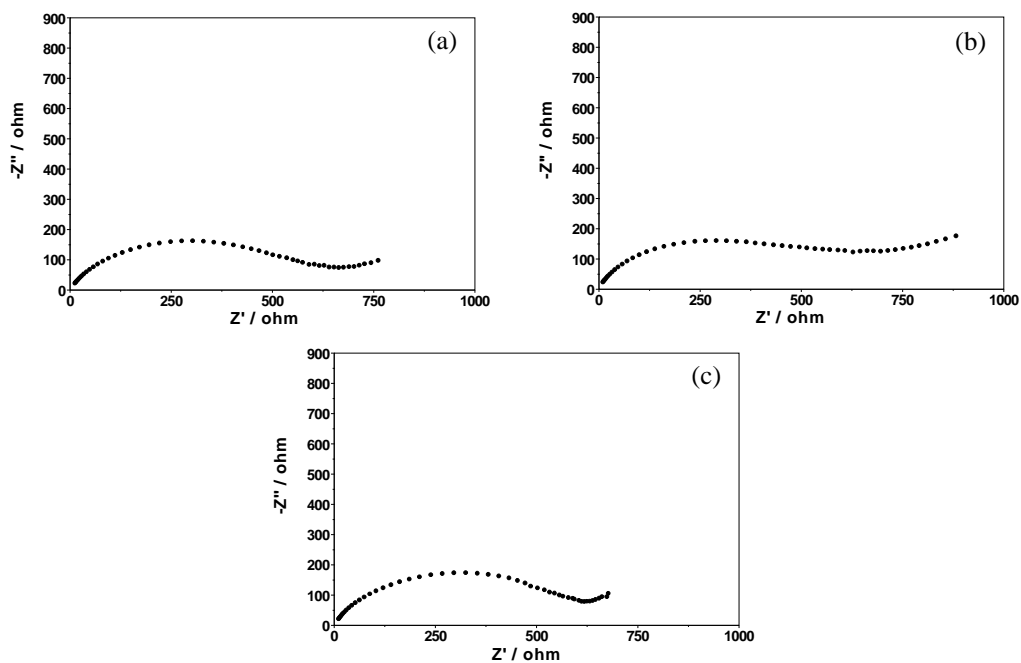


Figure 4.26 Complex-plane impedance spectra of electrochemical capacitors with electrode material made by the unsupported TiO_2 (TiO_2 100%) at various calcination temperatures of (a) 500°C, (b) 600°C, and (c) 700°C.

The specific capacitance values were obtained by fitting the impedance curve calculated by electrochemical software (Autolab PGSTAT 30, FRA software). Table 4.5 summarizes the specific capacitance of carbon, activated carbon, bulk TiO₂ and their composites which were calculated from electrochemical impedance spectroscopy. The specific capacitance of the carbon and activated carbon electrode is low and not different. Because of the carbon electrode is rather polarizable and the resulted polarization may reduce the diffusion of ions on double layer. It can be seen that the poor performance of pure TiO₂ electrodes provided the low capacitance in the range of 57-79 mF/g because the high resistance of TiO₂ electrodes.

The novel method A, TTIP impregnation before carbonization, provides the specific capacitance in the range of 92-381 mF/g while the conventional method B, TTIP impregnation after carbonization, provides the specific capacitance in the range of 67-423 mF/g. The specific capacitance values at the carbonization temperature of 500°C are the highest among those obtained from preparation methods and the Method B2 provides the highest capacitance values.

Table 4.5 The specific capacitance calculated from electrochemical impedance spectroscopy of the sample electrodes obtained from different preparation methods at carbonization temperatures of 500, 600, and 700°C

Conditions	Specific capacitance from electrochemical impedance spectroscopy (mF/g)		
	500°C	600°C	700°C
Carbonization temperature			
Method A: TTIP impregnation before carbonization			
- TiO ₂ /C (A1)	259	123	92
- TiO ₂ /C (A2)	381	146	103
Method B: TTIP impregnation after carbonization			
- TiO ₂ /C (B1)	187	95	67
- TiO ₂ /AC (B2)	423	216	158
Bulk TiO ₂	79	69	57
Carbon	52		
Activated carbon	59		

Table 4.6 shows the comparison between the specific capacitance values of the sample electrodes from cyclic voltammetric technique and those of from electrochemical impedance spectroscopic technique. Although the values of specific capacitance from electrochemical impedance spectroscopic technique are less than those calculated by cyclic voltammetric technique, the results show similar trend. The specific capacitance values of pure carbon, pure activated carbon, and bulk TiO₂ electrodes from both techniques are very low. To improve capacitive behavior, enhance stability, and increase conductivity, TiO₂ has been attached to carbon or activated carbon to form the composite. Thus, the specific capacitance values of the composite electrodes from both techniques are significantly increased. Especially, the carbonization temperature of 500°C at all preparation methods is the excellent carbonization temperature showing the highest specific capacitance values. The composite electrode prepared by the novel method and the conventional method shows the highest specific capacitance values from cyclic voltammetric technique of 932 and 1,592 mF/g, respectively. Whereas, the composite prepared by the novel method and the conventional method provides the highest specific capacitance values from electrochemical impedance spectroscopic technique are 381 and 423 mF/g, respectively.

Table 4.6 A comparison of the specific capacitance obtained from different techniques of the sample electrodes by different preparation methods at various carbonization temperatures of 500, 600, and 700°C

Conditions	Specific capacitance (mF/g)					
	Cyclic voltammetry			Electrochemical impedance spectroscopy		
Carbonization temperature	500°C	600°C	700°C	500°C	600°C	700°C
Method A:						
- TiO ₂ /C (A1)	462	156	105	259	123	92
- TiO ₂ /C (A2)	932	220	151	381	146	103
Method B:						
- TiO ₂ /C (B1)	224	130	83	187	95	67
- TiO ₂ /AC (B2)	1,592	1,346	932	423	216	158
Bulk TiO ₂	26	24	22	79	69	57
Carbon	35			52		
Activated carbon	80			59		

4.2 Effect of TiO₂ Contents in the Composite on Composite Properties

To study the effect of TiO₂ content in the composite on the capacitive performance of the composite electrode, all the composite samples were synthesized with various amounts of TiO₂ of 10, 20, 30, and 40 wt% in the composite. The carbonization temperature of 500°C was used.

4.2.1 XRD Patterns

XRD patterns of TiO₂/C composites prepared by Methods A1 and A2 at carbonization temperature of 500°C and at 10-40 wt% TiO₂ contents in the composites are shown in Figures 4.27 and 4.28, respectively. All XRD patterns of the samples are similar in intensities of five main characteristic peaks of anatase structure at the Bragg angles, 2θ of 25.3, 37.8, 48.0, 53.9, and 55.0 degrees. They are similar to that reported by *B. Jiang et al.* [50] and no other crystalline phase was observed in Method A1. It can be seen that with increasing TiO₂ content, the peak intensities of anatase increase, as shown in Figure 4.27. The broad bump of the baseline around 20-30 degrees due to the amorphous phase of carbon. For Method A2 in Figure 4.28, the significant change is that the pyrophosphate (TiP₂O₇) phase was found because this method was performed through phosphoric acid treatment followed by heating. It is well known that poly-anion type compound, such as TiP₂O₇ can keep their crystal structure during lithium ion intercalation/deintercalation process which brings excellent thermal stability and cyclic performance. It is demonstrated that TiP₂O₇ materials are able to deliver high reversible capacity at charge-discharge rate as lithium ion insertion materials [88]. The broadening of XRD peaks of the composite from Methods A1 and A2 is due to the small crystals compared to those of samples from Methods B1 and B2.

XRD patterns of the TiO₂/C and TiO₂/AC composites by Methods B1 and B2, respectively, prepared at the carbonization temperature of 500°C and at 10-40 wt% TiO₂ contents in the composites are shown in Figures 4.29 and 4.30, respectively. All the synthesized composites were identified as anatase TiO₂ incorporated on the carbon surface. All samples in both figures show the obvious increase in intensity of the anatase peak at 2θ of 25.3° due to the increase of the TiO₂ content in the composites. It implies that the decrease of TiO₂ content in the composites results in the increase of carbon that causes the presentation of broad peak of amorphous carbon.

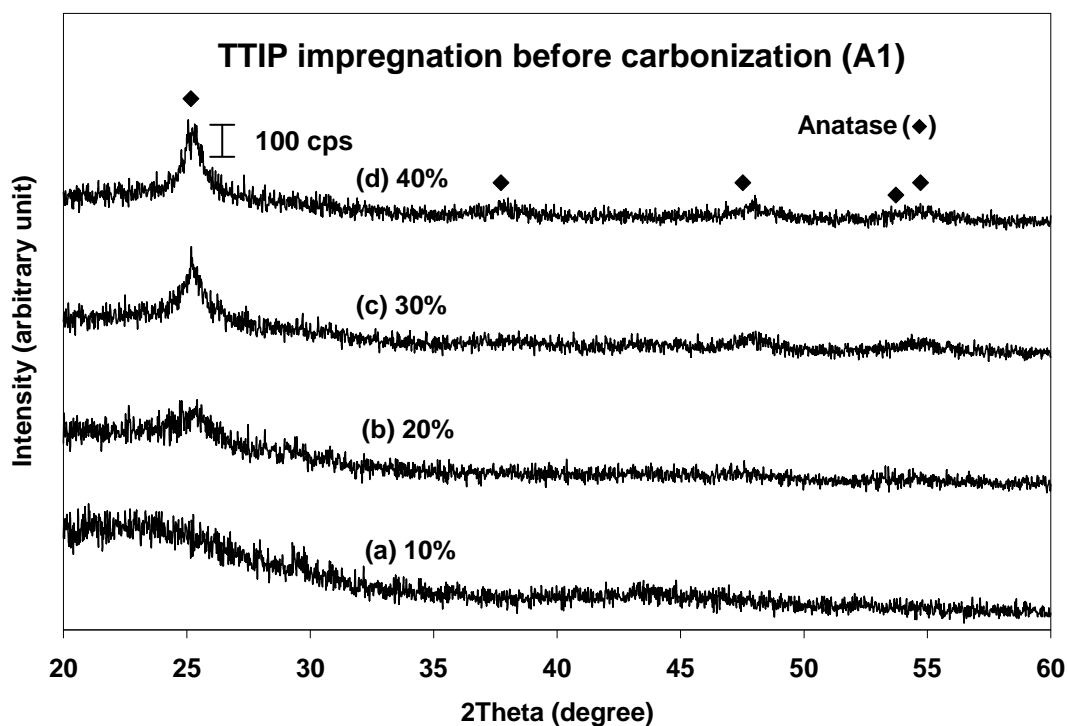


Figure 4.27 XRD patterns of TiO₂/C composites prepared by Method A1 at the carbonization temperature of 500°C at (a) 10%, (b) 20%, (c) 30%, and (d) 40% TiO₂ contents in the composites.

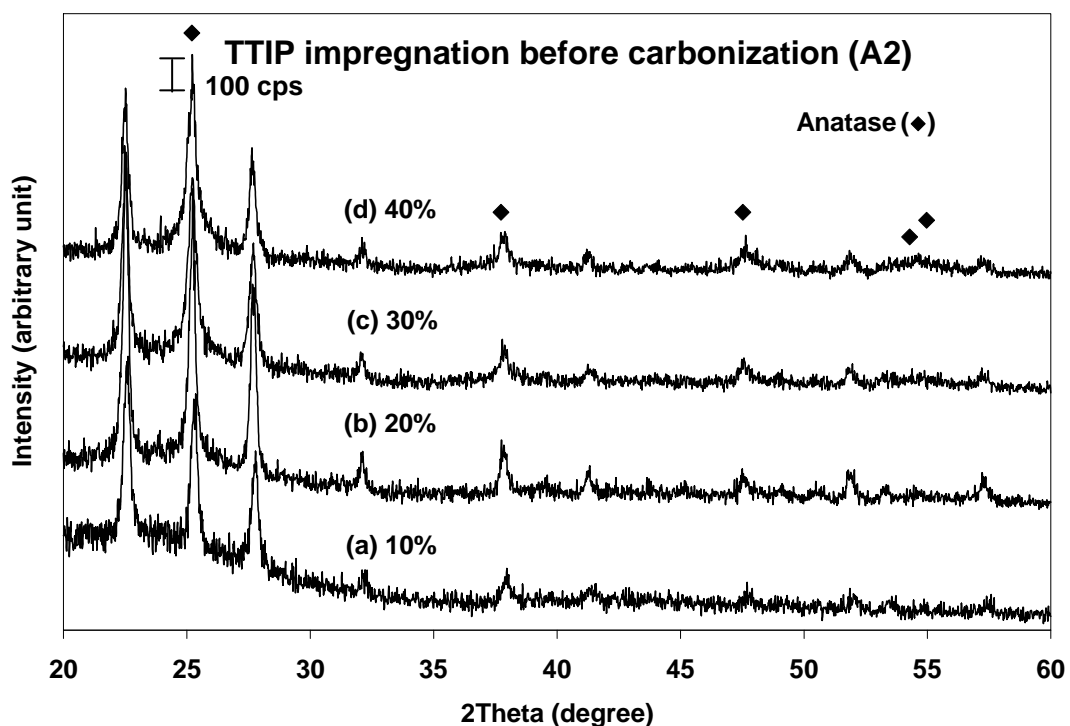


Figure 4.28 XRD patterns of TiO₂/C composites prepared by Method A2 at the carbonization temperature of 500°C at (a) 10%, (b) 20%, (c) 30%, and (d) 40% TiO₂ contents in the composites.

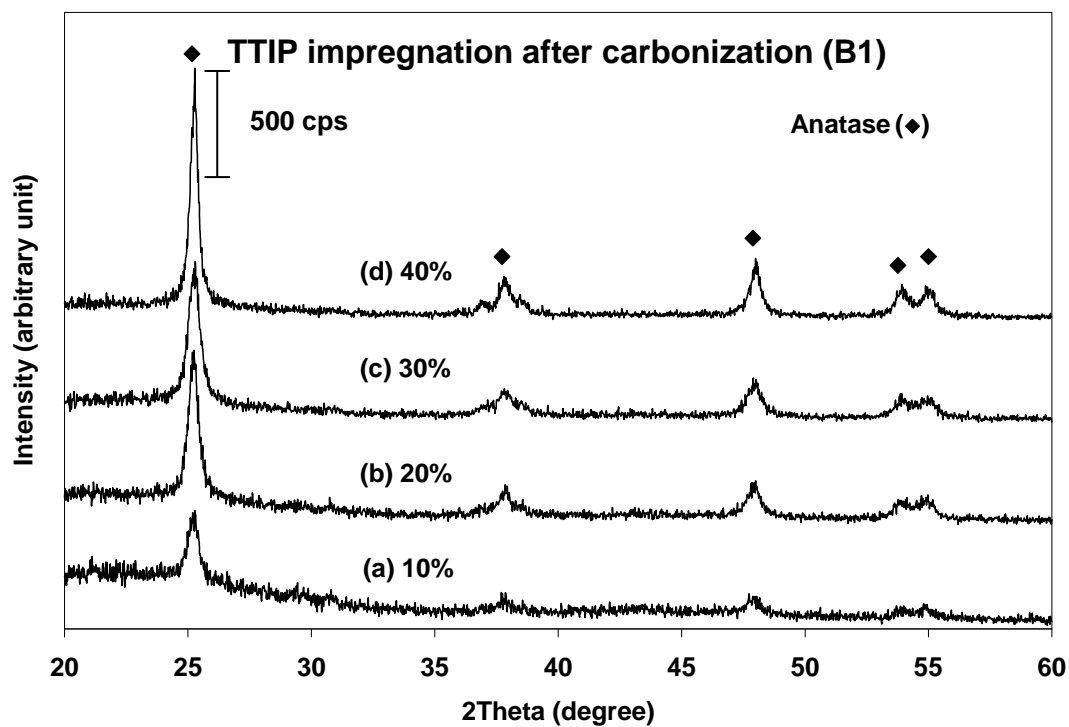


Figure 4.29 XRD patterns of TiO_2/C composites prepared by Method B1 at the carbonization temperature of 500°C at (a) 10%, (b) 20%, (c) 30%, and (d) 40% TiO_2 contents in the composites.

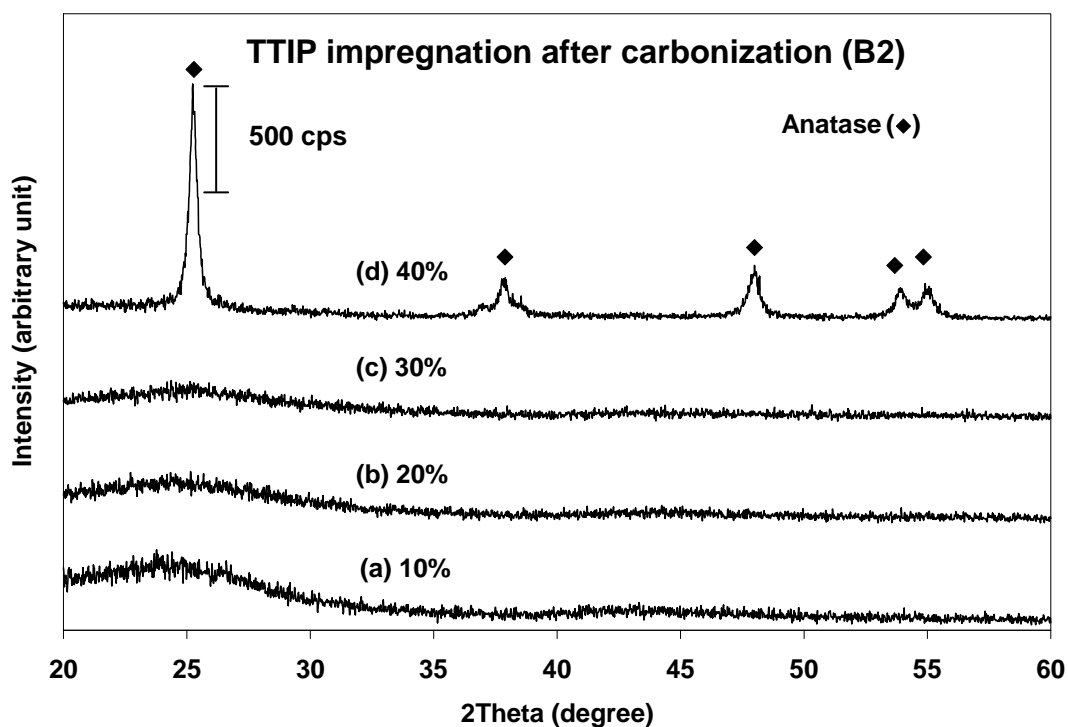


Figure 4.30 XRD patterns of TiO_2/AC composites prepared by Method B2 at the carbonization temperature of 500°C at (a) 10%, (b) 20%, (c) 30%, and (d) 40% TiO_2 contents in the composites.

The relative peak width of anatase in the composites was summarized in Table 4.7. From Scherrer formula, the crystal size is inversely proportional to a width at half height of a sample peak. In each method, the XRD peak width at half height of anatase is independent from the TiO₂ contents in the composite, especially the samples from Method B. However, the electrochemical properties of these composites will be reported.

Table 4.7 Relative peak width at half height for anatase crystals in the composites obtained from different preparation methods at the carbonization temperature of 500°C with various amounts of TiO₂ at 10-40 wt% in the composite

Conditions	Relative peak width at half height*(degree)			
	10%	20%	30%	40%
Carbonization temperature				
Method A: TTIP impregnation before carbonization				
- TiO ₂ /C (A1)	-	-	0.59	0.58
- TiO ₂ /C (A2)	0.29	0.37	0.37	0.38
Method B: TTIP impregnation after carbonization				
- TiO ₂ /C (B1)	0.42	0.44	0.47	0.33
- TiO ₂ /AC (B2)	-	-	-	0.35

*Based on the most intense characteristic peak at 2θ of 25.3

4.2.2 Nitrogen Adsorption

Figures 4.31-4.34 show the nitrogen adsorption isotherms for the resulting composites obtained from the novel method A and the conventional method B at the carbonization temperature of 500°C and at 10-40 wt% TiO₂ contents in the composites. All samples exhibit a type I adsorption isotherm which is a characteristic of a microporous material. The nitrogen adsorption isotherms of the composites at 40% TiO₂ content in the composites show the lowest absorbed amount of nitrogen. This indicates that the contents of TiO₂ in the composites have significant influence on the surface area of the composite. Applying the BET method, the specific surface area (S_{BET}) as shown in Table 4.8, is lowest with the maximum of TiO₂ content because of the aggregation of many TiO₂ crystals in the pores of carbon. The nitrogen isotherms of TiO₂/AC composites prepared by Method B2 as shown in Figure 4.34 shows larger absorbed amount of nitrogen than other methods. It is due to extremely high surface area provided by the activated

carbon obtained from this method while other methods gave only normal carbon materials with not so high specific surface areas.

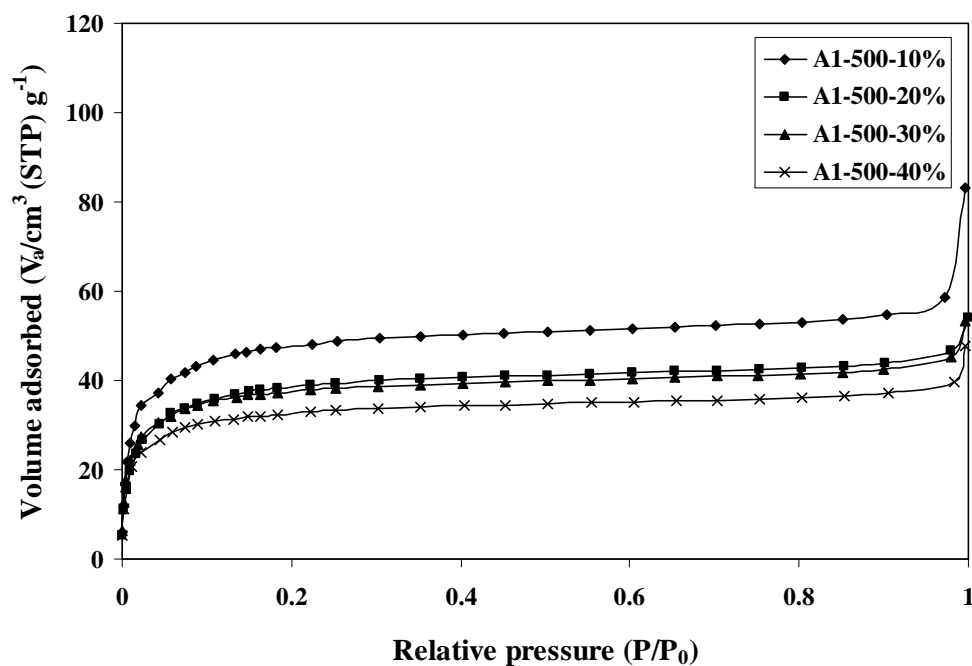


Figure 4.31 The N_2 adsorption isotherms of TiO_2/C composites prepared by Method A1 at the carbonization temperature of $500^\circ C$ at 10%, 20%, 30%, and 40% TiO_2 contents in the composites.

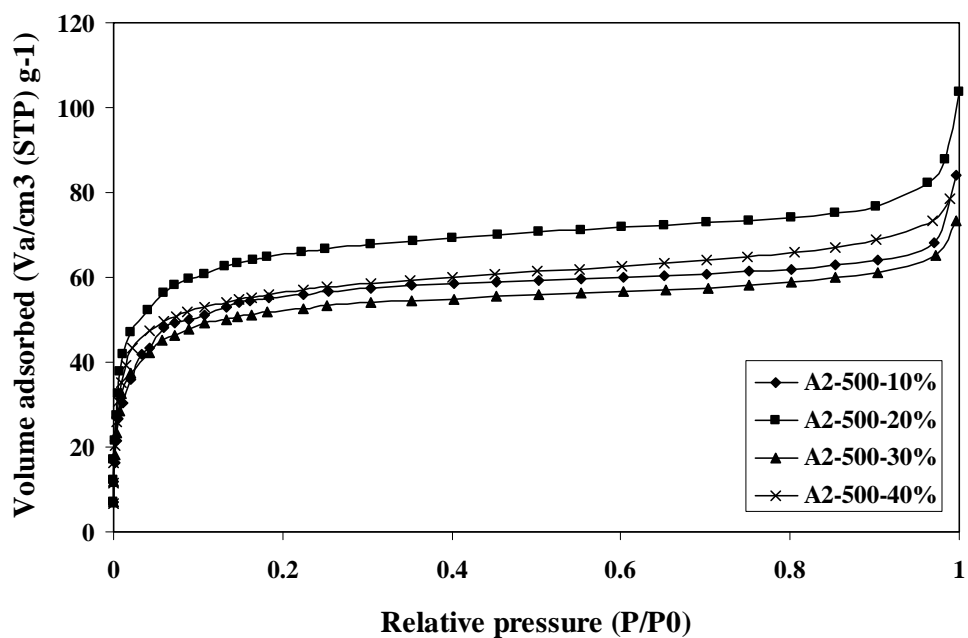


Figure 4.32 The N_2 adsorption isotherms of TiO_2/C composites prepared by Method A2 at the carbonization temperature of $500^\circ C$ at 10%, 20%, 30%, and 40% TiO_2 contents in the composites.

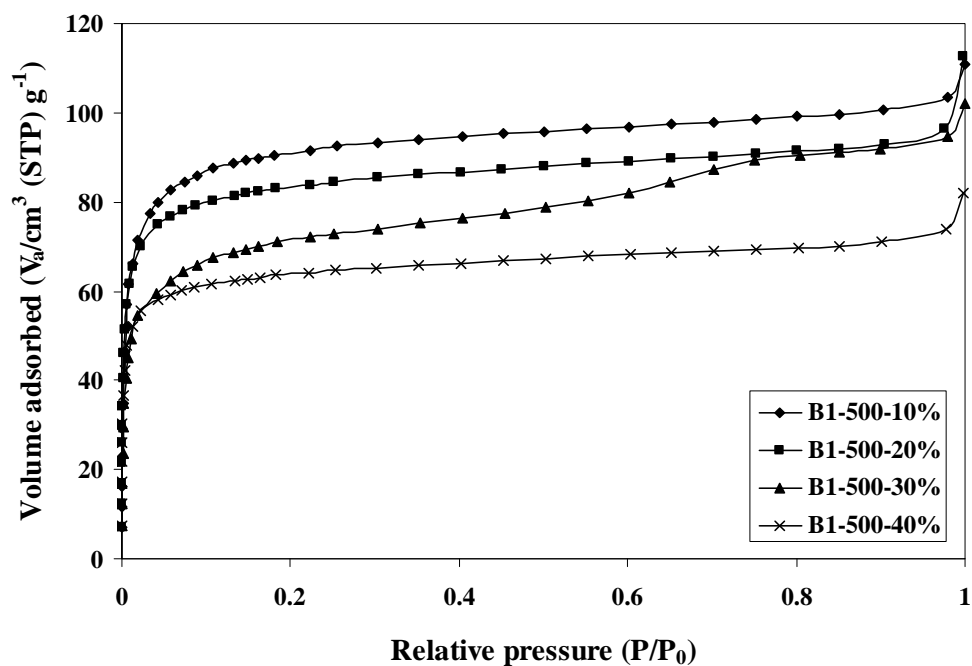


Figure 4.33 The N_2 adsorption isotherms of TiO_2/C composites prepared by Method B1 at the carbonization temperature of $500^\circ C$ at 10%, 20%, 30%, and 40% TiO_2 contents in the composites.

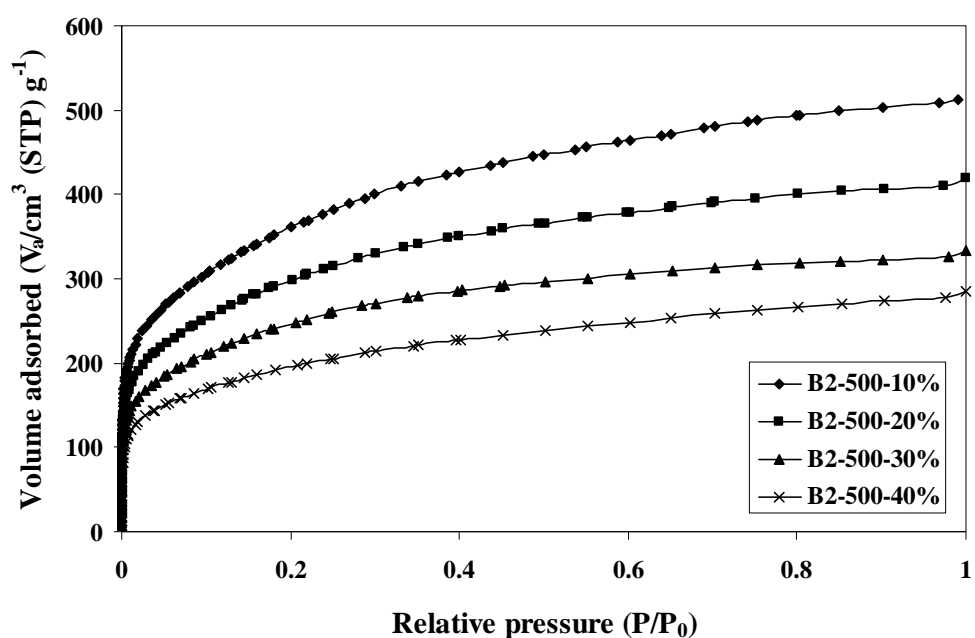


Figure 4.34 The N_2 adsorption isotherms of TiO_2/AC composites prepared by Method B2 at the carbonization temperature of $500^\circ C$ at 10%, 20%, 30%, and 40% TiO_2 contents in the composites.

Table 4.8 shows textural properties of TiO₂/C and TiO₂/AC composites obtained from different preparation methods at the carbonization temperature of 500°C at 10-40 wt% TiO₂ contents in the composites. The composites prepared by the novel method A have lower BET specific surface areas than those prepared by the conventional method B.

Table 4.8 Textural properties of TiO₂/C and TiO₂/AC composites obtained from different preparation methods at the carbonization temperature of 500°C at 10-40 wt% TiO₂ contents in the composites

Sample	S _{BET} ^a (m ² /g)	d _p ^b (nm)	S _{ext} ^c (m ² /g)	V _{micro} ^c (cm ³ /g)
A1-500-10%	181	0.8	17	0.0680
A1-500-20%	148	0.7	12	0.0564
A1-500-30%	141	0.8	9	0.0561
A1-500-40%	123	0.8	8	0.0490
A2-500-10%	215	0.7	17	0.0812
A2-500-20%	240	0.9	22	0.0961
A2-500-30%	196	0.8	21	0.0738
A2-500-40%	211	0.6	28	0.0778
B1-500-10%	346	0.7	30	0.1296
B1-500-20%	317	0.6	29	0.1181
B1-500-30%	262	0.6	66	0.0823
B1-500-40%	243	0.6	24	0.0890
B2-500-10%	1,280	1.0	396	0.4461
B2-500-20%	1,062	1.0	304	0.3773
B2-500-30%	880	1.0	221	0.3202
B2-500-40%	692	1.0	205	0.2429

^a Specific surface area determined by application of the BET-plot method

^b Micropore size determined by application of the MP-plot method

^c External surface area and micropore volume determined by application of the t-plot method

Method A provides the specific surface areas in the range of 123-240 m²/g. The composites from Method A2 were treated with phosphoric acid treatment thus the BET specific surface areas of the composites from Method A2 are higher than those from

Method A1. However, the specific surface areas of the composites after the treatment with phosphoric acid were significantly increased. Method B1 provides the BET specific surface areas in the range of 243-346 m²/g, while Method B2 provides the BET specific surface areas in the range of 692-1,280 m²/g. The BET specific surface areas of the composites from Method B2 are extremely higher than those of the composites from Method B1. Only normal carbon was formed in the composites prepared by Methods A1, A2, and B1 but it was not really activated as it was by Method B2. Pore sizes determined by the MP method falls in the range of 0.6-1 nm.

4.2.3 SEM Images

SEM images of TiO₂/C composite prepared by Method A1 at the carbonization temperature of 500°C and at 10-40% TiO₂ contents in the composites are presented in Figure 4.35. Obviously, the nanoparticles of TiO₂ were well dispersed over the supported carbon and held at around 100-150 nm with magnification of 10,000 to 40,000 times. The increase in the TiO₂ particle was restricted by the carbon surface in the nano-spaces in the carbon. It showed good agreement with the results of XRD that the novel method provided the small particles of TiO₂. The amount of TiO₂ on the carbon surface increases with increasing TiO₂ content. For the TiO₂/C composite from Method A2 treated by phosphoric acid, the particles are still well dispersed but slightly agglomerated as shown as in Figure 4.36. The SEM images show that the composites from Method A2 are slightly larger particle than Method A1. It has been discussed that chemical activation cause of the partial formation of TiP₂O₇ which has large crystal size the TiO₂.

SEM images of TiO₂/C (B1) and TiO₂/AC (B2) composites prepared by Method B at the carbonization temperature of 500°C and at 10-40% TiO₂ contents in the composites are presented in Figures 4.37 and 4.38, respectively. The composites from the conventional method were heavily aggregated with some bulk TiO₂ outside the carbon pore and some large particles appeared. This was in agreement with the XRD results.

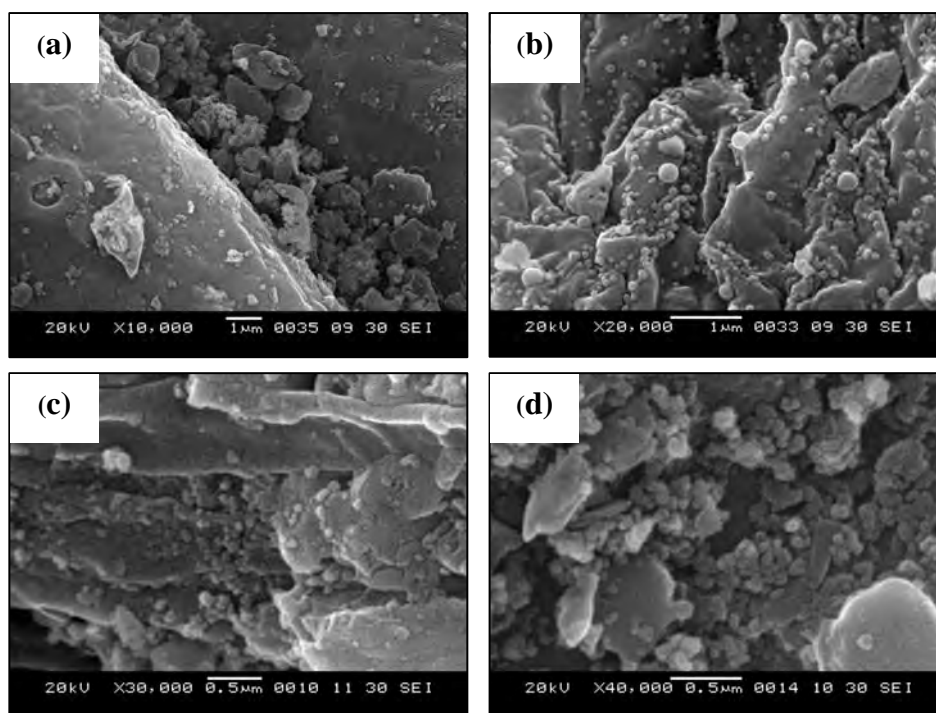


Figure 4.35 SEM images of TiO_2/C composites prepared by Method A1 at the carbonization temperature of 500°C at (a) 10%, (b) 20%, (c) 30%, and (d) 40% TiO_2 contents in the composites with magnification of 10,000x-40,000x, respectively.

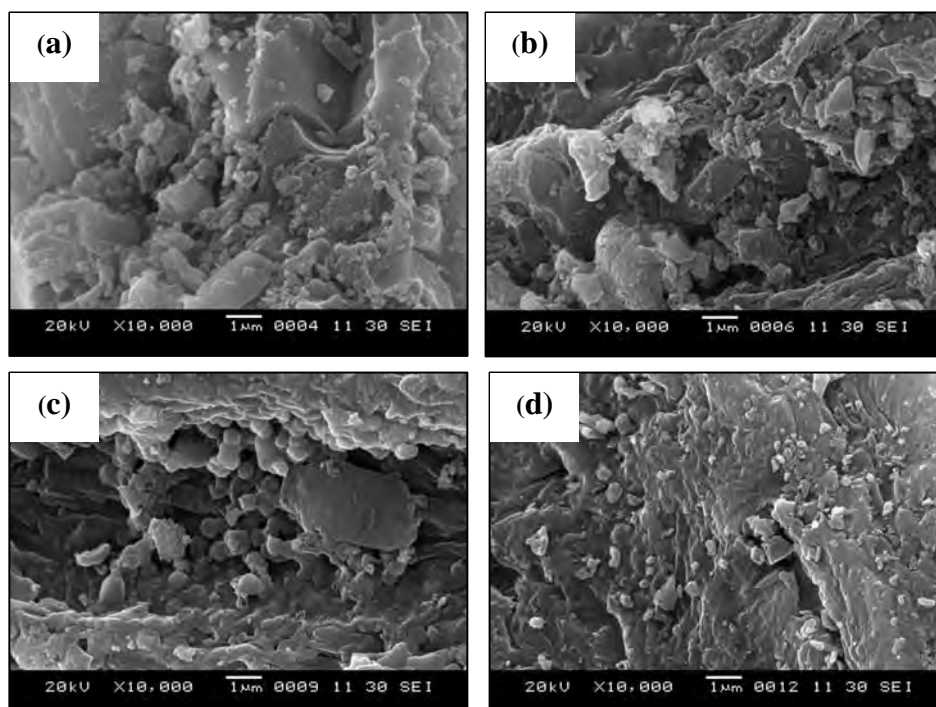


Figure 4.36 SEM images of TiO_2/C composites prepared by Method A2 at the carbonization temperature of 500°C at (a) 10%, (b) 20%, (c) 30%, and (d) 40% TiO_2 contents in the composites with magnification of 10,000x.

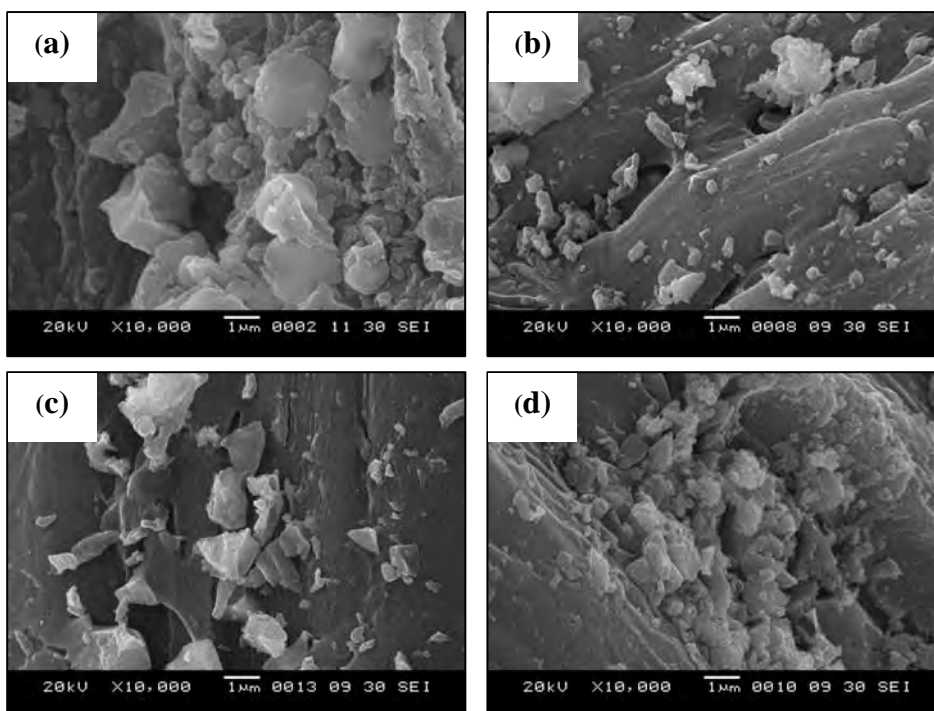


Figure 4.37 SEM images of TiO₂/C composites prepared by Method B1 at the carbonization temperature of 500°C at (a) 10%, (b) 20%, (c) 30%, and (d) 40% TiO₂ contents in the composites with magnification of 10,000x.

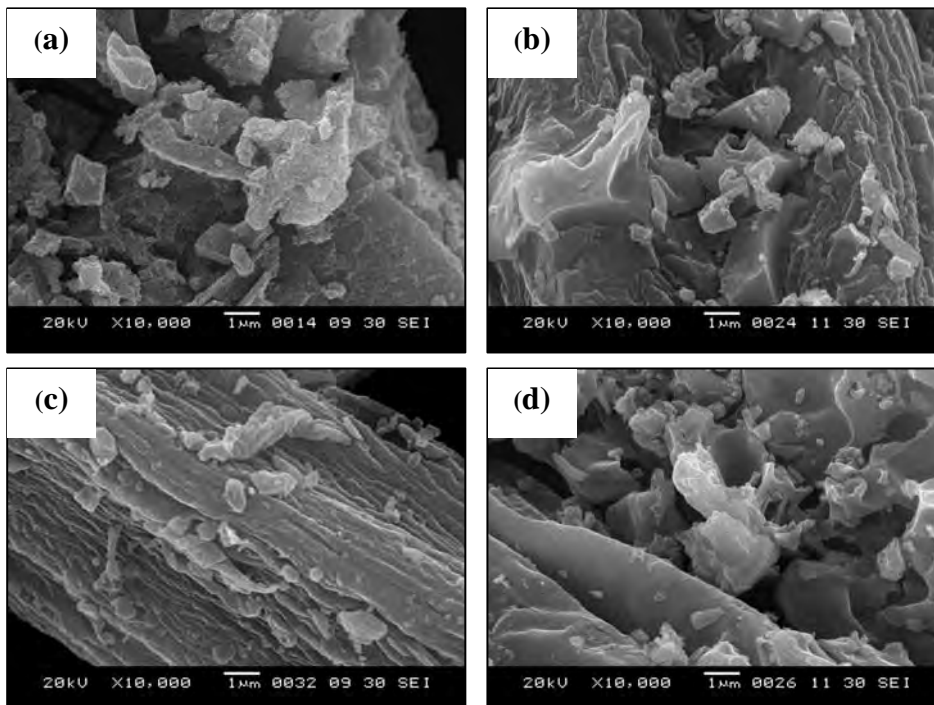


Figure 4.38 SEM images of TiO₂/AC composites prepared by Method B2 at the carbonization temperature of 500°C at (a) 10%, (b) 20%, (c) 30%, and (d) 40% TiO₂ contents in the composites with magnification of 10,000x.

4.2.4 Electrochemical Properties

4.2.4.1 Cyclic Voltammograms

In general, a cyclic voltammogram of an ideal double layer capacitor is in a rectangular shape, while that of the pseudocapacitor more or less detours from the rectangular shape [61]. Cyclic voltammograms of TiO₂/C and TiO₂/AC composite electrodes obtained from different preparation methods at carbonization temperature of 500°C with 10-40 wt% TiO₂ contents in the composites in 1 M H₂SO₄ are presented in Figures 4.39-4.42. Cyclic voltammetric measurements were carried out in the potential range of 0.5-1 V at a scan rate of 0.01 V/s. The profiles of the composite material electrodes are similar to those of carbon and activated carbon electrodes (see Figure 4.15) that present the typical box. Similar to the work done by *H. Liang et al.* [54], no redox peak behavior was observed when using the composite electrode. This result indicates that the capacitance obtained from our composite electrodes are mainly from double layer capacitive current and may be related to the less amount of titanium loaded.

From the cyclic voltammetric curve in the Figures 4.39-4.42, the average currents were obtained and listed in Table 4.9. It is shown that the average current of the composite electrode at 40% TiO₂ content is higher than that of other TiO₂ contents. The average current trends to increase with increasing TiO₂ content in the composites. It is also found that loading of TiO₂ increases the electric conductivity of the composite although TiO₂ itself had low electric conductivity when it stands alone.

Table 4.9 The average current calculated from cyclic voltammetry of the composite electrodes obtained from different preparation methods at the carbonization temperature of 500°C at 10-40 wt% TiO₂ contents in the composites

Conditions	The average current (Ampere, A)			
	10%	20%	30%	40%
% TiO ₂ in the composites				
Method A: TTIP impregnation before carbonization				
- TiO ₂ /C (A1)	8.58×10 ⁻⁸	1.69×10 ⁻⁷	1.03×10 ⁻⁶	3.10×10 ⁻⁶
- TiO ₂ /C (A2)	1.87×10 ⁻⁷	2.54×10 ⁻⁷	1.13×10 ⁻⁶	4.24×10 ⁻⁶
Method B: TTIP impregnation after carbonization				
- TiO ₂ /C (B1)	8.19×10 ⁻⁸	1.55×10 ⁻⁷	9.22×10 ⁻⁷	1.92×10 ⁻⁶
- TiO ₂ /AC (B2)	2.00×10 ⁻⁷	7.05×10 ⁻⁷	1.49×10 ⁻⁶	8.79×10 ⁻⁶

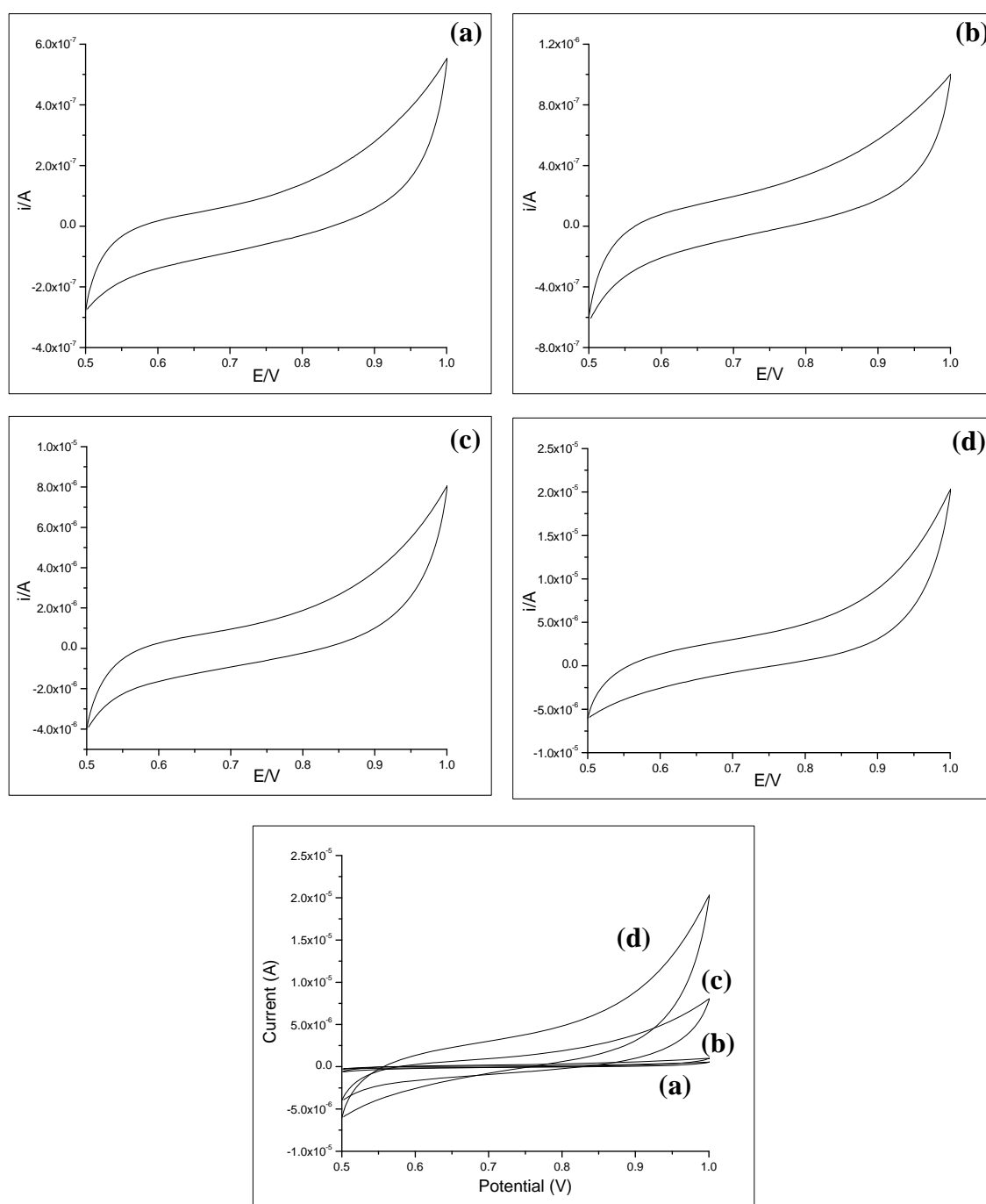


Figure 4.39 Cyclic voltammograms of TiO₂/C composites electrode prepared by Method A1 at carbonization temperature of 500°C at (a) 10%, (b) 20%, (c) 30%, and (d) 40% TiO₂ contents in the composites in 1 M H₂SO₄.

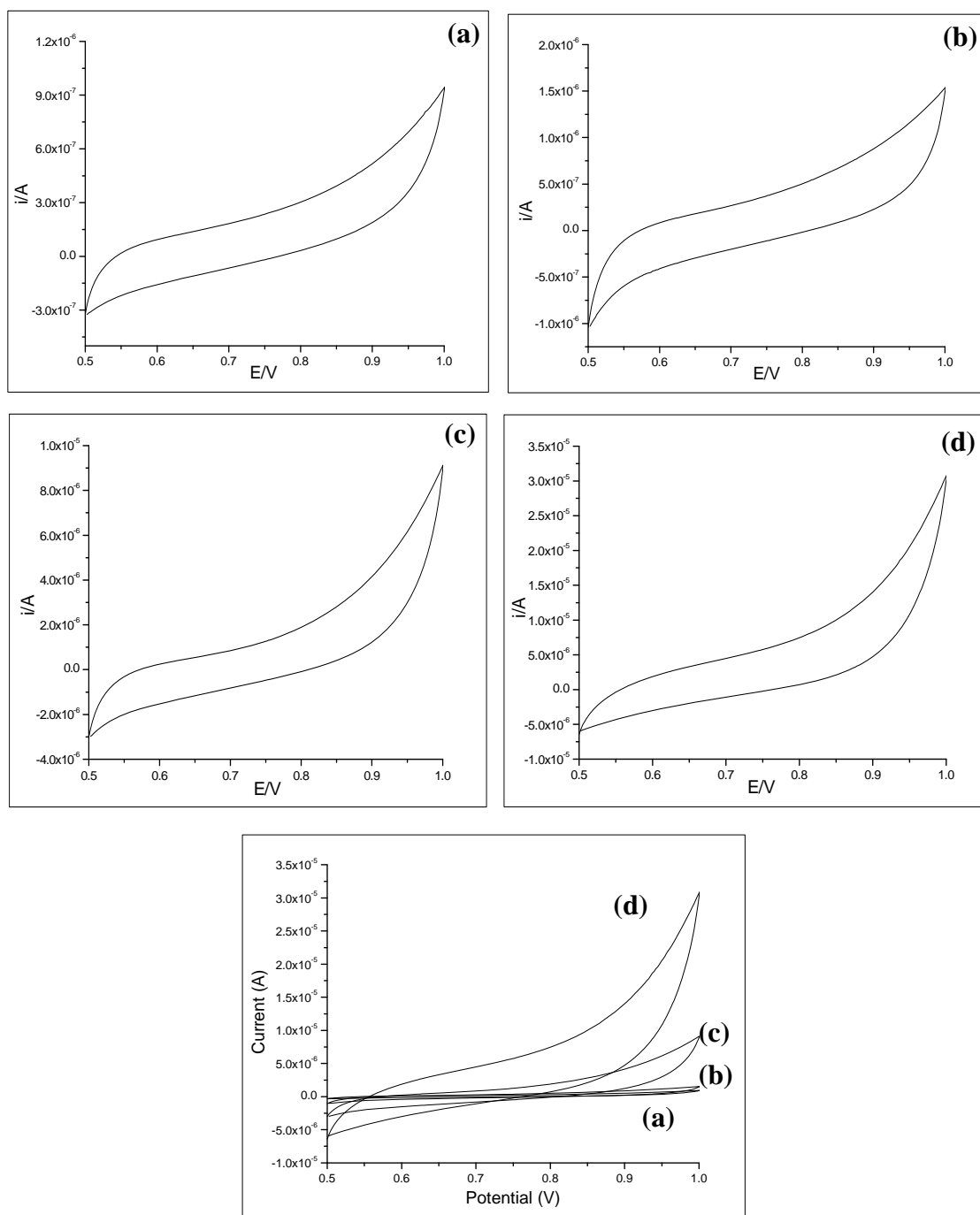


Figure 4.40 Cyclic voltammograms of TiO_2/C composites electrode prepared by Method A2 at carbonization temperature of 500°C at (a) 10%, (b) 20%, (c) 30%, and (d) 40% TiO_2 contents in the composites in 1 M H_2SO_4 .

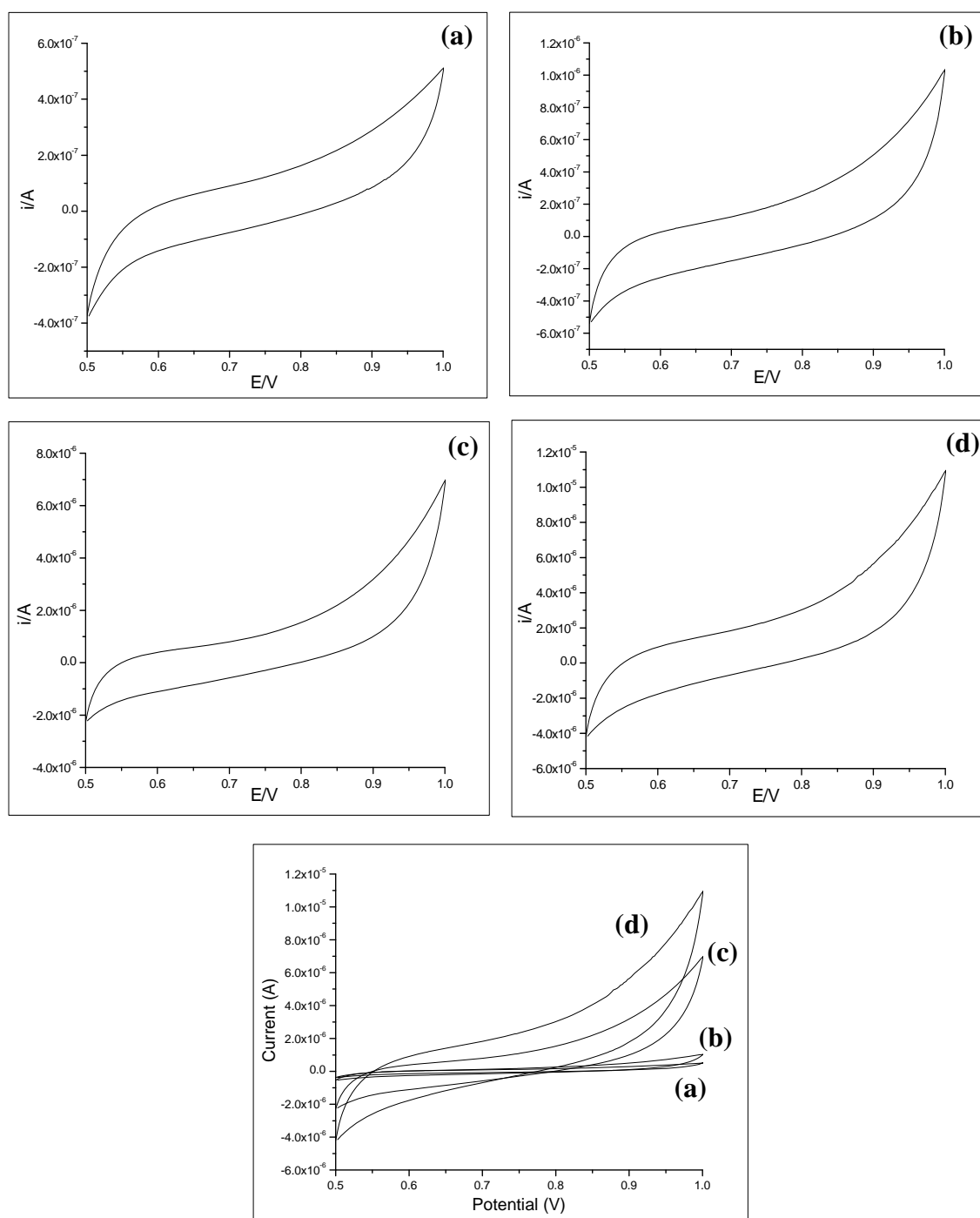


Figure 4.41 Cyclic voltammograms of TiO_2/C composites electrode prepared by Method B1 at carbonization temperature of 500°C at (a) 10%, (b) 20%, (c) 30%, and (d) 40% TiO_2 contents in the composites in 1 M H_2SO_4 .

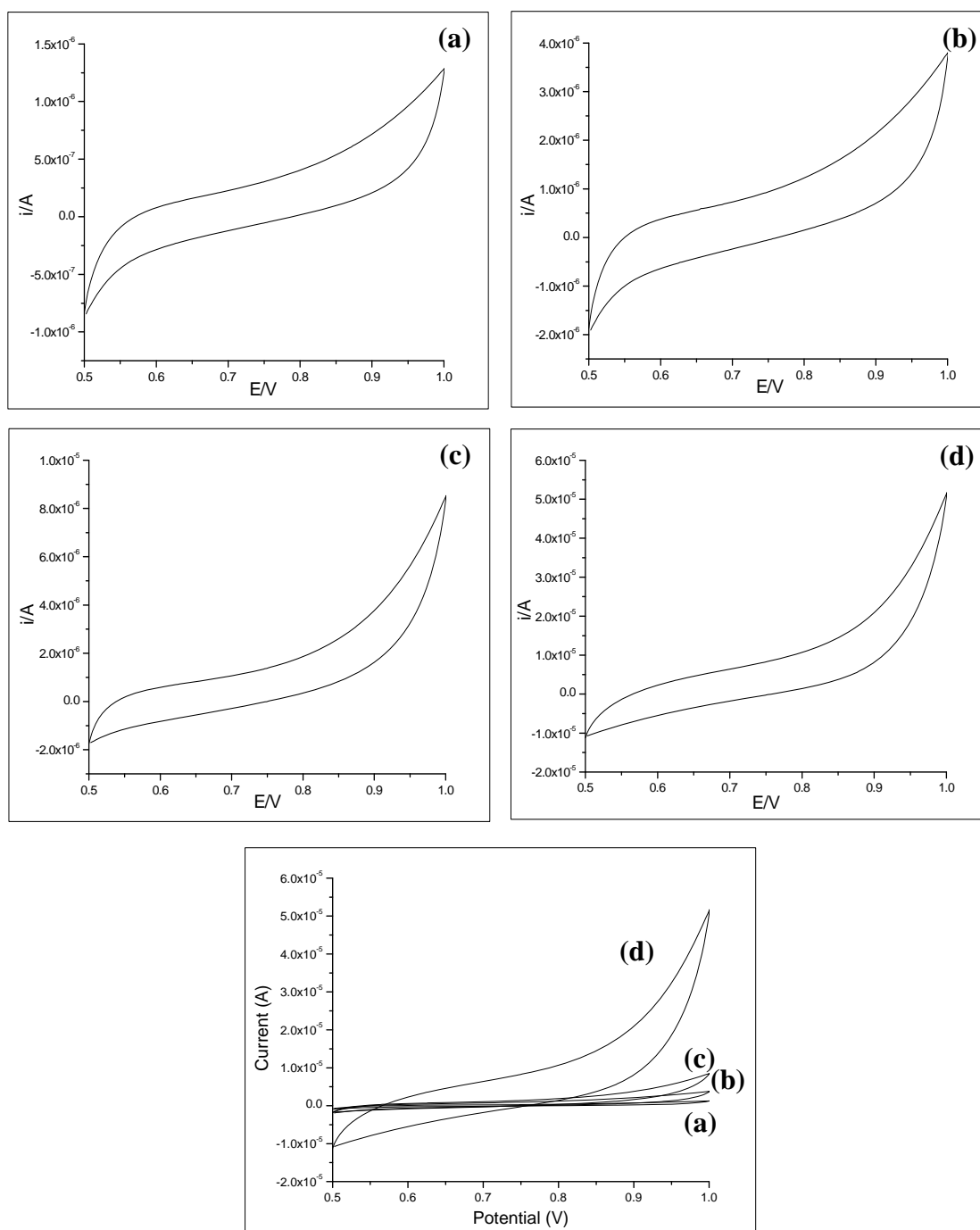


Figure 4.42 Cyclic voltammograms of TiO_2/AC composites electrode prepared by Method B2 at carbonization temperature of 500°C at (a) 10%, (b) 20%, (c) 30%, and (d) 40% TiO_2 contents in the composites in 1 M H_2SO_4 .

The effect of TiO_2 content in the composite on the capacitive performance of the composite electrode is summarized in Table 4.10. The novel method A provides the specific capacitance in the range of 17-848 mF/g while the conventional method B provides the specific capacitance in the range of 16-1,758 mF/g.

The specific capacitance of the composites prepared by the novel method A1 is higher than those from the conventional method B1, especially at 40% TiO₂ content in the composites where the specific capacitance value prepared by Method A1 is almost twice of Method B1. It indicates that our proposed method is effectively method to improve the capacitive performance of electrode. It can be explained that the novel method provides the very small crystals of TiO₂ (see Table 4.7). The nanosize of TiO₂ is expected to improve capacitive behavior of the electrode and increase the accumulation of the ion on double layer, although the specific surface areas from the novel method are lower than from the conventional method (see Table 4.8). The increase of TiO₂ content that causes the increase of the amount of nanosized TiO₂ in the carbon pores so the specific capacitance values are the highest at 40% TiO₂ content in the composites.

To compare Method A2 with Method B2, at all TiO₂ contents in the composites, Method B2 shows higher specific capacitance than Method A2. The specific capacitance values increase with the increase of the TiO₂ content in the composite and show the highest values of 848 and 1,758 mF/g from Methods A2 and B2, respectively, at 40% TiO₂ content. The tremendously high specific surface area is account for the very high capacitive performance of the electrode from Method B2. At the same TiO₂ content, all the composites from Method B2 provide higher specific capacitance values than Method A2. Among those composites from the same method, the increase of the TiO₂ content in the composite has an effect on the specific surface areas.

Table 4.10 The specific capacitance calculated from cyclic voltammetry of the composite electrodes obtained from different preparation methods at the carbonization temperature of 500°C at 10-40 wt% TiO₂ contents in the composites

Conditions	Specific capacitance from cyclic voltammetry (mF/g)			
	10%	20%	30%	40%
Method A: TTIP impregnation before carbonization				
- TiO ₂ /C (A1)	17	34	206	620
- TiO ₂ /C (A2)	37	51	226	848
Method B: TTIP impregnation after carbonization				
- TiO ₂ /C (B1)	16	31	184	384
- TiO ₂ /AC (B2)	40	141	298	1,758

The composite electrodes show enhanced specific capacitance when increasing TiO₂ content but the TiO₂ content in the composites must be appropriate to provide high capacitive performance of the composite electrode. If no TiO₂ but only carbon or activated carbon is used as electrode material, the capacitive performance is not so good. Similarly, if only TiO₂ without carbon is used, the capacitive performance is also low. The hybrid properties of TiO₂ along with carbon or activated carbon can provide the excellent capacitive performance of TiO₂/C or TiO₂/AC composite.

4.2.4.2 Electrochemical Impedance Spectra

Figures 4.43 and 4.44 present complex plane impedance plots for composites prepared by Method A1 and A2, respectively. The semicircular loop for the composites at 10-30% TiO₂ contents in the composite from both methods is not significantly different but they are obviously different from that at 40% TiO₂ content in the composite. The impedance (Z') is decreased and it indicates that the polarization resistance decreases and the electric conductivity increases. It can be explained that the increase of TiO₂ content can reduce the polarization of carbon in the composite causing the high electric double layer capacitance. However, diffusion of ions from aqueous solution to the interface layer between the electrode surface and the solution can create the impedance known as the Warburg impedance. At high frequencies the Warburg impedance is small as diffusing ions do not have to move very far. At low frequencies the ions have to diffuse farther, thus increasing the Warburg impedance [87].

Figures 4.45 and 4.46 present complex plane impedance plots for the TiO₂/C and TiO₂/AC composite prepared by Method B1 and B2, respectively. It is not different for the composites at 10-30% TiO₂ contents but obviously different from the composites at 40% TiO₂ content. The composite at 40% TiO₂ content in the composite from Method B2 in Figure 4.46(d) exhibits the lower Warburg impedance than Method B1 in Figure 4.45(d) indicating that this composite could enhance the diffusion of ions within pores of electrochemical electrodes, thus the electric double layer can be effectively increased. The results reveal that phosphoric acid treatment is the effective method to increase the electric double layer and significantly decrease the Warburg impedance, resulting in high specific capacitance.

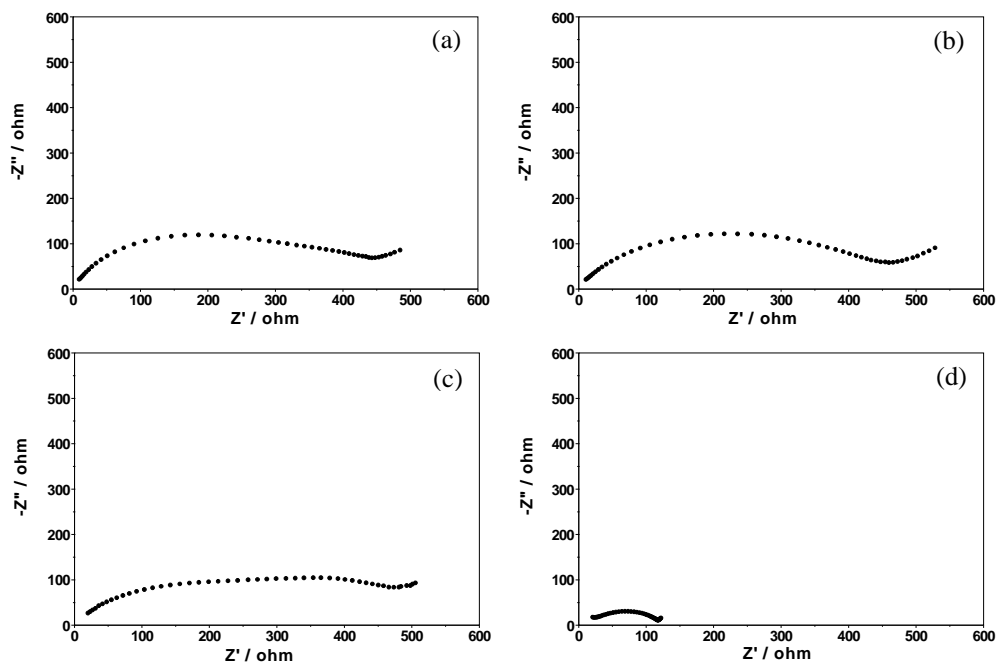


Figure 4.43 Complex-plane impedance spectra of electrochemical capacitors with electrode material made by Method A1 at the carbonization temperature of 500°C at (a) 10%, (b) 20%, (c) 30%, and (d) 40% TiO₂ contents in the composites.

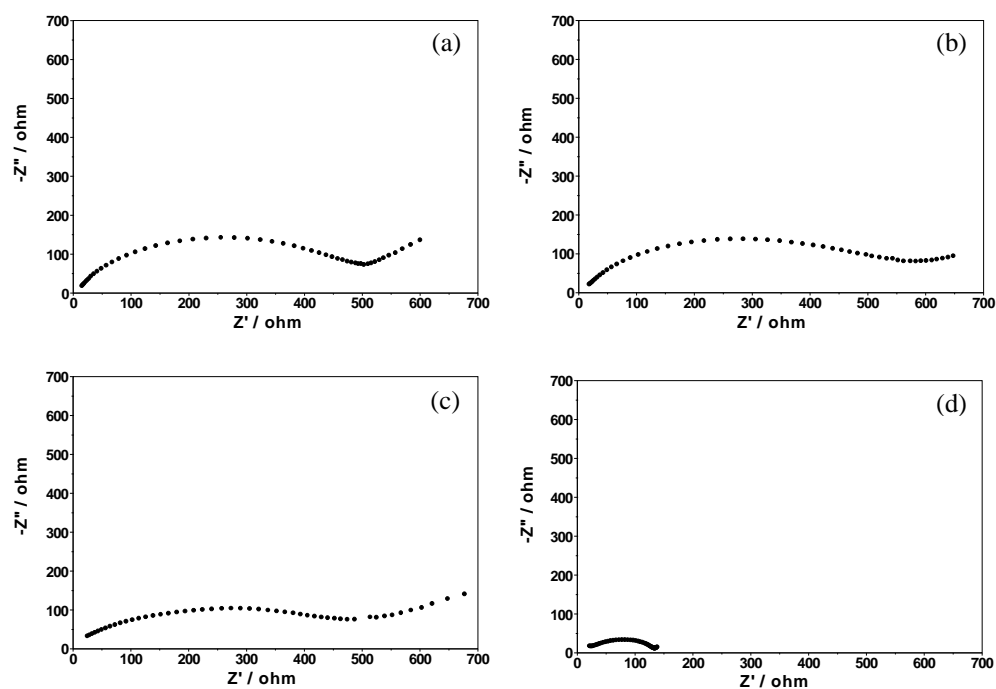


Figure 4.44 Complex-plane impedance spectra of electrochemical capacitors with electrode material made by Method A2 at the carbonization temperature of 500°C at (a) 10%, (b) 20%, (c) 30%, and (d) 40% TiO₂ contents in the composites.

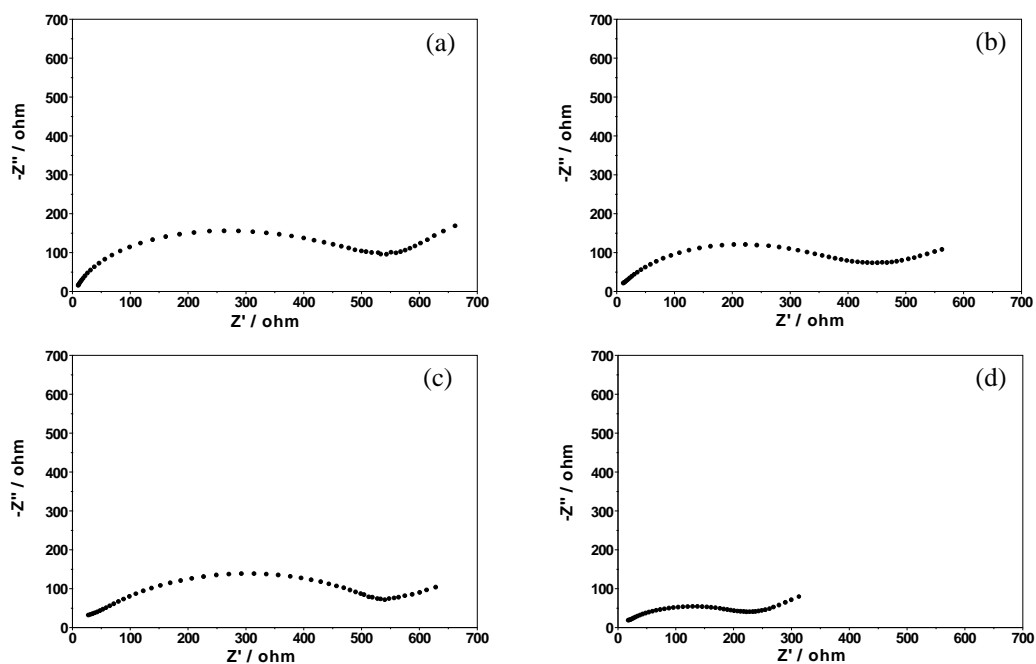


Figure 4.45 Complex-plane impedance spectra of electrochemical capacitors with electrode material made by Method B1 at the carbonization temperature of 500°C at (a) 10%, (b) 20%, (c) 30%, and (d) 40% TiO₂ contents in the composites.

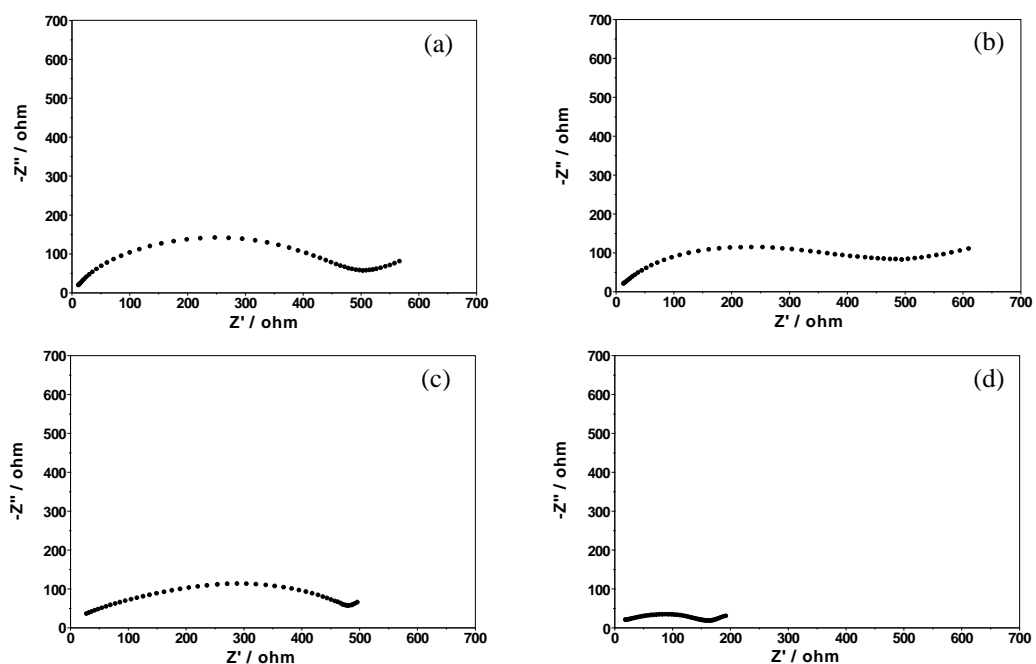


Figure 4.46 Complex-plane impedance spectra of electrochemical capacitors with electrode material made by Method B2 at the carbonization temperature of 500°C at (a) 10%, (b) 20%, (c) 30%, and (d) 40% TiO₂ contents in the composites.

The specific capacitance values were obtained by fitting the Nyquist plot curve calculated by electrochemical software (Autolab PGSTAT 30, FRA software). Table 4.11 summarizes the specific capacitance values of the composite electrodes obtained from different preparation methods with different TiO₂ contents in the composites. The novel method A, TTIP impregnation before carbonization, provides the specific capacitance in the range of 54-412 mF/g while the conventional method B, TTIP impregnation after carbonization, provides the specific capacitance in the range of 47-558 mF/g. The specific capacitance values of the composite at 40% TiO₂ content are the highest for all preparation methods and Method B2 gives the highest capacitance values.

Table 4.11 The specific capacitance calculated from electrochemical impedance spectroscopy of the composite electrodes obtained from different preparation methods at the carbonization temperature of 500°C at 10-40 wt% TiO₂ contents in the composites

Conditions	Specific capacitance from electrochemical impedance spectroscopy (mF/g)			
	10%	20%	30%	40%
% TiO₂ in the composites				
Method A: TTIP impregnation before carbonization				
- TiO ₂ /C (A1)	54	100	204	370
- TiO ₂ /C (A2)	59	105	217	412
Method B: TTIP impregnation after carbonization				
- TiO ₂ /C (B1)	47	91	179	313
- TiO ₂ /AC (B2)	67	122	259	558

It can be seen that the values of specific capacitance of the composites calculated from cyclic voltammetry (Table 4.10) are relatively higher than those from electrochemical impedance spectroscopy (Table 4.11) that is similar to other reports [53]. However, they provide the same trend that the increase in TiO₂ content results in both types of higher specific capacitance.

CHAPTER V

CONCLUSION

TiO₂/carbon composites can be prepared successfully through the novel method by impregnation of bamboo powder with TTIP solution in 2-propanol, followed by heating under nitrogen to form anatase-type TiO₂. This novel method can reduce the preparation steps because anatase formation and carbonization take place simultaneously in a single step at the same temperature. The composites containing the anatase crystals down to the size of 12 nm can be prepared successfully. The composite can be potentially applied further as electrode materials for electric double layer capacitor.

Anatase-type TiO₂ was readily formed in all preparation methods. The anatase phase obtained is very stable even at 700°C and no rutile phase was observed for all preparation methods. It indicates that carbon from bamboo can obviously stabilize the nano-anatase phase up to 700°C. The novel method (Method A), TTIP impregnation before carbonization, provides smaller crystal size than the conventional method (Method B), TTIP impregnation after carbonization and the sol-gel method. The increasing of the TiO₂ crystal size can be obtained when the composites were treated with phosphoric acid. This may result in a chemical activation inside the composite during calcination, thus leading to agglomeration of TiO₂ and increase in the crystal size. All composites exhibit a type I adsorption isotherm which is the typical isotherm of microporous material. The composites prepared by the novel method have lower BET specific surface areas than those prepared by the conventional method due to the composites prepared by Method A1, A2, and B1 are still composed of normal carbon or acid treated carbon not real activated carbon. From electrochemical studies, it indicated that introduction of TiO₂ dramatically increases capacity of carbon although TiO₂ itself had very low capacitance. The polarization of carbon which causes the decreasing accumulation of the ions on double layer can be reduced by modifying carbon with nanosize TiO₂. A high surface area of the composite and the small crystal sizes of TiO₂ are a key factor to increase the double layer at the surface of capacitor electrode in achieving a high capacitance.

The method which was performed through phosphoric acid treatment provided the high specific capacitance because the surface functional groups may play essential roles in the improvement and curing on the surface of the composite. The carbonized temperatures of 500°C is the effectively carbonization temperature. The composite electrode shows the highest specific capacitance values from voltammetric technique of 932 and 1,592 mF/g by the novel method and the conventional method respectively while those from electrochemical impedance spectroscopic technique are 381 and 423 mF/g by the novel method and the conventional method, respectively.

The effect of TiO₂ content (10-40 wt%) in the composite on the composite properties was studied at the carbonization temperature of 500°C. The suitable TiO₂ content in the composite is essential in the improvement on the total specific capacitance. The optimum content of TiO₂ is 40% for all preparation methods to provide the highest specific capacitance. The composite electrodes show the highest specific capacitance values from voltammetric technique of 848 and 1,758 mF/g by the novel method and the conventional method, respectively while those from electrochemical impedance spectroscopic technique are 412 and 558 mF/g by the novel method and the conventional method, respectively. It can be concluded that the specific capacitance of the composite electrode is affected by preparation methods, carbonization temperature, and the TiO₂ content in the composite.

In several countries in Asia including Thailand there is plenty of bamboo based chopsticks disposed as waste and it is worth converting such biomass towards the valued added material like TiO₂/carbon composite. Thus the novel method for preparing the TiO₂/carbon and TiO₂/activated carbon composite with high thermal stability using bamboo chopsticks as carbon source for further application in an electric double layer capacitor is interesting.

The suggestion for future work

1. Study of the methods of the activation of carbon in the presence of TiO₂ obtained from the novel method for improving BET surface area to get the real activated composite for enhancing the specific capacitance of the electrochemical capacitor electrode.
2. Study of the preparation method of the electrochemical capacitor electrode by decreasing the amounts of binder to increase the specific capacitance.

REFERENCES

- [1] Klass, D.L. *Biomass for Renewable Energy, Fuels and Chemicals*. San Diego CA: Academic Press, 1998.
- [2] Hu, Z. and Srinivasan, M.P. Preparation of high-surface-area activated carbons from coconut shell. *Microporous and Mesoporous Materials* 27 (1999): 11–18.
- [3] Ismadji, S.; Sudaryanto, Y.; Hartono, S.B.; Setiawan, L.E.K.; Ayucitra, A. Activated carbon from char obtained from vacuum pyrolysis of teak sawdust: pore structure development and characterization. *Bioresource Technology* 96 (2005): 1364–1369.
- [4] Yalçın, N. and Sevinç, V. Studies of the surface area and porosity of activated carbons prepared from rice husks. *Carbon* 38 (2000): 1943-1945.
- [5] Tsai, W.T.; Chang, C.Y.; Wang, S.Y.; Chang, C.F.; Chien, S.F.; Sun, H.F. Preparation of activated carbons from corn cob catalyzed by potassium salts and subsequent gasification with CO₂. *Bioresource Technology* 78 (2001): 203-208.
- [6] Avom, J.; Mbadcam, J.K.; Noubactep, C.; Germain, P. Adsorption of methylene blue from an aqueous solution onto activated carbon from palm-tree cobs. *Carbon* 35 (1997): 365-369.
- [7] Wu, F.C.; Tseng, R.L.; Juang, R.S. Pore structure and adsorption performance of the activated carbons from plum kernels. *Journal of Hazardous Materials* 69 (1999): 287-302.
- [8] Rajeshwarisivaraj.; Sivakumar, S.; Senthilkumar, P.; Subburam, V. Carbon from Cassava peel, an agricultural waste, as an adsorbent in the removal of dyes and metal ions from aqueous solution, *Bioresource Technology* 80 (2001): 233-235.
- [9] Tsai, W.T.; Chang, C.Y. Lin, M.C.; Chien, S.F.; Sun, H.F.; Hsieh, M.F. Adsorption of acid dye onto activated carbons prepared from agricultural waste bagasse by ZnCl₂ activation. *Chemosphere* 45 (2001): 51-58.

- [10] El-Sheikh, A.H. Newman, A.P. Characterization of activated carbon prepared from a single cultivar of Jordanian olive stones by chemical and physiochemical techniques. *Journal of Analytical and Applied Pyrolysis* 71 (2004): 151-164.
- [11] Girgis, B.S. and El-Hendawy, A.A. Porosity development in activated carbons obtained from date pits under chemical activation with phosphoric acid. *Microporous and Mesoporous Materials* 52 (2002): 105-117.
- [12] Aygün, A.; Yenisoy-Karakaş, S.; Duman, I. Production of granular activated carbon from fruit stones and nutshells and evaluation of their physical, chemical and adsorption properties. *Microporous and Mesoporous Materials* 66 (2003): 189-195.
- [13] Shin, F.G.; Xian, X. J.; Zheng, W.P.; Yipp, M.W. Analyses of the mechanical properties and microstructure of bamboo-epoxy composites. *Journal of Materials Science* 24 (1989): 3483.
- [14] Fox, M.A. and Dulay, M.T. Heterogeneous photocatalysis. *Chemical reviews* 93 (1993): 341-357.
- [15] Mills, A. and Hunte, S.Le. An overview of semiconductor photocatalysis. *Journal of Photochemistry and Photobiology A: Chemistry* 108 (1997): 1-35.
- [16] Fujishima, A.; Rao, T.A.; Tryk, D.A. Titanium dioxide photocatalysis. *Journal of Photochemistry and Photobiology C: Photochemistry Reviews* 1 (2000): 1–21.
- [17] Ding, Z.; Lu, G.Q.; Greenfield, P.F. Role of the crystallite phase of TiO₂ in heterogeneous photocatalysis for phenol oxidation in water. *Journal of Physical Chemistry B* 104 (2000): 4815-4820.
- [18] Yanqing, Z.; Erwei, S.; Zhizhan, C.; Wenjun, L.; Xingfang, H. Influence of solution concentration on the hydrothermal preparation of titania crystallites. *Journal of Materials Chemistry* 11 (2001): 1547-1551.
- [19] Yu, J.C.; Yu, J.; Zhao, J. Enhanced photocatalytic activity of mesoporous and ordinary TiO₂ thin films by sulfuric acid treatment. *Applied Catalysis B: Environmental* 36 (2002): 31–43.

- [20] Grzechulska, J. and Morawski, A.W. Photocatalytic decomposition of azo-dye acid black 1 in water over modified titanium dioxide. *Applied Catalysis B: Environmental* 36 (2002): 45–51.
- [21] Kominami, H.; Kohno, M.; Matsunaga, Y.; Kera, Y. Thermal decomposition of titanium alkoxide and silicate ester in organic solvent: a new method for synthesizing large-surface-Area, silica-modified titanium (IV) oxide of high thermal stability. *Journal of the American Ceramic Society* 84 (2001): 1178–80.
- [22] Chen, H.R.; Shi, J.L.; Zhang, W.H.; Ruan, M.L.; Yan, D.S. Incorporation of titanium into the inorganic wall of ordered porous zirconia oxide via direct synthesis. *Chemistry of Materials* 13 (2001): 1035-1040.
- [23] Jang, H.D. and Kim, S.K. Controlled synthesis of titanium dioxide nanoparticles in a modified diffusion flame reactor. *Materials Research Bulletin* 36 (2001): 627–637.
- [24] Andersson, M; Sterlund, L.; Ljungström, S.; Palmqvist, A. Preparation of nanosize anatase and rutile TiO₂ by hydrothermal treatment of microemulsions and their activity for photocatalytic wet oxidation of phenol. *The Journal of Physical Chemistry B* 106 (2002): 10674-10679.
- [25] Liu, D.; Zhang, J.; Han, B.; Chen, J.; Li, Z.; Shen, D.; Yang, G. Recovery of TiO₂ nanoparticles synthesized in reverse micelles by antisolvent CO₂. *Colloids and Surfaces A: Physicochemical and Engineering Aspects* 227 (2003): 45–48.
- [26] Stallings, W.E. and Lamb, H.H. Synthesis of nanostructured titania powders via hydrolysis of titanium isopropoxide in supercritical carbon dioxide. *Langmuir* 19 (2003): 2989-2994.
- [27] Liu, H.; Yang, W.; Ma, Y.; Cao, Y.; Yao, J.; Zhang, J.; Hu, T. Synthesis and characterization of titania prepared by using a photoassisted sol-gel method. *Langmuir* 19 (2003): 3001-3005.
- [28] Caruso, R.A.; Antonietti, M.; Giersig, M.; Hentze, H.P.; Jia, J. Modification of TiO₂ network structures using a polymer gel coating technique. *Chemistry of Materials* 13 (2001): 1114-1123.

- [29] Yin, H.; Wada, Y.; Kitamura, T.; Kambe, S.; Murasawa, S.; Mori, H.; Sakata, T.; Yanagida, S. Hydrothermal synthesis of nanosized anatase and rutile TiO₂ using amorphous phase TiO₂. *Journal of Materials Chemistry* 11 (2001): 1694–1703.
- [30] Yin, H.; Wada, Y.; Kitamura, T.; Sumida, T.; Hasegawa, Y.; Yanagida, S. Novel synthesis of phase-pure nano-particulate anatase and rutile TiO₂ using TiCl₄ aqueous solutions. *Journal of Materials Chemistry* 12 (2002): 378–383.
- [31] Kumar, S.R.; Suresh, C.; Vasudevan, A.K.; Suja, N.R.; Mukundan, P.; Warriar, K.G.K. Phase transformation in sol–gel titania containing silica. *Materials Letters* 38 (1999): 161–166.
- [32] Fu, X.; Clark, L.A.; Yang, Q.; Anderson, M.A. Enhanced photocatalytic performance of titania-based binary metal oxides: TiO₂/SiO₂ and TiO₂/ZrO₂. *Environmental Science and Technology* 30 (1996): 647–653.
- [33] Doolin, P.K.; Alerasool, S.; Zalewski, D.J.; Hoffman, J.F. Acidity studies of titania-silica mixed oxides. *Catalysis Letters* 25 (1994): 209–223.
- [34] Gun'ko, V.M.; Zarko, V.I.; Turov, V.V.; Leboda, R.; Chibowski, E.; Holysz, L.; Pakhlov, E.M.; Voronin, E.F.; Dudnik, V.V.; Gornikov, Y.I. CVD-titania on fumed silica substrate. *Journal of Colloid and Interface Science* 198 (1998): 141–156.
- [35] Tsumura, T.; Kojitani, N.; Izumi, I.; Iwashita, N.; Toyoda, M.; Inagaki, M. Carbon coating of anatase-type TiO₂ and photoactivity. *Journal of Materials Chemistry* 12 (2002): 1391–1396.
- [36] Przepiorski, J.; Yoshizawa, N.; Yamada, Y. Activated carbons containing TiO₂: Characterization and influence of a preparation method on the state of TiO₂ supported. *Journal of Materials Science* 36 (2001): 4249–4257.
- [37] Tryba, B.; Morawski, A.W.; Inagaki, M. Application of TiO₂-mounted activated carbon to the removal of phenol from water. *Applied Catalysis B: Environmental* 41 (2003): 427–433.
- [38] Matos, J.; Laine, J.; Hermann, J.M. Effect of the type of activated carbons on the photocatalytic degradation of aqueous organic pollutants by UV-irradiated titania. *Journal of Catalysis* 200 (2001): 10–20.

- [39] Janus, M.; Tryba, B.; Inagaki, M.; Morawski, A.W. New preparation of a carbon-TiO₂ photocatalyst by carbonization of *n*-hexane deposited on TiO₂. *Applied Catalysis B: Environmental* 52 (2004): 61–67.
- [40] El-Sheikh, A.H.; Newman, A.P.; Daffae, H.A.; Phull, S.; Cresswell, N.; York, S. Deposition of anatase on the surface of activated carbon. *Surface & Coatings Technology* 187 (2004): 284-292.
- [41] Li, Y.; Li, X.; Li, J.; Yin, J. TiO₂-coated active carbon composites with increased photocatalytic activity prepared by a properly controlled sol–gel method. *Materials Letters* 59 (2005): 2659 – 2663.
- [42] Ding, Z.; Hub, X.; Yue, P.L.; Lu, G.Q.; Greenfield, P.F. Synthesis of anatase TiO₂ supported on porous solids by chemical vapor deposition. *Catalysis Today* 68 (2001): 173–182.
- [43] Adhyapak, P.V.; Maddanimath, T.; Pethkar, S.; Chandwadkar, A.J.; Negi, Y.S.; Vijayamohanan, K. Application of electrochemically prepared carbon nanofibers in supercapacitors. *Journal of Power Sources* 109 (2002): 105–110.
- [44] Nishino, A. Capacitors: operating principles, current market and technical trends. *Journal of Power Sources* 60 (1996): 137-47.
- [45] Qu, D.; Shi, H. Studies of activated carbons used in double-layer capacitors. *Journal Power Sources* 74 (1998): 99-107.
- [46] Ioannides, T.; Verykios, X.E. Charge transfer in metal catalysts supported on doped TiO₂: a theoretical approach based on metal–semiconductor contact theory. *Journal of Catalysis* 161 (1996): 560-569.
- [47] Tatsuda, N.; Itahara, H.; Setoyama, N.; Fukushima, Y. Preparation of titanium dioxide/activated carbon composites using supercritical carbon dioxide. *Carbon* 43 (2005): 2358-2365.
- [48] Liu, S.X.; Chen, X.Y.; Chen, X. TiO₂/AC composite photocatalyst with high activity and easy separation prepared by a hydrothermal method. *Journal of Hazardous Materials* 143 (2007): 257–263.
- [49] Li, Z.; Hou, B.; Xu, Y.; Wu, D.; Sun, Y.; Hu, W.; Deng, F. Comparative study of sol–gel-hydrothermal and sol–gel synthesis of titania–silica composite nanoparticles. *Journal of Solid State Chemistry* 178 (2005): 1395–1405.

- [50] Jiang, B.; Yin, H.; Jiang, T.; Yan, J.; Fan, Z.; Li, C.; Wu, J.; Wada, Y. Size-controlled synthesis of anatase TiO₂ nanoparticles by carboxylic acid group-containing organics. *Materials Chemistry and Physics* 92 (2005): 595–599.
- [51] Kőrösi, L. and Dékány, L. Preparation and investigation of structural and photocatalytic properties of phosphate modified titanium dioxide. *Colloids and Surfaces A: Physicochemical Engineering Aspects* 280 (2006): 146–154.
- [52] Qiao, W.; Korai, Y.; Mochida, I.; Hori, Y.; Maeda, T. Preparation of an activated carbon artifact: oxidative modification of coconut shell-based carbon to improve the strength. *Carbon* 40 (2002): 351–358.
- [53] Dandekar, M.S.; Arabale, G.; Vijayamohanan, K. Preparation and characterization of composite electrodes of coconut-shell-based activated carbon and hydrous ruthenium oxide for supercapacitors. *Journal of Power Sources* 141 (2005): 198–203.
- [54] Liang, H.; Chen, F.; Li, R.; Wang, L.; Deng, Z. Electrochemical study of activated carbon-semiconducting oxide composites as electrode materials of double-layer capacitors. *Electrochimica Acta* 49 (2004): 3463–3467.
- [55] Yuan, G.H.; Jiang, Z.H.; Aramata, A.; Gao, Y.Z. Electrochemical behavior of activated-carbon capacitor material loaded with nickel oxide. *Carbon* 43 (2005): 2913–2917.
- [56] Arabale, G.; Wagh, D.; Kulkarni, M.; Mulla, I.S.; Vernekar, S.P.; Vijayamohanan, K.; Rao, A.M. Enhanced supercapacitance of multiwalled carbon nanotubes functionalized with ruthenium oxide. *Chemical Physical Letters* 376 (2003): 207–213.
- [57] Frackowaik, E.; Beguin, F. Electrochemical storage of energy in carbon nanotubes and nanostructured carbons. *Carbon* 40 (2002): 1775–1787.
- [58] Emmenegger, C.; Mauron, P.; Sudan, P.; Wenger, P.; Hermann, V.; Gallay, R.; Zuttel, A. Investigation of electrochemical double-layer (ECDL) capacitors electrodes based on carbon nanotubes and activated carbon materials. *Journal of Power Sources* 124 (2003): 321–329.

- [59] Probstle, H.; Schmitt, C.; Fricke, J. Button cell supercapacitor with monolithic carbon aerogels. *Journal of Power Sources* 105 (2002): 189–194.
- [60] Kierzek, K.; Frackowiak, E.; Lota, G.; Gryglewicz, G.; Machnikowski, J. Electrochemical capacitors based on highly porous carbons prepared by KOH activation. *Electrochimica Acta* 49 (2004): 515–523.
- [61] Frackowiak, E.; Beguin, F. Carbon materials for the electrochemical storage of energy in capacitors. *Carbon* 39 (2001): 937–950.
- [62] Xiao, Q.; Zhou, X. The study of multiwalled carbon nanotube deposited with conducting polymer for supercapacitor. *Electrochimica Acta* 48 (2003): 575–580.
- [63] Chen, W.C.; Wen, T.C.; Teng, H. Polyaniline-deposited porous carbon electrode for supercapacitor. *Electrochimica Acta* 48 (2003): 641–649.
- [64] Hu, C.C.; Wang, C.C. Effects of electrolytes and electrochemical pretreatments on the capacitive characteristics of activated carbon fabrics for supercapacitors. *Journal of Power Sources* 125 (2004): 299–308.
- [65] Watanabe, A.; Ishikawa, H.; Mori, K.; Ito, O. ESR study of electrochemical behavior of carbon black. *Carbon* 27 (1989): 863–867.
- [66] Satya Sai, P.M.; Ahmed, J.; Krishnaiah, K. Production of activated carbon from coconut shell char in a fluidized bed reactor. *Industrial & Engineering Chemistry Research* 36 (1997): 3625–3630.
- [67] Linares-Solano, A.; Salinas Mertz de Lecea, C.; Carzorra-Amors, D.; Merten-Gulln, I. Porosity development during CO and steam activation in a fluidized bed reactor. *Energy & Fuels* 14 (2000): 142–149.
- [68] Jagtoyen, M.; Derbyshire, F. Activated carbons from yellow poplar and white oak by H₃PO₄ activation. *Carbon* 36 (1998): 1085–1097.
- [69] Chen, W.C.; Hu, C.C.; Wang, C.C.; Min, C.K. Electrochemical characterization of activated carbon-ruthenium oxide nanoparticles composites for supercapacitors *Journal of Power Sources* 125 (2004): 292–298.
- [70] Zhang, F.; Zhou, Y.; Li, H. Nanocrystalline NiO as an electrode material for electrochemical capacitor. *Materials Chemistry and Physics* 83 (2004): 260–264.

- [71] Wu, M.; Snook, G.A.; Chen, G.Z.; Fray, D.J. Redox deposition of manganese oxide on graphite for supercapacitors. *Electrochimistry Communications* 6 (2004): 499–504.
- [72] Yin, H.; Wada, Y.; Kitamura, T.; Sumida, T.; Hasegawa, Y.; Yanagida, S. Novel synthesis of phase-pure nano-particulate anatase and rutile TiO₂ using TiCl₄ aqueous solutions. *Journal of Materials Chemistry* 12 (2002): 378–383.
- [73] Li, J.G.; Ishigaki, T.; Sun, X. Anatase, brookite, and rutile nanocrystals via redox reactions under mild hydrothermal conditons: phase-selective synthesis and physicochemical properties. *The Journal of Physical Chemistry C* 111 (2007): 4969-4976.
- [74] Chen, X. and Mao, S.S. Titanium dioxide nanomaterials: synthesis, properties, modifications, and applications. *Chemical Reviews* 107 (2007): 2891-2959.
- [75] Li, F. B.; Li, X. Z.; Hou, M. F. Photocatalytic degradation of 2-mercaptobenzothiazole in aqueous La³⁺-TiO₂ suspension for odor control. *Applied Catalysis B: Environmental* 48 (2004): 185-194.
- [76] Nagaveni, K.; Hegde, M. S.; Madras, G. Structure and photocatalytic activity of TiMO (M=W, V, Ce, Zr, Fe, and Cu) synthesized by solution combustion method. *The Journal of Physical Chemistry B* 108 (2004): 20204-20212.
- [77] Shen, M.; Wu, Z.; Huang, H.; Du, Y.; Zou, Z.; Yang, P. Carbon-doped anatase TiO₂ obtained from TiC for photocatalysis under visible light irradiation. *Materials Letters* 60 (2006): 693-697.
- [78] Khan, S. U. M.; Al-Shahry, M.; Ingler, W. B. Efficient photochemical water splitting by a chemically modified n-TiO₂. *Science* 297 (2002): 2243-2245.
- [79] Beydoun, D.; Amal, R.; Low, G.; McEvoy, S. Role of nanoparticles in photocatalysis. *Journal of Nanoparticle Research* 1 (1999): 439.
- [80] Bard, A.J. and Faulkner, L.R. *Electrochemical Methods: Fundamentals and Applications*. 2nded: John Wiley & Sons Inc.
- [81] Kotz, R.; Carlen, M. Principles and applications of electrochemical capacitors. *Electrochimica Acta* 45 (2000): 2483-2498.

- [82] Available from: http://www.gamry.com/App_Notes/EIS_Primer.htm#Model1
[2009, January 25]
- [83] Analysis software user's manual, BELSORP, BEL JAPAN, INC. 57.
- [84] Sawyer, D.T.; Sobkowiak, A.; Roberts, J.L. *Electrochemistry for Chemists*.
2nded. New York: Wiley Interscience, 1995.
- [85] Settle, F.A.; *Handbook of Instrumental Techniques for Analytical Chemistry*.
New Jersey: Prentice Hall, 1997.
- [86] Thomas, F.G. and Henze, G. *Introduction to Voltammetric Analysis*
Collingwood. Australia: CSIRO Publishing, 2001.
- [87] Xi-miao, Liu.; Rai, Z.; Liang, Z. ; Dong-hui, L. ; Wen-ming, Q. ; Jun-he, Y.;
Li-cheng, L. Impedance of carbon/aerogel activated carbon composites
as electrodes of electrochemical capacitors in aprotic electrolyte. *New*
Carbon Materials 22 (2007): 153-158.
- [88] Shi, Z.; Wang, Q.; Ye, W.; Li, Y.; Yang, Y. Synthesis and characterization
of mesoporous titanium pyrophosphate as lithium intercalation
electrode materials. *Microporous and Mesoporous Materials* 88
(2006): 232–237.
- [89] Leela Mohana Reddy, A. and Ramaprabhu. S. Nanocrystalline metal oxides
dispersed multiwalled carbon nanotubes as supercapacitor electrodes.
Journal of Physical Chemistry C 111 (2007): 7727-7734.

APPENDICES

Table A-2 Specific capacitance of electrodes with effect of TiO₂ contents in the composite calculated from cyclic voltammetric technique

Conditions	Specific capacitance from cyclic voltammetry (mF/g)															
	10%				20%				30%				40%			
% TiO ₂ in the composite	1	2	3	average capacitance	1	2	3	average capacitance	1	2	3	average capacitance	1	2	3	average capacitance
Method A																
- A1	18	17	17	17	38	33	30	34	210	202	204	205	564	694	600	619
- A2	42	37	33	37	51	51	51	51	226	220	230	225	980	726	840	849
Method B																
- B1	16	16	16	16	32	31	30	31	184	188	181	184	436	378	338	384
- B2	43	38	38	40	158	139	126	141	324	294	276	298	2,06 0	1,72 0	1,49 6	1,759

APPENDIX B

Results from electrochemical impedance spectroscopic technique

Table B-1 Specific capacitance of electrodes with effect of preparation methods and carbonization temperature calculated from electrochemical impedance spectroscopic technique

Conditions	Specific capacitance from electrochemical impedance spectroscopy (mF/g)					
	Carbonization temperature	500°C				
1		2	3	4	5	average capacitance
Method A						
- A1	256	242	292	264	242	259
- A2	380	390	382	365	390	281
Method B						
- B1	191	184	182	196	184	187
- B2	439	434	390	460	390	423
Bulk TiO ₂	74	75	76	81	88	79
Carbonization temperature	600°C					
	1	2	3	4	5	average capacitance
Method A						
- A1	126	121	117	129	122	123
- A2	134	148	153	139	158	146
Method B						
- B1	98	97	100	94	88	95
- B2	218	220	220	212	212	216
Bulk TiO ₂	69	70	71	67	68	69
Carbonization temperature	700°C					
	1	2	3	4	5	average capacitance
Method A						
- A1	96	94	90	92	87	92
- A2	100	113	102	100	102	103
Method B						
- B1	60	79	60	66	72	67
- B2	185	167	131	139	167	158
Bulk TiO ₂	43	65	54	60	65	57
Materials	1	2	3			average capacitance
Carbon	54	54	49			52
Activated carbon	56	59	62			59

Table B-2 Specific capacitance of electrodes with effect of TiO₂ contents in the composite calculated from electrochemical impedance spectroscopic technique

Conditions	Specific capacitance from electrochemical impedance spectroscopy (mF/g)															
	10%				20%				30%				40%			
	1	2	3	average capacitance	1	2	3	average capacitance	1	2	3	average capacitance	1	2	3	average capacitance
Method A																
- A1	52	54	57	54	98	100	101	100	198	206	208	204	346	370	394	370
- A2	58	58	62	59	105	105	106	106	217	219	214	217	412	414	410	412
Method B																
- B1	49	41	52	47	88	91	95	91	188	178	172	179	318	320	300	313
- B2	64	68	70	67	109	126	130	122	264	268	244	259	564	546	546	558

APPENDIX C

Micropore size determined by application of the MP-plot method

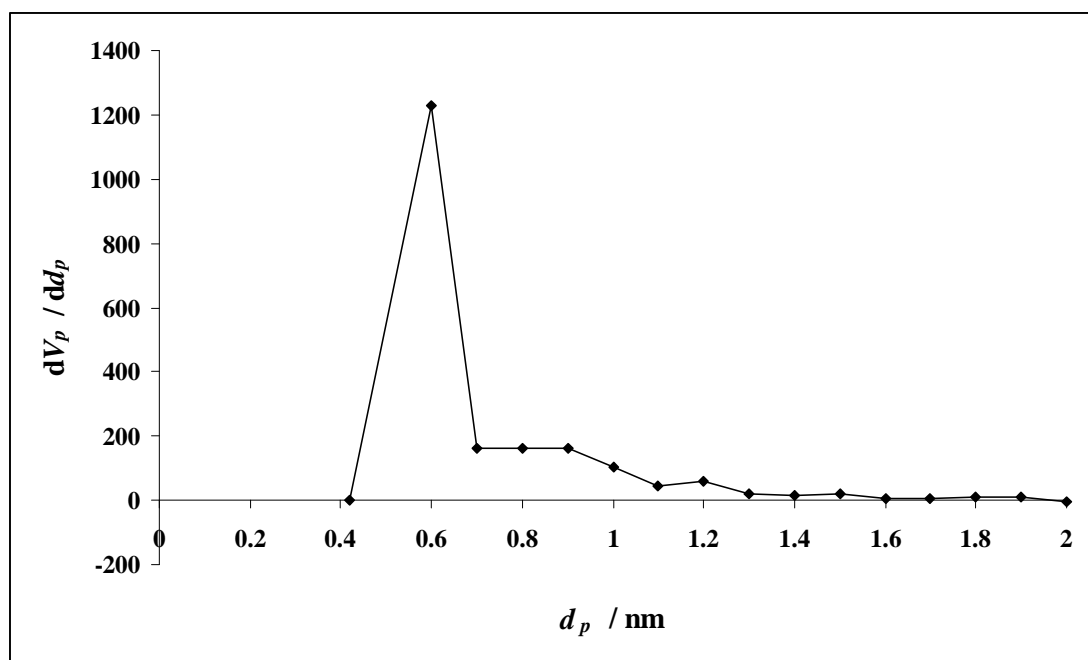


Figure C-1 MP pore-size distribution of the TiO₂/C composite.

VITAE

Miss Chamaiporn Mungthangtham was born on March 10, 1983 in Thailand. She graduated with high school degree from Suankularb Wittayalai Nonthaburi School, in 2001. She graduated with Bachelor's Degree in Chemistry from Faculty of Science, Kasetsart University in 2005. She continued her study in Petrochemistry and Polymer Science Program, Faculty of Science, Chulalongkorn University in 2005 and completed her Master of Science degree in 2009.

Her present address is 25/109 Moo.6 Srirachong 3, Changwattana Road, Bangtalard, Pakkred, Nonthaburi, Thailand 11120.